Investigation of Variations in the Saturated Hydraulic Conductivity of Sand and the Influencing Factors in the Laboratory

A thesis submitted in partial fulfilment of the requirements for the degree

of

Doctor of Philosophy in Engineering

by

Saeed Nikghalb Ashouri

Division of Health, Engineering & Computing and Science

THE UNIVERSITY OF
WAIKATO
Te Whare Wānanga o Waikato

2024

Abstract

The most critical hydraulic property of soil is the saturated hydraulic conductivity (Ks) of its matrix. Accurate determination of Ks is vital for understanding and simulating flow and transport phenomena. Hydrologists require accurate estimations of soil moisture content and retention to better discern rainfall distribution between runoff and infiltration; agronomists similarly rely on this data to inform crop yield models and formulate appropriate irrigation timetables. A diverse range of methodologies currently exists to determine the Ks, with the constant head test in the laboratory being a common approach. Traditionally, it is presumed that the Ks values obtained from both field and laboratory assessments remain constant. In addition, Ks is considered as a constant in various applications, such as solute transport modelling and surface water as well as groundwater simulations.

Given that soils can undergo saturation and desaturation they can be subjected to gradual and/or rapid changes in the hydraulic head, and thus the Ks of the soil will be affected. Consequently, any changes in Ks will affect the hydraulic properties of the soil. Therefore, to fully understand the hydraulic behaviour of a soil requires investigating the changes in Ks during short and long timeframes.

A primary objective of this study was to systematically investigate the changes that could occur in Ks during short-term and long-term constant head tests. Two soil columns were prepared and subjected to continuous constant head tests for a duration exceeding 50 days The hydraulic heads were increased gradually in a similar way as for a constant head test, with the only difference being that the hydraulic heads were increased every 5 to 7 days. The outcomes reveal that Ks exhibits negligible variations over short intervals, showing minor daily fluctuations. However, the long-term variations highlight significant shifts in Ks, with a maximum decrease in value of approximately 90% from the onset of the experiments, followed by intermittent brief periods of slight increase. These findings challenge the notion of Ks as a constant value over time. Moreover, a comparative analysis of soil properties before and after the tests indicates notable modifications in the sample characteristics. Specifically, the particle size distribution and particle density differ pre and post-experiment, with an observable migration of fine, low-density particles towards the upper section of the sample closer to the outlet, and aligned with the flow direction. This phenomenon results in an increased particle density at the lower part of the sample

adjacent to the water inlet. The migration of particles is evidence of the constant head test impact on the distribution of particles. The change in the distribution of the particles pre and post experiment, caused by the standard procedure of the tests, shows that the Ks value determined in the lab through constant head tests is influenced by the tests, and might not reflect the actual Ks of the sample.

In addition, a series of short-term experiments were carried out on 10 samples that were prepared with different particle size mixtures. These mixtures featured varying proportions of fine and coarse materials to study the range of changes in the Ks in different mixtures. The hydraulic heads of the tests on these samples were systematically adjusted in ascending increments, to investigate the range of changes in Ks under low and high hydraulic heads during short-term tests. This test series revealed a distinctive 3-phase pattern exhibited by the samples: a low and relatively consistent Ks was initially observed prior to a transition through a phase change as the hydraulic head escalates, leading to a stable constant Ks under high hydraulic gradients. These observations underscore the significance of the changes of Ks during constant head tests, and show a need to consider that Ks has a range of values over time rather than being a constant value.

Determining a suitable value for Ks in the lab and field is time consuming, it can be costly, and test results can be impacted by the test conditions. For instance, in the lab, ensuring the full saturation of the samples before the tests needs determination of solid particle density, which requires a pycnometer. Moreover, due to the spatial variations in Ks, the number of samples needed to represent the typical Ks in a study area can be costly to retrieve. Similarly, to investigate the spatial variation of Ks, the field tests (slug tests, pumping tests, or tracer tests) add extra cost and time to projects. Additionally, taking soil samples or performing Ks field tests in remote areas or harsh weather conditions is an arduous task. Therefore many researchers have endeavoured to establish predictive relationships to estimate Ks accurately without relying on resource-intensive laboratory or field tests. Indirect estimation methods are generally based on easily obtainable data such as soil texture, particle size distribution, specific surface area, or porosity. These relationships are developed into pedotransfer functions and aim to provide estimations of Ks. However, the reliability of these functions remains uncertain due to discrepancies observed when comparing the results obtained using different pedotransfer functions with actual field or laboratory measurements.

To address this issue, the Ks derived from Darcy's equation for the short-term tests were compared with those computed using 7 of the most commonly used pedotransfer functions. The objective of the comparison was to evaluate the effectiveness of these equations in predicting Ks. The analysis revealed that the majority of pedotransfer functions tend to underestimate the Ks values of the soil samples. Subsequently, a novel method was employed to adjust the parameters of one of the equations, which is suitable for non-plastic sandy soils as used in the earlier experiments, by linking the equation parameters to the coefficient of uniformity and void ratio of the samples. This modification led to a more precise estimations of Ks for the range of sandy samples used in the research.

Given the inaccuracies related to the constant head tests and the impact on Ks determination (such as the disturbance in connection of drainable pores due to varying hydraulic heads, inaccuracies in reading the flow rate and sample head gradient, improper sample saturation, effect of air entrapment in the sample), it was necessary to look for improvements in determining the Ks in the soil.

Tracer tests on soil samples in the laboratory and field have been used by several researchers to estimate the soil hydraulic properties. These tests offer essential insights into site hydrogeology, aiding in the delineation of crucial factors such as natural groundwater velocity and hydraulic connectivity between neighbouring aquifers and aquitards. When coupled with groundwater flow and transport models, tracer tests can enhance the precision of defining Ks and its spatial distribution accurately.

In order to acquire soil hydraulic properties from tracer tests, a tracing element is injected into the samples, and the changes of concentration in the outflow is plotted over time. The resulting graph is called a break through curve (BTC). In order to acquire soil hydraulic properties from BTCs, advection-dispersion equations (ADE) and the models that are built upon ADE equations are widely used. The ADE links soil hydraulic properties (Ks and dispersivity coefficient) to the BTC. Trial and error is required to achieve the best fit between predicted and measured BTC which can be challenging and may require several trials to process multiple sets of BTCs.

In this study, the use of a statistical distribution, specifically the Inverse Gaussian distribution (IG), was examined for fitting BTCs obtained from 94 tracer tests utilizing sodium chloride as the tracer compound. The results of fitting the BTCs using the IG distribution revealed that solute transport in porous media could be effectively articulated using this distribution, particularly given its suitability for positively skewed data. The

majority of the tracer tests fitted with the IG distribution exhibited model efficiencies exceeding 0.9 (based on Nash–Sutcliffe model efficiency coefficient), indicating a strong fit of the BTCs. A comparison of the IG method with alternative methodologies from existing research further underscored the superior fit achieved by the IG distribution in modelling BTCs.

The test series outlined in this thesis represent a significant advancement in the comprehension of saturated hydraulic conductivity within porous media. The noticeable long-term changes of Ks in the laboratory show this parameter cannot be considered as a constant, and the assumption of linearity between the hydraulic head and flow in the samples is only valid in the short-term tests. Additionally, Ks can have a range of low and high values, during rapid changes of the hydraulic head. The implications of these findings offer potential revisions to the existing approaches for integrating saturated hydraulic conductivity within equations of surface and groundwater models. Furthermore, the study highlights the viability of employing statistical methods to analyse the BTCs from tracer tests. The use of statistical methods with the tracer tests can save time and cost in the post-processing of the tracer test results.

Acknowledgements

I would like to express my heartfelt gratitude to the following individuals who have played a significant role in supporting me throughout my academic journey:

To my supervisor, Ali Shokri, I am truly thankful for your guidance, support, and scientific expertise that have been invaluable in shaping my research and thesis. Your mentorship has been instrumental in my growth.

I extend my sincere appreciation to my co-supervisor, Adrian Pittari, for your continuous guidance, scientific insights, and unwavering support during challenging times. Your input has been crucial to the success of my work.

I want to acknowledge Kim de Graaf for stepping in after Ali's resignation and taking on the role of chief supervisor. Your support and assistance were crucial in helping me complete my thesis successfully. I am truly grateful for your dedication.

A special thank you goes to my wife, Dalareen Fernandez, my pillar of strength and unwavering source of support. Your encouragement, positivity, and heartwarming words have kept me going through the toughest of times. Having you by my side has been a blessing beyond words.

I also want to express my gratitude to my wife's family, as well as my parents, for their endless support and encouragement. Your belief in me has meant the world.

To my dear friends in New Zealand, thank you for the great moments we shared during the course of my PhD journey. Special mentions to Hadley Craig, Amin Rahdarian, Jaber Abbaszadeh, Jamal Abarashi, Ali Haji Wahabzadeh, Sanush Abeysekera, Jeremy Toms, and Lia Missena. Your friendship and camaraderie have been a source of joy and strength.

Last but not least, I am thankful to my colleagues at Te Miro Water Consultants for their support, encouragement, and understanding as I balanced my thesis work and professional responsibilities. Your support has been invaluable.

Thank you all for being part of this significant chapter in my life.

Table of contents

List of figures

List of tables

Chapter 1. Introduction

1.1. Introduction

Saturated hydraulic conductivity (Ks) is a pivotal parameter in soil science and hydrology that quantifies the ease with which water travels within saturated soil pores (Deb, 2012; Naik et al., 2024; Novák & Hlaváčiková, 2019). Its significance lies in its fundamental role in predicting and managing water flow and distribution in diverse environmental contexts. High Ks values indicate soils with rapid drainage potential, which are crucial in agriculture (Islam et al., 2019; Keïta et al., 2023) to prevent waterlogging and ensure adequate root aeration. In urban planning, an in-depth understanding of this parameter is essential for designing effective stormwater management systems, thereby minimizing flood risks (Ghibus et al., 2023; Olson et al., 2013). Additionally, Ks is vital for groundwater recharge and sustainable management of water resources (Hwang et al., 2017; Olson et al., 2013; Zebarth et al., 1989), influencing infiltration rates and the overall hydrological cycle. By precisely assessing Ks, scientists and engineers can make informed decisions to bolster agricultural productivity, urban development, and environmental conservation.

The determination of Ks can be approached via several direct and indirect methods. Direct methods (or hydraulic methods) use soil's hydraulic properties (rate of flow and hydraulic gradient) and apply Darcy's equation to determine Ks (Águila et al., 2023; H. Hwang et al., 2017). Conversely, indirect methods correlate other properties (such as electric conductivity, electrical resistance, transport of tracing elements, particle size distribution, gravity of particles, void ratio, and specific surface area) with the soil's hydraulic behaviour (Águila et al., 2023). These methods are further categorized into laboratory and field determinations (Islam et al., 2019).

Various standards have been developed for determining Ks in both laboratory (ASTM D2434-19, 2019; ASTM D5856-15, 2015) and field settings (ASTM 6034-96, 2010; ASTM D4044M, 2015). Additionally, numerous methods have been developed (Field, 2003; Liu et al., 2012; Melville et al., 1991) or enhanced (Águila et al., 2023; Batlle-Aguilar et al., 2016; Pucko & Verbovšek, 2015; Vienken & Dietrich, 2011) to improve the accuracy of Ks determination. These methods range from highly detailed setups to desktop approaches based on easily measurable soil parameters, like particle size distribution. Furthermore,

comparative research on different methodologies for determining Ks has been extensive to evaluate their accuracy and generalizability, with findings indicating variability in Ks results from different methods (Águila et al., 2023; Butler, 2005; Hangen & Vieten, 2018; Lee & Lee, 1999; Pedescoll et al., 2011).

Despite the critical nature of Ks in various contexts concerning water movement in soil, significant knowledge gaps persist. Many established standard methods (ASTM 6034-96, 2010; ASTM D2434-19, 2019; ASTM D4044M, 2015; ASTM D5856-15, 2015) overlook the impact of hydraulic heads on the test, which significantly influence Ks results.

Given that field and laboratory Ks determinations are time and labour-intensive, alternative estimation methods utilizing easily measurable soil parameters (such as particle size distribution and void ratio) have been developed (Aubertin et al., 2005; R. P. Chapuis, 2012a; Kozeny, 1927b; Mbonimpa et al., 2002; Slichter, 1898; C. Terzaghi, 1925). These methods, known as pedotransfer functions, are widely used for initial Ks estimates. Several countries have developed maps based on these functions to facilitate Ks estimation for designers and hydraulic-hydrological modelers. Although pedotransfer functions are widely used for estimation of Ks, concerns about the accuracy and reliability of these functions persist (Águila et al., 2023; Cheong et al., 2008; Mbonimpa et al., 2002). Improving the accuracy of Ks estimations from pedotransfer functions can save time and reduce labour costs that are related to the field or lab determination of Ks.

Tracer methods are among the more reliable means of determining Ks (Field, 2003; Nowak & Cirpka, 2006). Nevertheless, they are often impractical due to their time-consuming and costly nature. The associated time and costs are not solely from field or laboratory measurements but also from the complex interpretation of data, including the analysis of breakthrough curves. Estimating soil hydraulic parameters often involves trial and error, which is time-intensive. Hence, developing efficient methods for estimating soil hydraulic parameters would be beneficial, significantly reducing the required time and effort.

1.2. Aims and objectives

1.2.1. Investigate long-term changes in Ks and the reliability of standard constant head tests

The variations in Ks significantly affect studies related to water movement through soil. One objective of this thesis is to investigate the reliability of Ks acquired from standard constant head tests. Specifically, the aim is to monitor if the Ks remains constant when the constant head tests are extended for several days. It is hypothesised that initial Ks results from the first few hours of testing, whether in the lab or field, may be unreliable because of the rearrangement in pore connections. Long-term variations in Ks will be explored using two samples under constant head until a stable value of Ks is reached.

1.2.2. Determine the impact of rapid changes of hydraulic head on Ks

The dynamic interconnections between soil pores can be affected by sudden hydraulic heads imposed on samples in both laboratory and field settings, potentially causing the rearrangement of drainable pore connections. To investigate the changes in Ks under rapid fluctuations of hydraulic heads, ten samples with different particle size mixtures are designed to be tested using a constant head setup. The hydraulic heads are altered relatively quickly, and the behaviour of the samples under these conditions are thoroughly evaluated.

1.2.3. Improve the accuracy of the Ks estimate from pedotransfer functions

Pedotransfer functions are simple tools that offer quick estimates of saturated Ks. To evaluate the usability and reliability of these functions, seven widely used methods were selected, and their predictions were compared with Ks values obtained through constant head tests. Additionally, the parameters of one method were adjusted to enhance the accuracy of its predictions.

1.2.4. Simplify the analysis of tracer test data and estimation of breakthrough curve fitting parameters

The analysis of breakthrough curves from tracer tests is typically time-consuming and computationally intensive. Developing and testing a novel method to streamline the estimation of soil hydraulic parameters from these curves could significantly reduce the time required for data analysis. The objective of this study is to evaluate the effectiveness of the Inverse Gaussian distribution in interpretation of tracer test breakthrough curves and compare its performance with conventional advection-dispersion methods.

1.3. Structure of thesis and research questions

This section provides a concise introduction to the chapters and outlines the key research questions addressed in the thesis. It offers an overview of the entire thesis, facilitating a better understanding of the subsequent parts.

Chapter 2- A literature review of the methods for determining the Ks. This chapter briefly explains the concept of the following 3 chapters.

Chapter 3- Research article 1: Examining the mid to long-term variability in saturated hydraulic conductivity of sandy soils and its influencing factors under constant head test in the laboratory:

- In this chapter, the methods of determining the Ks in the laboratory and the advantages and disadvantages are discussed.
- The reliability of standard constant head tests for determination of Ks is investigated by Ks tests on 2 samples for more than 50 days.
- In order to study the causes of changes in Ks during constant head tests, the properties of the samples before and after the tests are compared and the possible reasons for the variations are discussed.

Chapter 4- Research article 2: Range of variations in the saturated hydraulic conductivity of sand and gravel samples in the laboratory by constant head method in a rigid wall cell and comparison of results from Darcy's equation with predictive methods.

- In this chapter, the impact of changing the fine and coarse particle content composition on the Ks during short Ks tests in the laboratory will be investigated. Then the efficiency

of pedotransfer functions for estimation of Ks will be evaluated, followed by modification of one of the equations in order to achieve more accurate predictions of Ks.

- How does the saturated hydraulic conductivity change in sets of short-term constant head tests, in samples with different particle size distributions?

Chapter 5: Research article 3: Using inverse Gaussian distribution for analysis of breakthrough curves in tracer tests for sandy samples in rigid wall cell.

- In this chapter, the focus is on interpretation of tracer test data. The breakthrough curves from several tracer tests are used to test the potential of employing Inverse Gaussian distribution for predicting travel times.
- The results of other studies using advection-dispersion models for analysis of breakthrough curves are compared with the Inverse Gaussian method.

  The effectiveness of the Inverse Gaussian equation for predicting the breakthrough curves is compared with advection-dispersion models, through the use of the Nash-Sutcliffe model efficiency coefficient.

Chapter 2. Background

In this chapter, a comprehensive review of preceding research relevant to the thesis topic is undertaken. The chapter commences with an in-depth account of the historical methods employed in determining saturated hydraulic conductivity (Ks). Subsequently, the factors that influence variations in Ks are presented. Following this, the applications of pedotransfer functions for estimation of Ks are explained. In the last section, an analysis of methods for the interpretation of tracer test data and the estimation of soil hydraulic parameters is discussed.

2.1. Methods of determining Ks

Ks is an essential soil property that profoundly impacts numerous engineering and environmental applications. Libohova et al. (2018) highlight that measuring Ks is one of the most expensive soil properties to quantify. Ks delineates the soil's ability to conduct water, influencing several vital processes such as water retention, groundwater recharge, and water availability for plant growth (Duan et al., 2012; Hoseini, 2023; Ibrahim & Aliyu, 2016). Therefore, accurate estimation of Ks is paramount in the design and construction of embankment slopes, waste disposal sites, roadways, and building foundations (Feng & Vardanega, 2019).

Moreover, Ks is integral to equations employed in modelling surface and subsurface water flow and in predicting the transport of contaminants within the soil (Ghanbarian et al., 2017). It is one of the most critical parameters in hydrological modelling (Libohova et al., 2018) and serves as a primary variable for modelling solute transport in the soil or estimating the flood retention capacity of soil (Hangen & Vieten, 2018). Specifically, accurate assessment of Ks is indispensable for simulating water movement in the unsaturated zone of soil through Richard's equation (Zhang & Schaap, 2019). Consequently, precise measurements of Ks are crucial for effective water resources management and the successful execution of diverse environmental and engineering projects. Nevertheless, accurately determining Ks remains a challenging undertaking in hydrogeological investigations (Vienken & Dietrich, 2011).

Various methodologies exist for determining the Ks of soil, with the selection of a specific method typically influenced by factors such as time constraints, budget limitations, and

the required level of accuracy. Butler (2005) provides a comprehensive review of these methods. The techniques for determining Ks include pumping tests, slug tests, laboratory tests on both disturbed and undisturbed soil cores, geophysical logging, borehole flowmeter tests, direct push methods, and hydraulic tomography. Generally, these methodologies can be categorized into three groups: field tests, laboratory tests, and predictive equations.

Further classification of these methods can be delineated based on whether they determine Ks through the assessment of hydraulic soil properties or by utilizing other non-hydraulic soil characteristics, such as electrical conductivity, particle size distribution, and porosity. Therefore, methods for determining Ks can be classified as either direct or indirect based on these distinctions.

Direct field methods for determining the Ks include the pumping test, auger hole test (or soakage test), and slug test (ASTM 6034-96, 2010; ASTM D4044M, 2015; Pucko & Verbovšek, 2015; Vienken & Dietrich, 2011). In essence, these methods involve the excavation of soil layers to a specified depth, followed by the injection, extraction, or sudden alteration of the water level with a known head or flow rate, and subsequently recording the modifications in the hydraulic head or flow rate within the aquifer or targeted saturated soil layer (Águila et al., 2023). The Ks can then be determined through analysis of the drawdown curve or the temporal variation in the water level.

Specifically, in the pumping test, a pump is employed to displace water, while in the slug test, a slug is abruptly introduced into the borehole, and the resultant changes in the water level are documented in the observation or monitoring wells (Batlle-Aguilar et al., 2016).

Having multiple observation wells in a pumping test or slug test enables researchers to investigate the heterogeneity of Ks within the aquifer. By recording the changes in water levels in these observation wells, researchers can develop hydraulic tomography or hydraulic profiles (Liu et al., 2012) of the aquifer, facilitating the examination of the soil layer's heterogeneity in the field.

In contrast, the auger hole test involves creating a borehole in the aquifer using an auger, followed by the addition of water to the borehole. The subsequent drop in the water level is then recorded over time to determine Ks.

Indirect field methods for determining Ks include tracer tests (Melville et al., 1991). In tracer tests, a tracer element (such as NaCl, Bromide, KCl, or Rhodamine) is injected into a

borehole, and the concentration of the tracer is measured in observation wells (Field, 2003; Masipan et al., 2016; Melville et al., 1991). The Ks is then calibrated by analysing breakthrough curves (BTCs) using advection-dispersion or convection-dispersion models (Mallants, 2014; Piccinini et al., 2016) or through mass balance numerical models to match the measured and modelled BTCs. One of the most widely used software packages for analysing tracer test BTCs is STANMOD (van Genuchten et al., 2012), which offers various modules for modelling the movement of tracers in groundwater (Piccinini et al., 2016).

Other indirect field methods include measuring electrical conductivity, electromagnetic pulses, and heat energy pulses, which correlate other soil properties to Ks. These methods are generally used in conjunction with direct methods to calibrate correlation equations. The cone penetrometer test (CPT) is a direct-push method commonly employed to investigate the heterogeneity of Ks in an aquifer (Águila et al., 2023; Elhakim, 2016). The CPT involves a transducer inside the probe that measures the pressure of injected water. Ks is determined by recording changes in the injected water pressure and discharge (Águila et al., 2023).

The instantaneous profile method is another indirect approach for determining Ks (Hangen & Vieten, 2018; Su et al., 2018). This method posits a linear correlation between the instantaneous Ks and macroscopic flow velocity, potential gradient, and water content at any given time in the soil (Watson, 1966). Water content can be measured using time domain reflectometry (TDR) probes, which offer a non-destructive and easily automated technique (He et al., 2023).

Ks determined from direct field methods is typically more reliable than other methods due to reduced variability in Ks values (Águila et al., 2023). However, there are numerous scenarios in which field measurements of Ks are impractical. For example, in many projects, excavated materials are sourced from borrows and transported to the project site, where the backfilled materials must meet specific compaction and Ks requirements. In such cases, the only feasible way to determine Ks is through laboratory measurements.

Direct laboratory methods for determining Ks include constant and falling head tests (ASTM D2434-19, 2019; ASTM D5856-15, 2015). In these methods, a disturbed or undisturbed soil sample is placed in a hydraulic conductivity cell. The sample is then fully saturated and connected to a water supply, after which a constant head, falling head, or constant flow rate is applied (Amoozegar, 2020; Pedescoll et al., 2011). Changes in the hydraulic head within the sample are recorded along with the flow rate, and Ks is

determined using Darcy's equation. The constant head method is generally suitable for samples with moderate to high Ks, while the falling head method is more appropriate for samples with low Ks (Butler, 2005).

Indirect laboratory methods include tracer tests (Qiu et al., 2023). This method includes injection of the tracing element in the sample and measuring the concentration at the other end. The tracer tests in the laboratory can be carried out on the permeability cells, but the results will show the dispersivity of the tracer in one dimension (1D). But there are several studies that investigate dispersion of tracers in a sandbox that account for the lateral transport of the tracing element (Zhao et al., 2022).

Given that determining Ks in the field or laboratory can be both costly and time-consuming, especially for large-scale measurements (Abdelbaki, 2021), scientists have developed relationships between soil properties and Ks. These desktop methods, known as pedotransfer or empirical functions, utilize readily available soil data such as particle size distribution, bulk density, porosity, and organic matter content (Abdelbaki, 2016). Pedotransfer functions are generally applied to coarse soils with a limited proportion of fine particles. Estimating Ks from particle size distribution (PSD) is one of the most prevalent approaches within this category (Vienken & Dietrich, 2011).

Numerous equations have been developed to estimate Ks based on soil properties such as porosity, PSD, specific surface area, and Atterberg limits (Aubertin et al., 2005; Carman, 1939; Mbonimpa et al., 2002; Slichter, 1898; Terzaghi, 1925). However, the accuracy of these methods remains unclear (Hangen & Vieten, 2018; Vienken & Dietrich, 2011). While pedotransfer functions provide quick and easy initial estimates of Ks, they can exhibit considerable error; some studies have reported discrepancies as large as 500% compared to field or laboratory methods (Águila et al., 2023). Hangen & Vieten (2018) and Vienken & Dietrich (2011) note that the primary reason for the preference for using pedotransfer functions is their ease of use and reduced labour compared to field methods.

Additionally, there are pedotransfer tables containing databases of numerous soil types along with their measured Ks values in the laboratory. The Ks of a target sample can be estimated by matching the sample's texture and bulk density with entries in these tables. Databases such as ROSETTA, HYPRES, and the German Ad-hoc Committee on Soil fall into this category of methods for determining Ks (Hangen & Vieten, 2018).

The Ks of the vadose zone, extending up to a few meters from the surface (Amoozegar, 2020), can be assessed using devices like infiltrometers or permeameters. Various

infiltrometers have been devised for this purpose, including hood infiltrometers, disk infiltrometers for topsoil, and constant head permeameters that can measure deeper soil layers as well (Amoozegar, 2020; Hangen & Vieten, 2018).

Other techniques for determining Ks are location-specific. In coastal regions, the Tide-Aquifer interaction method is utilized, relying on the sinusoidal water level fluctuations in coastal aquifers (Ferris, 1952). Geophysical methods are also deployed in the field, encompassing the use of natural gamma logs, electrical conductivity, or resistivity logs (Butler, 2005). The dipole flow test (DFT) involves the isolation of a specific aquifer layer using packers, followed by water injection and measurement of drawdown in the isolated layer using pressure transducers (Kabala, 1993). A relatively recent approach, the multilevel slug test (Melville et al., 1991), is akin to the DFT and isolates an aquifer layer for evaluating soil hydraulic parameters through slug tests.

Advancements in computational capabilities have led to the utilization of numerical models for determining Ks in recent years (Cheong et al., 2008). The MODFLOW model (McDonald & Harbaugh, 1988) stands out as a popular numerical model widely utilized in aquifer analysis (Strom, 1998).

2.2. Variations of Ks between different methods and within each method

Various studies have highlighted significant variations in Ks values obtained from different methods, influenced by several factors. In a coastal sand aquifer study by Águila et al. (2023), where 8 different direct and indirect methods were utilized (including field methods, pedotransfer functions, and numerical models), the resulting Ks values ranged from 3.6 to 58.3 m/day. The study concluded that Ks is not necessarily scale-dependent when significant aquifer heterogeneity is absent. Pedescoll et al. (2011) examined the reliability, repeatability, and accuracy of the falling head method, determining it to be sufficiently accurate for assessing clogging in constructed wetlands. Hangen & Vieten (2018) compared 5 different Ks determination methods, ranking the Ks values from smallest to largest as borehole permeameter, PSD-based pedotransfer function, pedotransfer table, instantaneous profile, and soil core in the laboratory. The presence of clay layers in specimens can lead to significant discrepancies between Ks values obtained from pedotransfer functions and field measurements (Vienken & Dietrich, 2011).

Furthermore, Vienken & Dietrich (2011) highlighted that results from pedotransfer functions may not be adequate for high-resolution modelling of water transport in aquifers.

Studies have shown diverse results and considerations on Ks measurements and the factors influencing them. Butler (2005) observed differences of 16% and 39% for undisturbed and disturbed samples, respectively, compared to pumping tests. Lee & Lee (1999) recommended conducting multiple replicates of pumping and slug tests to obtain reliable estimates of aquifer hydraulic parameters. In a study by Cheong et al. (2008) on an alluvial system, they compared Ks results from pedotransfer functions, slug and pumping tests, and numerical modelling, concluding that Ks values from pedotransfer functions were 3.33 times greater than those from pumping tests.

Moreover, several studies have delved into the long-term changes in Ks in both laboratory and field settings, particularly focusing on changes due to pore clogging in aquifer storage and recovery (ASR) or aquifer recharge, as well as in constructed wetlands (CW) for water storage and treatment. Researchers such as Goldenberg et al. (1983), Konikow et al. (2001a), Oliveira et al. (2014), Rinck-Pfeiffer (2000), and Yang et al. (2008) have explored Ks fluctuations in such systems. For instance, Jeong et al. (2018a) highlighted how injecting water with minimal suspended solids can lead to rearrangement of silt and clay particles, causing clogging and altering Ks. Segismundo et al. (2016) discussed the variability of Ks in sand and zeolite, attributing it to internal particle mobility and rearrangement. Cihan et al. (2022a) suggested that Ks decrease could be due to clays separating from grains and relocating within the sample. Torkzaban et al. (2015a) investigated Ks changes in aquifer sandstones, linking these alterations to variations in injected water salinity affecting fine particle mobility and clogging. Additionally, Goldenberg et al. (1983) raised questions about models that assume a constant Ks, particularly regarding changes at the seawater-freshwater front in a coastal aquifer.

Research on determining Ks in various soils has been extensive, but there has been relatively limited focus on the duration of Ks tests. The gradual displacement of fine particles in soil can occur slowly over time. Standards for conducting Ks tests in the laboratory (ASTM D2434-19, 2019; ASTM D5856-15, 2015) typically do not specify test duration. The only reference to test conclusion criteria is found in ASTM D5856-15 (2015), where it suggests ending the test when four consecutive Ks measurements fall within ±25% of the average of all measurements. However, this criterion raises questions about

instances where measurements stay within the range for a period and then change gradually over a longer duration. Some studies have noted longer-term changes in Ks in laboratory tests after permeation with freshwater, but without delving into the underlying reasons (Mavis & Wilsey, 1936; Pillsbury & Appleman, 1945).

Currently, there is a need for an assessment of Ks determination methods and the establishment of a benchmark standard (Águila et al., 2023). While there are multiple methods documented in literature for determining Ks, the existing standards primarily focus on core soil testing in laboratories using constant or falling head tests (Hangen & Vieten, 2018). Discrepancies between field and laboratory Ks values may stem from imperfect laboratory procedures and aquifer heterogeneity (Butler, 2005). Commonly employed standard methods for Ks determination include falling head and constant head tests in the laboratory (ASTM D2434-19, 2019; ASTM D5856-15, 2015), and slug tests and pumping tests in the field (ASTM 6034-96, 2010; ASTM D4044M, 2015). Other methods developed by researchers for Ks determination are credible but deviate from standard practices and are not widely adopted in industry.

2.3. Evaluation of pedotransfer functions for estimation of Ks

Pedotransfer functions (PTFs) have a long history of use for estimating Ks. Hazen's formula, established in 1892 and later confirmed by other researchers like Loudon (1952), was one of the earliest relationships linking particle size to Ks. This formula correlates Ks with the square of D_{10} (the size at which 10% of the material is smaller) and a correlation coefficient. Subsequent studies by researchers such as Breyer (1964), Carman (1939), Kozeny (1927b), Slichter (1898), Terzaghi (1922) further reinforced the correlation between Ks and the square of D_{10} while incorporating additional soil properties like porosity and coefficient of uniformity into the correlation coefficient.

Among these classical PTFs, the Kozeny-Carman formula, introduced by Carman (1939), is particularly popular for estimating Ks as it considers the shape of particles. Mbonimpa et al. (2002) modified Hazen's PTF by incorporating surface characteristics through factors like particle density and specific surface area. While many researchers still assume Ks is associated with the square of D_{10}, Chapuis (2004) introduced a power function for estimating Ks that offers a different relationship with D_{10} compared to Hazen's formula,

making it applicable across a broader range of material sizes. These classical PTFs continue to be studied and refined by researchers in pursuit of more accurate Ks estimates.

In large-scale applications for extrapolating point-measured data to entire catchments and countries, artificial neural networks (ANNs) have been utilized in developing PTFs to create maps of Ks. Minasny et al. (1999) and Schaap et al. (2001) employed ANNs to generate Ks maps. Schaap et al. (2001) notably created the ROSETTA program, which utilizes an extensive database of soil hydraulic properties, incorporating ANN and bootstrap analysis to provide estimations of Ks.

Similarly, Lebron et al. (1999) applied neural networks and bootstrap analysis to predict the formation factor utilized in the Kozeny-Carman formula, achieving excellent agreement between predicted and measured data. Ferrer Julià et al. (2004) focused on developing a Ks map for Spain, comparing the results of regression-based PTFs with ANN-generated estimations. They concluded that regression-based PTFs utilizing the percentage of sand as a soil property tended to provide more accurate estimates of Ks. Additionally, Picciafuoco et al. (2019) employed two regression methods to extrapolate point measurements of Ks obtained via infiltrometers to cover an entire area within a small catchment.

Rehman et al. (2022) used machine learning (ML) intelligent modelling, such as ANN multi-expression programming (MEP) and genetic expression programming (GEP) for predicting the Ks of a wide range of sandy samples, using soil parameters including particle size distribution and dry density. Their findings showed reasonable performance of ML models for prediction of Ks. Pásztor et al. (2025) also use machine learning to predict the Ks of soils in Hungary. Zeitfogel et al. (2023) used machine learning models, including eXtreme Gradient Boosting (XGBoost) and feed-forward neural network (FNN), and demonstrated the effectiveness of these models to predict Ks in areas lacking soil information. However, they emphasize the importance of field investigation to validate the Ks predictions. Wang et al. (2025) developed three multi-modal machine learning models to predict Ks in the field using field measured Ks and tracer tests data. They concluded that the models that use combined inputs of hydraulic head and tracer concentration outperform the models that use sole hydraulic head for predicting the field value of Ks. Araya & Ghezzehei (2019) used a database of over 18,000 soils and related Ks to the soil properties, such as particle size indicators, clay content, bulk density, and organic carbon content, and developed generic ML PTFs for estimating Ks. Other researchers have also

used ML models to develop PTFs and to predict Ks (Devi et al., 2025; Kotlar et al., 2019; Moosavi et al., 2024; Tan et al., 2023; Y. Wang et al., 2024).

Pedotransfer functions specific to New Zealand soils have been developed by McNeill et al. (2018) and are accessible through the SMAP database provided by Landcare Research (2023). The SMAP tool serves as a valuable resource for estimating soil types and water retention parameters across the country, commonly utilized for stormwater modelling in New Zealand. However, criticisms have been raised regarding the tool's accuracy in providing Ks values, with earlier work by Cichota et al. (2013) noting a wide and potentially inaccurate range of Ks estimates for each region of New Zealand.

In a groundwater movement simulation model, Weihermüller et al. (2021) explored the use of various pedotransfer functions and highlighted how the selection of these functions can impact both the results and runtime of the model. This underscores the importance of carefully considering which pedotransfer functions to employ as they can significantly influence the outcomes of groundwater modelling studies.

The studies mentioned indicate that pedotransfer functions play a key role in estimating saturated hydraulic conductivity (Ks) and are commonly used for this purpose. However, the credibility and accuracy of these functions are subjects of ongoing investigation. It is clear that there is a continuing need to enhance the accuracy of Ks predictions through pedotransfer functions. Researchers are working to refine these functions to improve their predictive capabilities and ensure more reliable estimations of soil hydraulic properties such as Ks. By advancing the accuracy of these predictions, we can further enhance our understanding of soil behavior and improve modelling efforts in various environmental and engineering applications.

2.4. Methods of interpretation of tracer test data

Tracer tests have been established as reliable methods for estimating Ks and are frequently employed by researchers to evaluate the hydraulic properties of aquifers (Field, 2003; Lei et al., 2023; Nowak & Cirpka, 2006; Seifert & Engesgaard, 2007a). In a comprehensive study conducted by Millham & Howes (1995) comparing five methods for field estimation of Ks, the tracer method was found to exhibit higher reliability and reproducibility compared to other methods, with the slug test and permeameter deemed the least reliable.

Seifert & Engesgaard (2007a) utilized tracer tests to scrutinize changes in hydraulic properties within porous media columns resulting from bioclogging processes. Additionally, Monego et al. (2010) employed electrical resistivity in combination with a saline tracer to generate tomographic representations of the hydraulic properties of the aquifer. These studies underscore the effectiveness and significance of tracer tests in assessing hydraulic properties and investigating alterations in porous media caused by various factors like bioclogging.

Tracer tests indeed provide reliable estimates of Ks but can be costly and time-consuming, especially in terms of data interpretation (Melville et al., 1991). Typically, the solute transport in porous media is elucidated using the advection-dispersion equation (ADE) or convection-dispersion (CDE) framework. In the ADE, the dispersivity coefficient and pore velocity can be iteratively adjusted to align predicted breakthrough curves (BTCs) with measured data through a trial and error process. Subsequently, Ks can be determined based on the estimated pore velocity and dispersivity coefficient.

To facilitate this process, various software packages are available that aid in fitting BTCs and estimating ADE parameters, such as STANMOD or HYDRUS (Radcliffe & Simunek, 2018; Simunek et al., 1999). These tools assist in streamlining the analysis, calibration, and determination of hydraulic parameters from tracer test data, enhancing the efficiency and accuracy of estimating Ks in porous media.

The iterative process of adjusting solute transport parameters to match BTCs can be time-consuming, particularly when using traditional trial-and-error methods. Rajabi et al. (2022) introduced a deep convolutional neural network to optimize parameter estimation in heat transport models within porous media, showcasing a more efficient approach to parameter optimization.

Groundwater models utilized for simulating solute transport are computationally demanding, especially when applied to large spatial extents. In scenarios where multiple tracer tests are conducted to characterize aquifers, accurate estimation of hydraulic parameters like pore velocity, dispersivity, and Ks requires multiple iterations to align modelled and measured BTCs effectively. This repetitive process can be laborious, time-consuming, and computationally intensive.

Streamlining this process by directly predicting hydraulic properties of solute transport in porous media offers a promising solution to save time and effort. By harnessing advanced computational techniques like neural networks, researchers aim to enhance the efficiency

and accuracy of estimating hydraulic parameters in groundwater models, ultimately reducing the computational burden and simplifying the parameter estimation process.

Chapter 3. Examining the mid to long-term variability in saturated hydraulic conductivity of sandy soils and its influencing factors under constant head test in the laboratory

Saeed Nikghalb Ashouri[1], Adrian Pittari[2], Vicki Moon[2], Ali Shokri[1]

1. School of Engineering, University of Waikato, Hamilton, New Zealand
2. School of Science, University of Waikato, Hamilton, New Zealand

Abstract

Saturated hydraulic conductivity (*Ks*) is a crucial parameter that influences water flow in saturated soils, with applications in various fields such as surface water runoff, soil erosion, drainage, and solute transport. However, accurate determination of *Ks* is challenging due to temporal and spatial uncertainties. This study addresses the knowledge gap regarding the long-term behaviour of *Ks* in sandy soils with less than 10% fine particles. The research investigates the changes in *Ks* over a long period of constant head tests and examines the factors influencing its variation. Two sandy samples were tested using a hydraulic conductivity cell, and the hydraulic head and discharge were recorded for over 50 days. The results show a general decline in *Ks* throughout the test, except for brief periods of increase. At the end of both tests, there are noticeable reductions in the saturated hydraulic conductivities of the samples, with one sample being 96% and the other sample 91% less than the maximum recorded saturated hydraulic conductivity during the tests. Furthermore, the relationship between flow rate and hydraulic head gradient does not follow the expected linear correlation from Darcy's law, highlighting the complex nature of sandy soil saturated hydraulic conductivity. The investigation of soil properties in three different sections of the samples before and after the tests revealed a decrease in the percentage of fine particles and a shift in specific gravity from the bottom to the top of the sample, suggesting particle migration along the flow direction. Factors such as clogging by fine particles and pore pressure variation contribute to the changes in *Ks*. The findings of this research show the importance of considering changes of saturated hydraulic conductivity during constant-head laboratory tests. Therefore, this study

provides evidence for the requirement to further assess the laboratory methods for measurement of the saturated hydraulic conductivity in sandy soil mixtures.

Keywords: Saturated hydraulic conductivity, constant head test, clogging, sandy soil, drainable pores

THE UNIVERSITY OF WAIKATO
Te Whare Wānanga o Waikato

Co-Authorship Form

School of Graduate Research
The University of Waikato
Private Bag 3105
Hamilton 3240, New Zealand
Phone +64 7 838 5096
Email: SGR@waikato.ac.nz
Website: http://www.waikato.ac.nz/students/research-degree

This form is to accompany the submission of any PhD that contains research reported in published or unpublished co-authored work. **Please include one copy of this form for each co-authored work**. Completed forms should be included in your appendices for all the copies of your thesis submitted for examination and library deposit (including digital deposit).

Please indicate the chapter/section/pages of this thesis that are extracted from a co-authored work and give the title and publication details or details of submission of the co-authored work.
Thesis chapter 3: Nikghalb Ashouri. S., Pittari. A., Moon. V., Shokri. A. (Submitted to journal of Water Resources Research). Examining the mid to long-term variability in saturated hydraulic conductivity of sandy soils and its influencing factors under constant head test in the laboratory

Nature of contribution by PhD candidate	Experimental setup- data collection and analysis- writing and editing of the manuscript
Extent of contribution by PhD candidate (%)	90%

CO-AUTHORS

Name	Nature of Contribution
Ali Shokri	Provided supervision and input during experimental setup, study design, data interpretation, and reviewwing the manuscript
Adrian Pittari	Provided consultation and input during data interpretation, and reviewing the manuscript
Vicki Moon	Provided supervision and reviewing the manuscript

Certification by Co-Authors

The undersigned hereby certify that:

- the above statement correctly reflects the nature and extent of the PhD candidate's contribution to this work, and the nature of the contribution of each of the co-authors; and
- that the candidate wrote all or the majority of the text.

Name	Signature	Date
Ali Shokri		21/06/2024
Adrian Pittari	Adrian Pittari	21/06/2024
Vicki Moon	V. Moon	21/06/2024

3.1. Introduction

The saturated hydraulic conductivity (*Ks*) plays a crucial role in determining the water flow rate within the saturated zone of soils. This parameter is essential in various fields of study, including surface water runoff, soil erosion, deep percolation, drainage, crop simulation models, and solute transport (Ben-Hur et al., 2009; Boadu, 2000; Hwang et al., 2017; Suleiman & Ritchie, 2001). Using the Darcy equation, *Ks* can be defined as the ratio of water flow (Q) in the unit section of saturated soil (A) to the hydraulic gradient (i). The parameter *Ks* is present in the majority of equations related to water flow in a saturated medium, yet its determination can be challenging both in the laboratory and the field due to temporal and spatial uncertainties (Suleiman & Ritchie, 2001).

Laboratory determination of *Ks* utilise three standard methods: constant head, falling head, and constant flow rate, as detailed in ASTM D5856-15 (2015). When dealing with granular and disturbed samples containing less than 10% of fine particles passing 75 μm or No. 200 sieve, the recommended approach is the constant head method, as outlined in ASTM D2434-19 (2019). Conversely, samples comprising more than 10% of fine particles can be analysed using any of the three mentioned methods. However, *Ks* measurements are conducted using a rigid-wall, compaction-mold permeameter, with specific criteria provided in ASTM D5856-15 (2015).

Extensive research has been conducted on the long-term variations of saturated hydraulic conductivity in low-permeability soils, which are commonly employed in landfill sites and artificial wetlands. From the perspective of an Earth scientist, these materials might be perceived as loose sediment or deposits rather than the conventional 'soil,' which typically encompasses a mixture of inorganic and organic constituents. In landfills, leachate, and artificial wetlands, contaminated water from roads needs to be contained to gradually remove the pollutants from the water and prevent pollution of underground water resources (Fang et al., 2022; Li et al., 2023; Shaver, 2020; Touze-Foltz et al., 2006; Valencia-González et al., 2022; Wang et al., 2023). Therefore, the application of a layer with very low permeability is necessary to reduce the infiltration of contaminated water into the soil while simultaneously eliminating pollutants. Several studies have shown that the *Ks* in low permeability soil samples change with infiltration of the water that contains chemical or biological agents (Francisca & Glatstein, 2010; Y. Liu & Liu, 2020; Lu et al., 2020; Montoro & Francisca, 2010).

Chemical substances present in the fluid can create a chemical imbalance and interfere with ion exchange processes in the soil, leading to fluctuations in *Ks*. According to a study conducted by Jo et al. (2005), a 3-year test observed a tenfold variation in *Ks* of a clay liner permeated by leachate-containing chemical agents. In their tests, the saturated hydraulic conductivity of one of the samples reached stability after about 1.5 years of the test. On the other hand, the formation of microorganisms and the presence of nutrients to feed them can cause clogging in the soil and, hence, a reduction in the drainable pores and *Ks* (Fang et al., 2022; VanGulck & Rowe, 2004).

In sandy soils, the duration of the test is usually relatively short. It is commonly assumed that the test can be concluded when four samples yield values within ±25% of the mean calculated from these four samples throughout the test (ASTM D5856-15, 2015). Also, there is no reference to the length of the test in ASTM D2434-19 (2019). However, several studies suggest that the saturated hydraulic conductivity of sandy soils can change over time. For example, there has been extensive research on the variation of saturated hydraulic conductivity in groundwater artificial recharge (Konikow et al., 2001b; Mays & Hunt, 2005; Siriwardene et al., 2007; Song et al., 2020; Ye et al., 2019). Vanderzalm et al. (2020) and Du et al. (2018) subjected sandy samples to water permeation containing suspended solids and *Fe (III)* ions, respectively, for an extended period (40 days in the former case and seven days in the latter study), leading to observed fluctuations in *Ks* that demonstrate a prevalent declining pattern over time. These studies identified physical and biological clogging mechanisms as dominant factors for *Ks* variation. However, neither of the above studies has tested a sample permeated with distilled water or tap water with minimum suspended solids or chemicals to ensure that *Ks* remains constant under minimum influent contamination. Du et al. (2013) and Wang et al. (2012) used tap water with and without suspended solids in a constant head test on quartz sand samples and observed a noticeable drop in *Ks* over four days. Siriwardene et al. (2007) also reported a reduction in the *Ks* when the sample was permeated with tap water containing suspended solids. They noticed clogging of the suspended solids in the lower section of the sample as the main reason for the noticeable drop in the *Ks*, whereas Wang et al. (2012) showed that finer suspended solids could travel deeper in the sample and cause blockage of the drainable pores.

Clogging can also be caused by the internal mobilisation or swelling of fine particles in the soil (Jeong et al., 2018b; Konikow et al., 2001b; Mohan et al., 1993; Torkzaban et al., 2015b) . Additionally, clay minerals like *Illite*, *Kaolinite*, and *Montmorillonite* can be transported

with water, leading to the blockage of drainable pores in the sample and a reduction in *Ks* (Cihan et al., 2022; Jeong et al., 2018; Wang et al., 2021). The migration of fine particles in soil is a phenomenon that occurs due to various factors such as seepage forces, hydraulic gradients, and soil deformation. Fine particle migration can lead to geotechnical damage, failures of earth dams and soil slopes, and changes in the properties of the soil. It has been observed that seepage forces induce the migration of fine soil particles along the water flow direction, causing redistribution and reconsolidation of sand particles (Wang et al., 2022). Dikinya et al. (2006) observed a substantial decrease in hydraulic conductivity due to structural breakdown and pore clogging caused by dispersion and re-deposition of fine particles.

In a research on the transportation of fine particles in petroleum and groundwater reservoirs, Tangparitkul et al. (2020) performed an analytical study on the mobilization of the fine particles and concluded that size distribution of the fine particles and velocity of the permeant fluid dominate the mobilization of the particles. Wang et al. (2022) studied the impact of the hydraulic gradient on seepage failure in sandy samples in a set of 15 minutes constant head tests and resulted that the distribution of particles in the samples change due to water flow, leading to transportation of fine particles to the top, and coarse particles to the bottom.

Stormwater management devices like artificial soakage basins and soak pits are commonly recommended in new urban developments with high infiltration rates (Shaver, 2020). Furthermore, with the widespread use of artificial groundwater recharge, the long-term behaviour of *Ks* in sandy materials gains significant importance. Variations in *Ks* and pore blockages can profoundly influence the effectiveness of design strategies employed in stormwater management and groundwater recharge scenarios.

Currently, there is a lack of research focusing on the extended-duration variations in *Ks* within sandy soils due to fluctuating hydraulic levels. Observing *Ks* over the long term provides insights into the sustained groundwater movement within the aquifer, with changes in hydraulic levels indicating shifts in aquifer water levels during and after rainfall events. This study aims to bridge the knowledge gap regarding the prolonged behaviour of saturated hydraulic conductivity in sandy soils. Although various research has explored short-term *Ks* variations, particularly in the context of stormwater management devices, a comprehensive understanding of how *Ks* evolves over extended timeframes remains limited. Grasping the mid to long-term behaviour of *Ks* holds critical significance in

modelling water flow and solute transport in the soil. Increasing the accuracy of estimates of the *Ks* provides better design of soakage systems and safeguarding subsurface water resources. Thus, this paper illuminates the key factors shaping *Ks* variations over prolonged periods.

3.2. Materials

3.2.1. Sample source and physical properties

The soil examined in this study is river sand, commercially referred to as pit sand, often employed for embankments and raised areas like pathways. A batch of pit sand was purchased from a supplier in Hamilton, New Zealand, that provides different types of aggregates for garden and home purposes. According to the statement of the supplier, they acquire the pit sands from sand quarries situated in Ngahinapouri and Te Kowhai, located along the Waipa River in Waikato, New Zealand, as depicted in Figure 3.2.1. A bag of 10 kilograms of pit sand was purchased and brought to the laboratory, and the samples were prepared according to the procedure explained in the following section. For this study, two samples (sample *A* and sample *B*) were taken from the same batch of pit sand provided by a supplier.

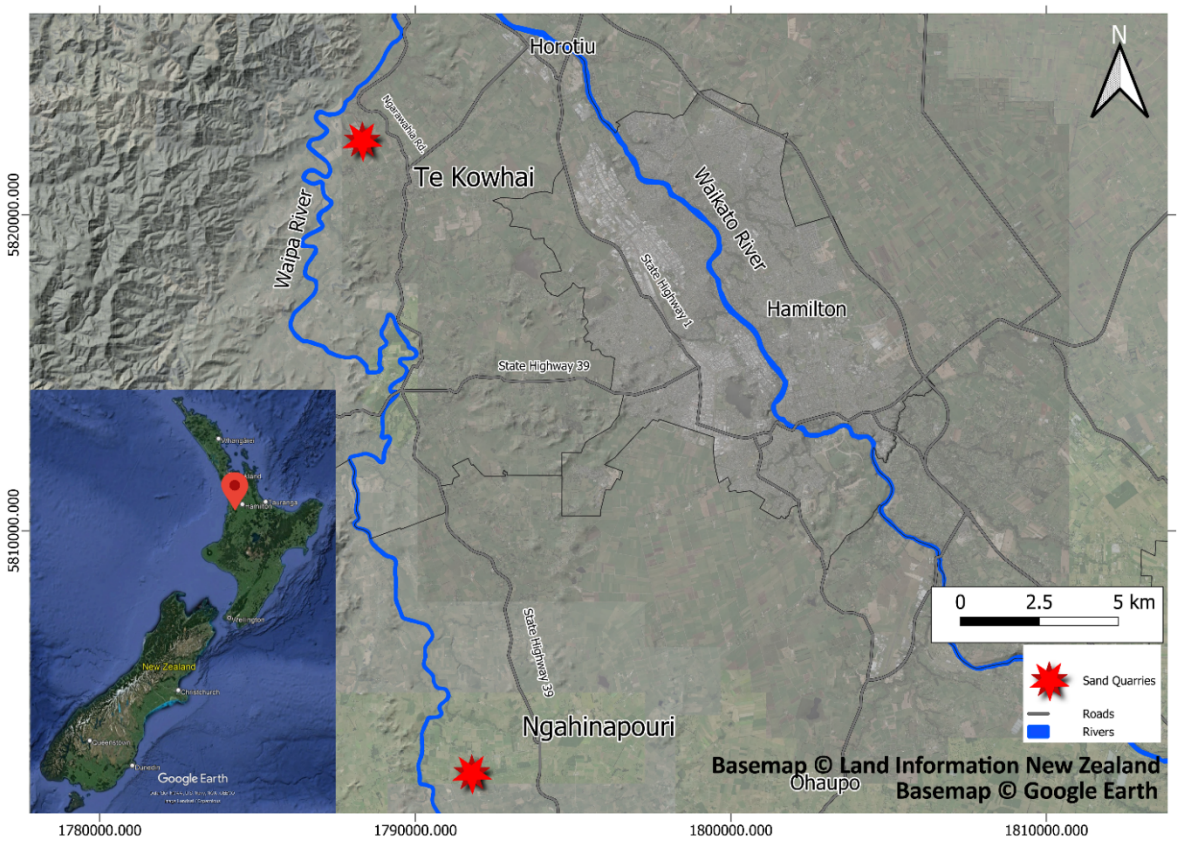

Figure 3.2.1. The geographical location of the Waipa River in New Zealand, with the samples originating from sand quarries located near the Waipa riverbanks. The locations of the sand quarries are approximate

Table 3.2.1 outlines the physical properties of the samples. Upon microscopic examination and particle separation, five distinct groups are discerned (Figure 3.2.2): quartz and feldspar (approximately 60%), pumice (approximately 11%), rock fragments and ferromagnesian minerals (approximately 6%), magnetic minerals (approximately 10%), and glass shards (approximately 13%). The magnetic minerals were isolated through magnetic separation. X-ray diffraction (XRD) analysis was employed to assess mineral composition, while the loss on ignition (LOI) method was utilised to estimate the presence of organic material in the samples. The analysis of XRD data peak patterns confirms that quartz and feldspar constitute the majority of minerals in the sample (Figure 3.2.3). The observed low dry bulk density can be attributed to the presence of pumice within the samples (Table 3.2.1). As per the Digital Soil Map (SMAP) database, the dry bulk density of deposits along the banks of the Waipa River typically spans from 0.8 to 1.3 g/cm^3 (Landcare Research, 2023). The dry bulk density values of the analysed samples align within the aforementioned range. Given that the samples are derived from the same batch,

it is assumed that both samples A and B exhibit comparable specific gravity (Gs). The Gs (which is density of grains proportional to the density of water) was determined as the average value derived from 5 measurements conducted using a gas pycnometer.

A laser diffractometer (Malvern Mastersizer 3000, Malvern Instruments Ltd., UK) was used to determine the particle size distribution of the samples. For this study, the particles below 75 μm were considered as fines, which aligns with the classification of ASTM for fine and coarse particles (ASTM D2487, 2020). The particle size distribution results indicate that the samples are primarily sandy, with less than 10% of fine materials. Particles below 5 μm were considered mobile colloidal particles (Kretzschmar et al., 1999), and the percentages of these particles are also mentioned in Table 3.2.1. Based on Standard Proctor tests (ASTM, 2012), the optimal compaction moisture of the samples was determined to be 12% by mass.

Table 3.2.1. Properties of tested samples

Parameter	Sample A	Sample B
Specific gravity of grains (-)	2.6739	-
Specific surface (m^2/kg)	84.60	102.90
Particles < 5 µm (%)	2.3	2.6
Particles 5-75 µm (%)	5.06	5.83
Particles > 75 µm (%)	92.61	91.56
Dry bulk density (g/cm^3)	1.289	1.261
Optimal gravimetric compaction moisture (%)	12	12
Sample gravimetric moisture (%)*	8.1	11.8
Organic matter (%)	1.7	1.7

* Sample gravimetric moisture was measured when the sample was compacted in the mould. A small amount of sample A and B was taken and dried in the oven, and moisture was measured.

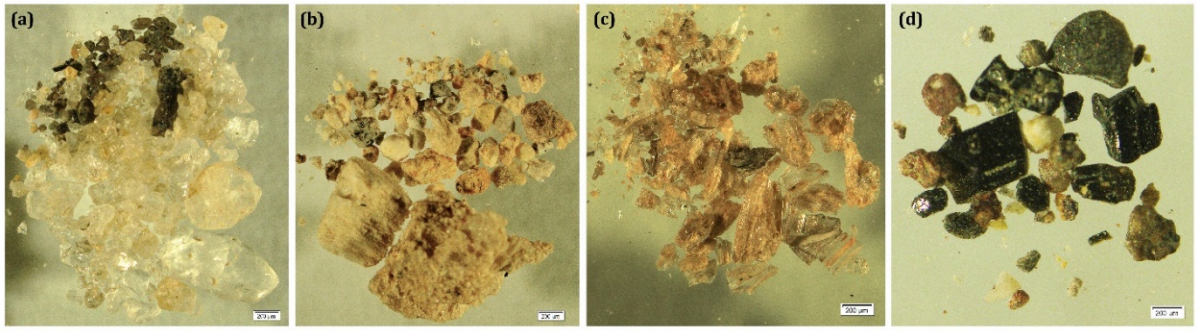

Figure 3.2.2. Separation of particles under microscope: (a) Quartz and feldspar, (b) Pumice, (c), glass shards, and (d) rock fragments and ferromagnesian minerals, and magnetic minerals - The magnetic minerals were separated by magnet, but there is not a separate picture of them

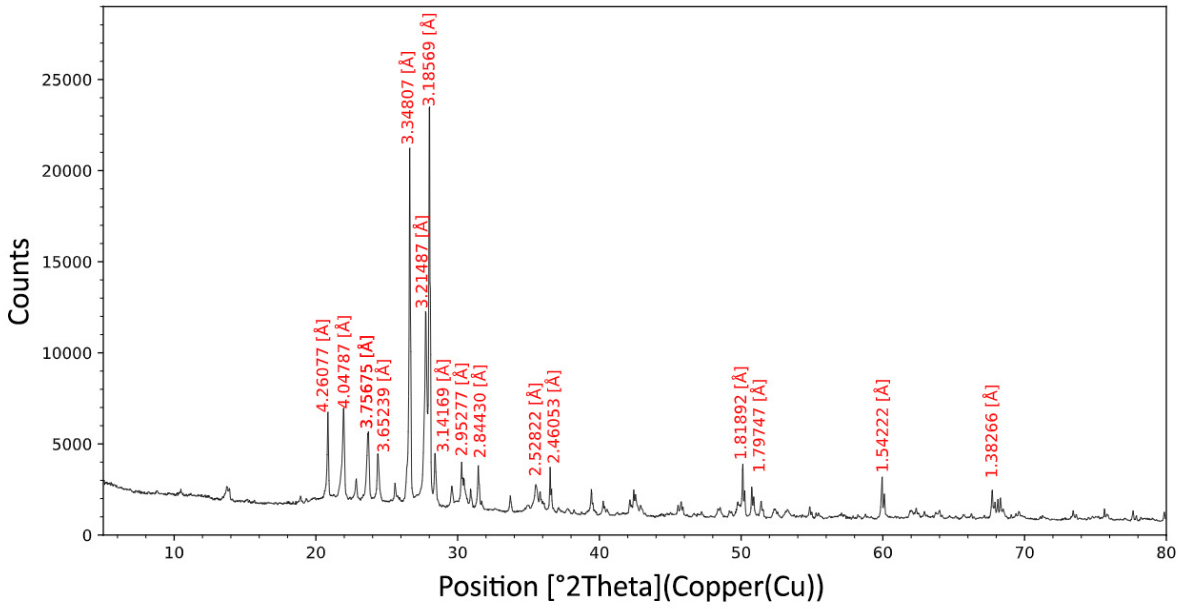

Figure 3.2.3. XRD analysis of the sample: Major peaks are related to the quartz and feldspar content in the sample

3.3. Methods

3.3.1. Sample preparation

Prior to conducting the tests, the samples underwent a preparation process that involved drying in an oven at 105℃ for 24 hours and passing through a 2 *mm* sieve. The moist tamping method was used to prepare the samples, which is based on a technique described

by Ladd (1978). This method allows for achieving a uniform distribution of density in the sample. A specific amount of soil was weighed, and distilled water was sprayed onto the samples to attain an initial moisture content of 8.1% (Sample A) and 11.8% (Sample B). The choice of 8.1% moisture for sample A was intended to explore the influence of initial compaction moisture on the extended-term variations of *Ks*. The samples were then covered and left for approximately 24 hours to achieve moisture balance before testing. The samples were compacted in a constant head test cell with an interior diameter and height of 76.2 *mm* and 292 *mm*, respectively. Compaction was carried out in layers of 12 *mm*. Before the compaction, subsamples were taken to measure the actual moisture, particle size distribution, and XRD. The final dry density of the samples was calculated from the net dry soil used and compacted sample volume, and is listed in Table 3.2.1.

To achieve saturation, the samples were first connected to a vacuum pump for one hour. Distilled and de-aired water was then introduced into the test cell in an upward direction, following the procedure outlined in ASTM D2434-19 (ASTM, 2019), to minimise air entrapment. The samples were left saturated overnight to reduce the chances of air entrapment further.

3.3.2. Constant head saturated hydraulic conductivity tests

The schematic experimental apparatus used for the constant head saturated hydraulic conductivity test is shown in Figure 3.3.1. The adjustable water head tank enabled the alteration of the hydraulic head during the experiment without the need to terminate the test. In addition, there were porous disks with a 1 *mm* mesh size and a spring on top to hold the sample stable in the cell. The mesh size of the porous disk was selected in a way to prevent the formation of clogging and pressure drops on the disk.

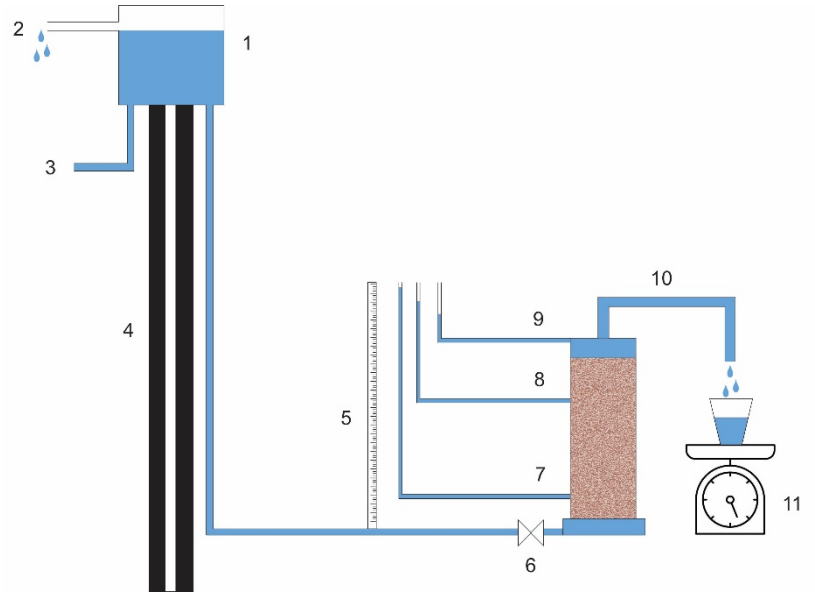

Figure 3.3.1. Schematic constant head saturated hydraulic conductivity apparatus-(1) Water tank, (2) overflow outlet, (3) water supply hose, (4) adjustable level board, (5) ruler, (6) water entrance valve, (7) piezometer 1, (8) piezometer 2, (9) piezometer 3, (10) water outlet, (11) scale for measuring the discharge

The water flow and head gradient were measured at least thrice daily. The collection of effluent in a bucket was carried out for each flow measurement, and the duration of the effluent collection was recorded. Subsequently, the discharge was calculated by dividing the weight of the collected effluent by the collection duration.

Formation of air bubbles during the test can change *Ks*. However, because the *Ks* of the sandy soils is relatively high compared to the silty and clayey soils, it was not possible to provide de-aired water for the whole period of the tests. In order to minimise the air entrapment during the test, permeation was from bottom to the top so that the air bubbles can escape. The samples were also regularly checked during the test for formation of any air bubbles in the transparent cell.

The tests were conducted in a back-and-forth pattern with water heads ranging from 963 *mm* to 1765 *mm*, with increments and decrements of approximately 200 *mm*. The hydraulic head began at a minimum of 963 *mm* and was incrementally increased by around 200 *mm* until it reached a maximum of 1765 *mm*. Subsequently, the head followed the same pattern of decrease in sequential steps. The testing period has lasted for approximately 53 days. Detailed information on the test phases, hydraulic heads, and durations can be found in Table 3.3.1. The tests were conducted in a laboratory with

controlled temperature. Throughout the tests, the temperature variations were below 4°C. Consequently, the potential impact of temperature changes on *Ks* can be deemed negligible.

The hydraulic heads applied in this research are not representative of the place where the samples are originated. Since the pit sand is used in disturbed form for construction work as filter material to facilitate infiltration of water, it will be under different head gradients depending on the storm events and subsurface water levels. Therefore, the hydraulic gradients were selected to cover a wide range.

Table 3.3.1. Hydraulic Head and Durations of Constant Head Tests on Samples A and B

Test Phase	**1**	**2**	**3**	**4**	**5**	**6**	**7**	**8**	**9**	**10**
Hydraulic head (mm)	963	1163	1365	1558	1765	1558	1365	1163	963	Varies
Sample A Duration (days)	5	6	6	6	5	3	7	6	7	1
Sample B Duration (days)	5	5	5	5	5	5	5	5	31	N/A

During the testing process, the pressure and discharge readings were recorded simultaneously by three piezometers. As depicted in Figure 3.3.1, the pressure inside the sample was measured by two piezometers located at points 7 and 8, while the piezometer at point 9 measured the water head at the discharge point on the opposite end of the cell.

In order to minimise the systematic error which results from measurement devices, including measurement of discharge by weight, and reading of the water heads in the piezometers, each reading set of discharge and head was done twice, and the mean value was used for calculating the *Ks*. If the difference between two reads was more than 1%, then the discharge and heads were measured for the third time. And the final *Ks* in each read would be the mean of the two closest measurements.

To minimise the accidental changes in the *Ks*, the constant head hydraulic conductivity system was set up in a laboratory with limited access, with warning signs so that unauthorised individuals do not touch the cell accidentally.

After completing phase 9 on sample *A*, the water flow was not stopped, and a moderately rapid constant head test was conducted using the same hydraulic heads as phases 1 to 9. This phase, designated as "Phase 10", and as mentioned, continued from end of phase 9, lasted approximately 16 hours, with each constant head being run for about 2 hours. The purpose of Phase 10 was to observe any changes in *Ks* under a shorter duration and to determine if the *Ks* during the head-increasing stage were similar to the reciprocal *Ks* during the head-decreasing stage.

In the case of sample *B*, Phase 9 was allowed to run for 31 days at the minimum head (963 *mm*) after an increasing trend in the *Ks* of the sample was observed from day 53 onwards. The purpose was to determine how long the *Ks* would continue to change and whether it would return to a value similar to the beginning of the test.

The *Ks* was calculated using Darcy's law (Wang et al., 2020) as follows (Eq. 1):

$$K_s = \frac{Q}{i \,.\, A} \tag{1}$$

where *Ks* is the saturated hydraulic conductivity of the sample (m/s), *Q* is the rate of flow in the sample (m^3/s), *i* is the hydraulic gradient (m/m), and *A* is the cross-sectional area of the sample (m^2).

3.3.3. Post-processing of the samples

In order to examine changes in soil properties before and after the tests, the samples were recovered from the saturated hydraulic conductivity cell. After extraction, the samples were divided into three sections: bottom, middle, and top. Sub-samples were extracted from these sections to perform further analysis. In order to ensure the sub-samples are representative of the sections that they belong to, minimum of five sub-samples at each section were utilized for particle size distribution (PSD) and specific gravity (Gs) measurements.

The sub-samples were dried in the oven for 24 hours. Measurements of Gs were carried out by a gas pycnometer (Ultra Pycnometer 1000- Anton Paar QuantaTec Inc., USA). Five samples from each section were separated to measure the Gs and each measurement was

repeated 4 times in the pycnometer. Therefore, 20 measurements for each section were recorded. In order to measure the particle size distribution, a laser diffractometer was used (Malvern Mastersizer 3000, Malvern Instruments Ltd., UK) and 5 measurements were recorded for each section.

Fine particles can mobilize with water flow and leave the system. In order to measure the fine particles leaving the system, two approaches were considered: Particle size analysis before and after the tests; measurement of the weight of the saturated cells before and after the tests. There could be another approach that includes installing a very fine mesh in the outlet pipe. However, there was the risk of blockage in the outlet pipe, and as a result, the whole test could have failed. Therefore, the latter approach was not applied.

3.4. Results

3.4.1. Mid to long-term *Ks* Test

The mid to long-term change in *Ks* calculated for both samples is illustrated in Figure 3.4.1. The *Ks* values of the samples showed a general decline throughout the test, as shown in Figure 3.4.1, except for three brief periods. These periods occurred between days 36 to 38 for sample *A* and between days 0 to 1 and 37 to 40 for sample *B*.

Furthermore, there are two distinct periods of a noticeable increase in *Ks* in both samples, which coincide closely in timing, specifically between days 35 and 40. In sample *A*, the increase in *Ks* starts at 1365 *mm* head and ends at the same head in Figure 3.4.1a. However, in sample *B*, *Ks* starts increasing at 1163 *mm* head and starts decreasing again at 963 *mm* head in Figure 3.4.1b. At the end of the tests on sample A, the final Ks value reaches to 0.5×10^{-4} m/s approximately that is 96% less than the maximum value (12.3×10^{-4} m/s). In sample B, the final Ks is 1×10^{-4} m/s approximately that is 91% less than the maximum value (12.2×10^{-4} m/s). Figure 3.4.1 illustrates that sample *A*, with initial moisture of 8.1%, achieved its maximum *Ks* within the first few hours of commencing the test. In contrast, sample *B*, with the initial moisture of 11.8%, took approximately two days to reach its peak *Ks*. From the peak point onwards, the *Ks* followed a reducing trend.

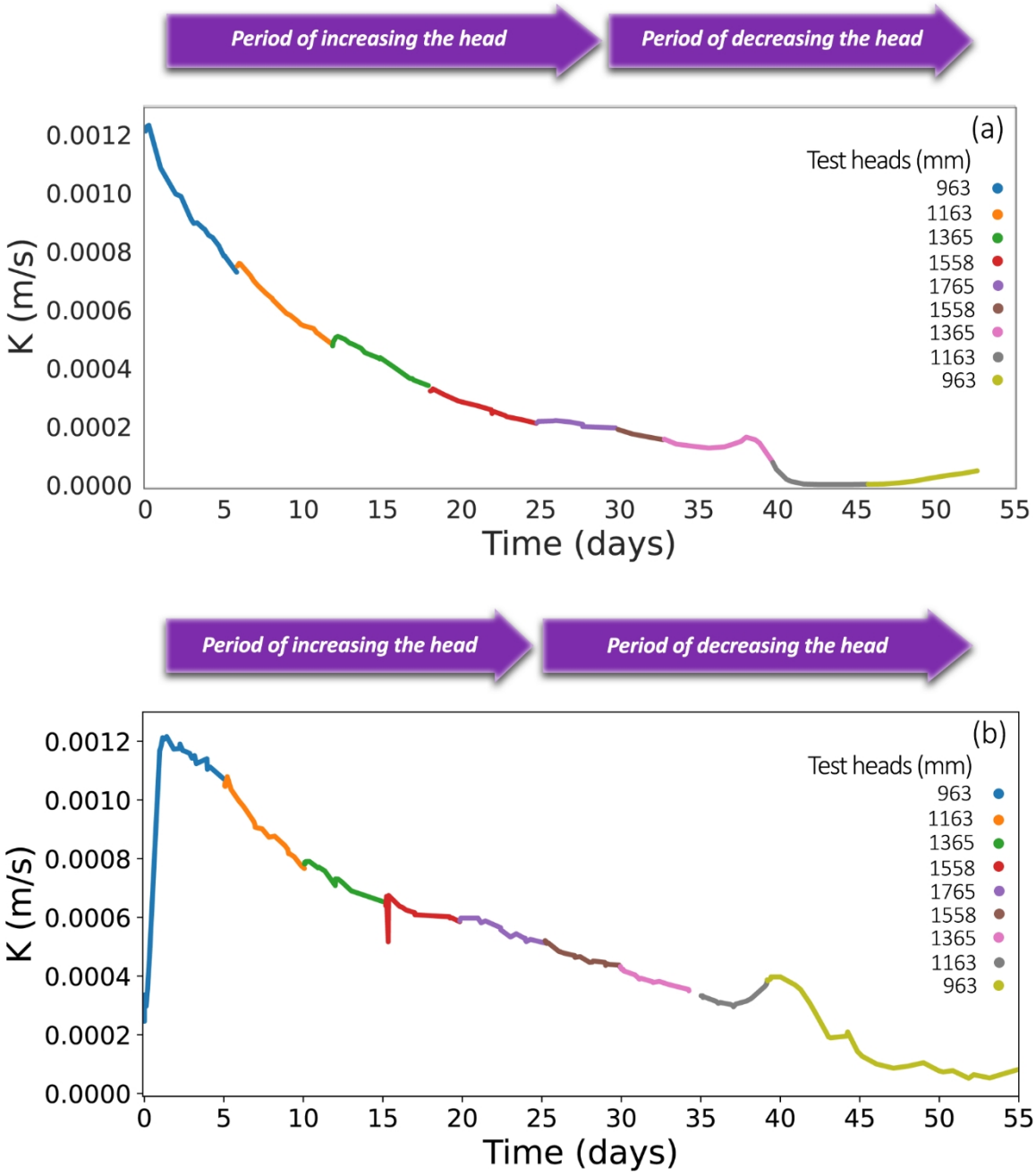

Figure 3.4.1. Changes of Ks over time for samples A (a) & B (b)- the generally reducing trend in Ks is noticeable in both samples

3.4.2. Flow-head gradient relationship

In the hypothetical scenario, where the samples remained unchanged throughout the tests, Darcy's law would anticipate the clustering of all data points at each hydraulic head increment around a single point, forming a unified line. Figure 3.4.2 illustrates the

relationship between flow rate (Q) and hydraulic head gradient (i) within samples A and B across varying hydraulic head levels. The symbol "R" signifies the period characterised by a decreasing head. The scatterplots demonstrate the absence of a straightforward linear correlation between Q and i.

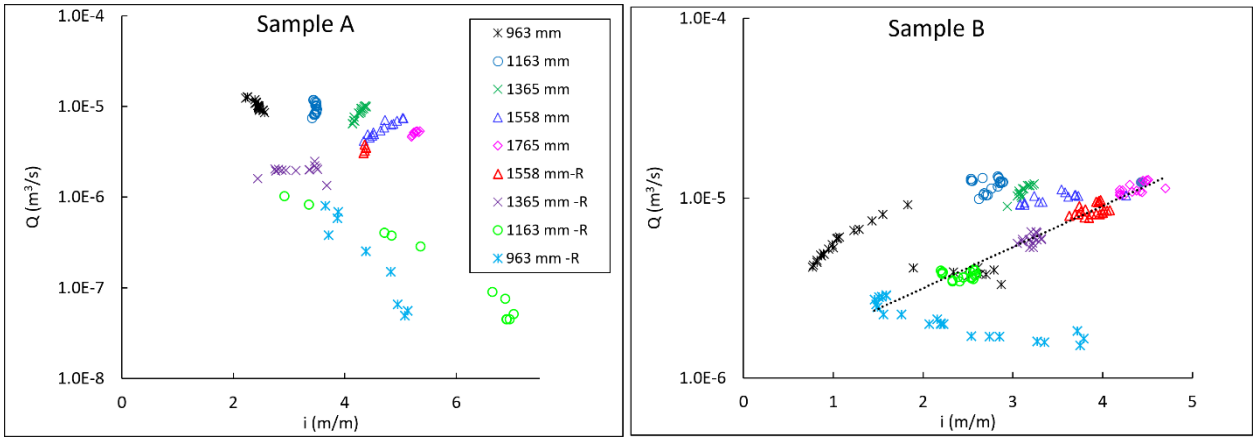

Figure 3.4.1. Scatterplots exploring the correlation between head gradient (i) and flow rate (Q) in samples A and B with different hydraulic head levels. The symbol "R" signifies the period characterised by a decreasing hydraulic head. Y axis is in logarithmic scale. A hypothetical line is added to the graph of sample B to show the linearity

In the case of sample A, during test phases 1 to 4, wherein the head is incrementally raised every 5 or 6 days from 963 to 1765 mm, a decrease in flow accompanied by an increase in head gradient becomes evident. Interestingly, even within each step, the scatterplot does not exhibit the expected convergence around a single point, as outlined by Darcy's law. This suggests a dynamic nature of the sample during this period, with the saturated hydraulic conductivity undergoing continuous changes. However, phase 5, characterised by the maximum head of 1765 mm and a 5-day observation period, showcases a remarkable consistency in both head gradient and flow rate, implying a phase of stability.

Furthermore, as the head is reduced to 1558 mm, this stability persists, with the scatterplot points clustering around a single location and both flow rate and head gradient diminishing. On the contrary, during phases 7 to 9, where the head drops from 1365 to 963 mm, the scatterplot points display unpredictable distribution, deviating significantly from the expectations of Darcy's law. This observation indicates a departure from the anticipated behaviour of the sample.

In sample B, the initial phase with a head of 963 mm shows an unexpected trend where both the head gradient and flow rate increase, deviating from the expected convergence

around a single point. As we move through phases 2 to 4, involving a hydraulic head increase from 1163 to 1558 mm, a distinct behaviour emerges: despite the elevated hydraulic head, the head gradient rises while the flow rate unexpectedly drops. This pattern suggests a shift in the hydraulic properties of the samples.

Nevertheless, when the hydraulic head is raised to 1765 mm and subsequently reduced to 1163 mm over four 5-day intervals, the sample aligns somewhat better with the predictions of Darcy's law. Data points cluster more closely around a central location, and the flow rate responds to changes in the hydraulic head. However, variations still exist at each step. In contrast, at the lowest head level of 963 mm, there's an increase in head gradient while the flow rate remains stable.

3.4.3. Sample A behaviour in a relatively short-duration test

Interestingly, this relatively quick test (Phase 10) demonstrated a strong linear correlation between the water flux and the gradient within the sample, as expected by the Darcy law. The saturated hydraulic conductivity was determined to be 1.53×10^{-4} m/s during the increasing stage of the test head and 1.75×10^{-4} m/s during the decreasing stage. The correlation between *Q* and *i* is illustrated in Figure 3.4.3. Contrary to Figure 3.4.2, a notably stronger correlation between *Q* and *i* can be observed.

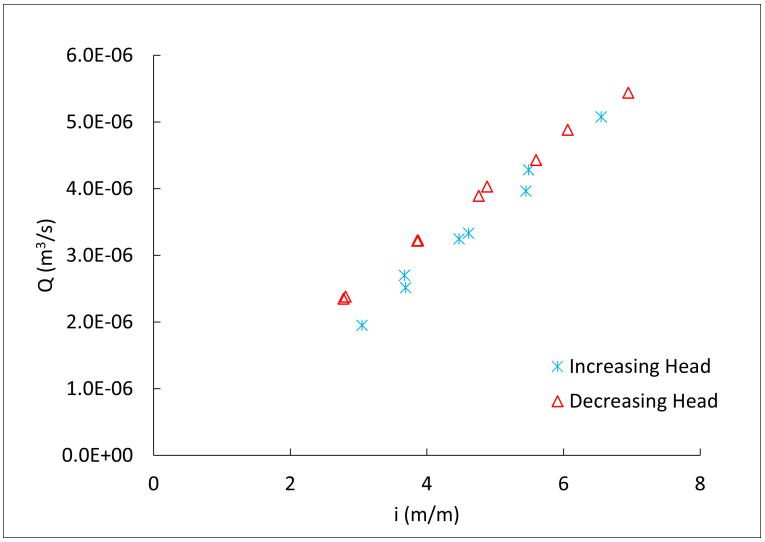

Figure 3.4.1. The relationship between Q and i in phase 10 for sample A, where the gradients are varied. The blue and orange arrows represent the periods of increasing and decreasing test heads, respectively.

3.4.4. Extending sample B in the minimum constant head for 31 days

Test B has been extended for an additional 31-day period under the minimum head condition (963 mm). This extension aims to investigate whether saturated hydraulic conductivity comes into stability without any disruptions.

Figure 3.4.4.(a) depicts the correlation between flow rate and head gradient during extended Phase 9 period. The *Q-i* correlation exhibits unpredictable fluctuations in both hydraulic gradient and flow rate, mirroring the patterns observed in the preceding 45 days, as shown in Figure 3.4.2.

The temporal evolution of *Ks* is visually outlined in Figure 3.4.4(b). The variability of *Ks* spans from 1.25×10^{-4} m/s to 0.5×10^{-4} m/s, centring around a median value of 1.0×10^{-4} m/s. In summary, the continuation of the testing procedure with a consistent hydraulic head maintained over the course of 31 days does not result in the stabilisation of the saturated hydraulic conductivity of the sample. The *Ks* values persistently oscillate within a range of +33% and -46% around the median value, thereby underscoring the absence of stability in the system. However, a decreasing trend is absent in contrast to previous observation periods.

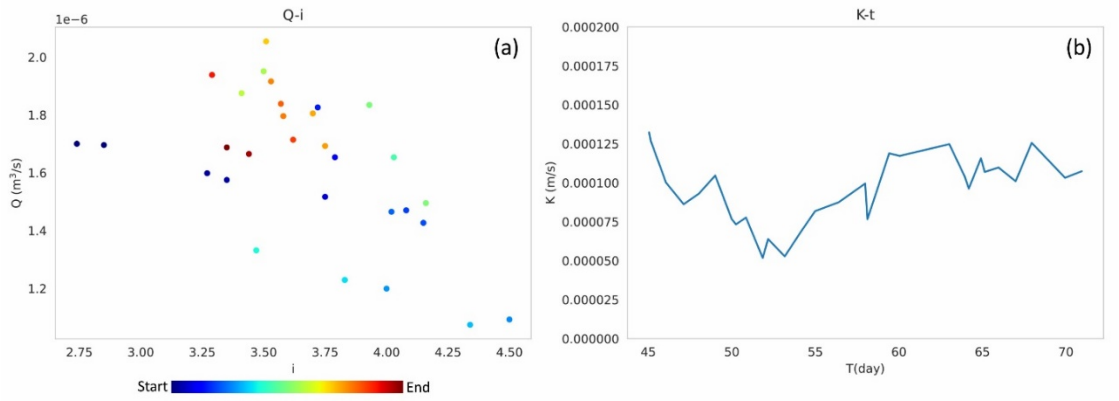

Figure 3.4.1. (a) The relationship between Q and i for sample B during an extended period (31 days) of running phase 9 at the minimum hydraulic head. The colour spectrum and arrows depict the temporal sequence of the measurements. (b) The changes in Ks over time for sample B during the same 31-day duration of phase 9 at the minimum hydraulic head.

3.4.5. Comparison of soil properties before and after the tests

Figure 3.4.5 shows the *PSD* of the sample's top, middle, and bottom sections and the original sample prior to the test. Additionally, Table 3.4.1 compares the total particles below and above 75 μm for reference. The results in Table 3.4.1 indicate that the sample's total percentage of fine particles decreased after the tests. Approximately 2% of fine particles in sample *A* and 1% in sample *B* were washed away during the long-term tests which is negligible. Measurements of saturated weight of the cells before and after the tests aligns with the particle size distribution data and confirms the latter. Because the rate of outflow was high during the tests, it was impossible to observe the fine particles leaving the sample or track the changes in the water colour. It is noteworthy that samples *A* and *B* contained less than 9% of fine particles (below 75 μm).

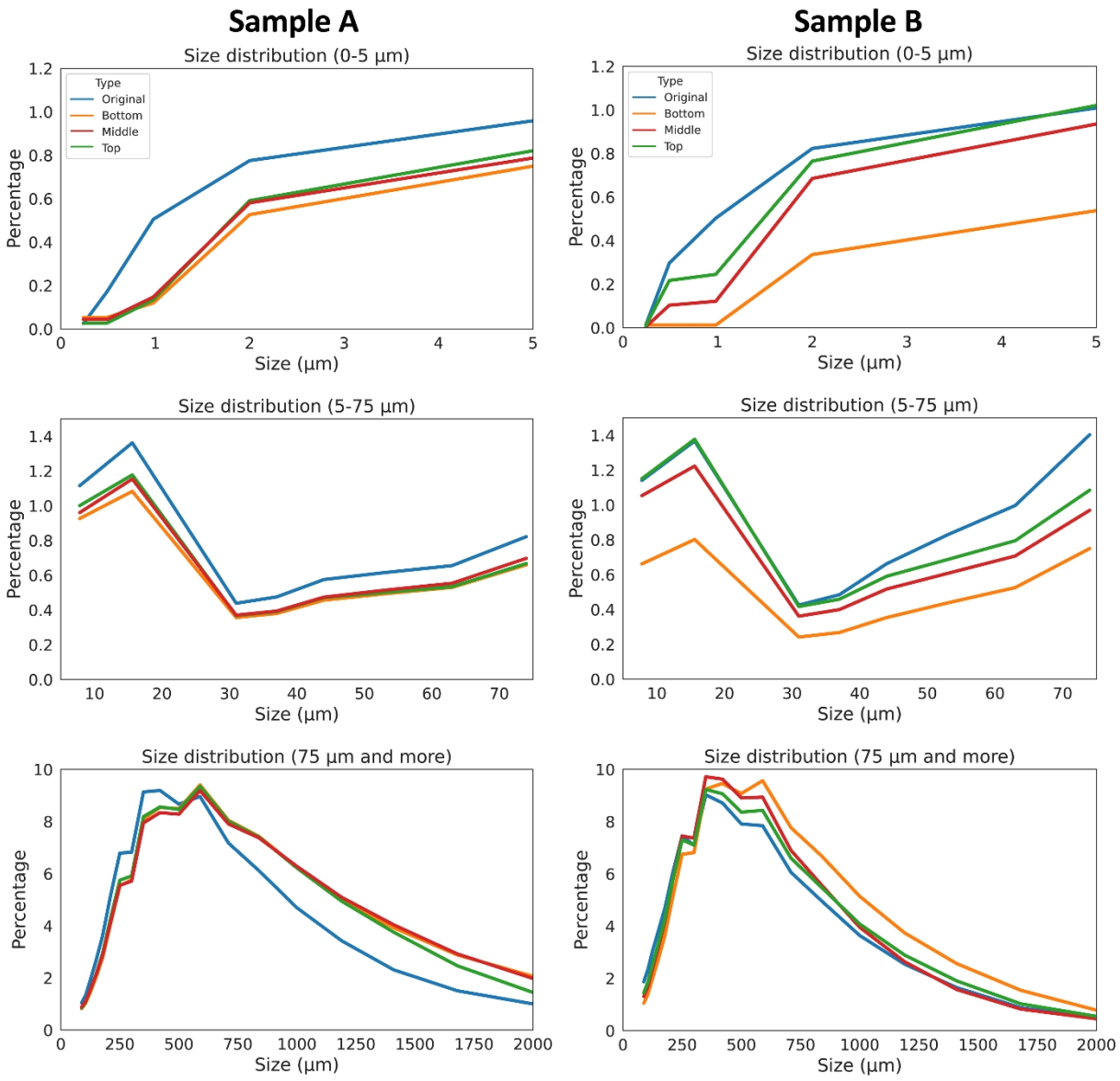

Figure 3.4.1. Particle size analysis of the samples (comparison of the samples before tests and after tests, divided by sub-samples of different sections)

Table 3.4.1. Comparison of total percentage of particles below and above 75 µm before and after tests divided by different sections in the sample

		Sample A					Sample B		
Totals (%)	Original	Bottom	Middle	Top		Original	Bottom	Middle	Top
Below 75 µm	7.37	5.09	5.41	5.74		8.42	4.06	6.68	7.63
Above 75 µm	92.61	94.91	94.59	94.26		91.58	95.94	93.32	92.37

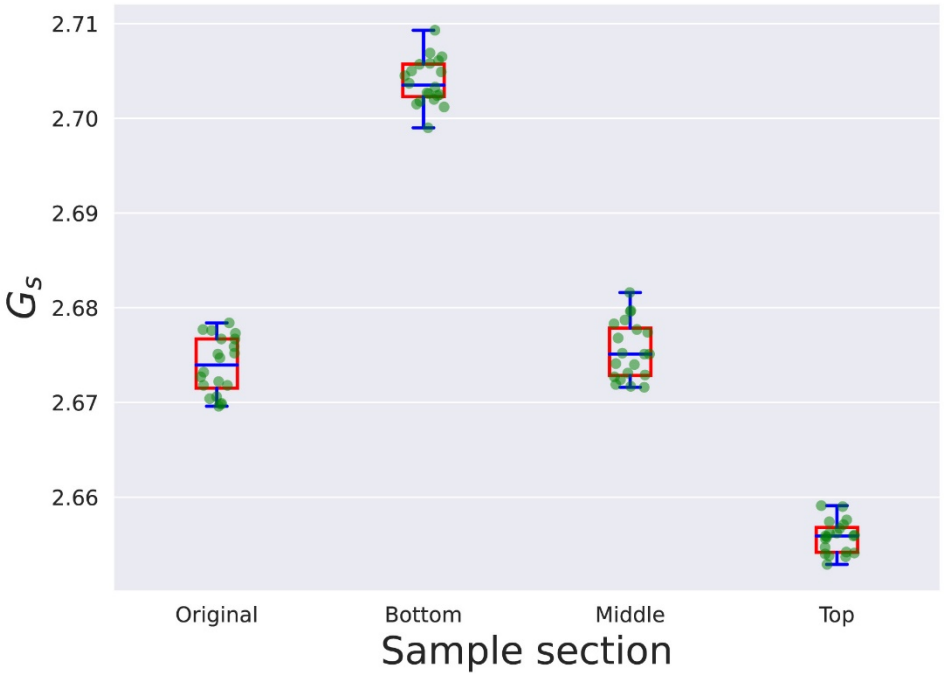

Figure 3.4.2. Gs (density of grains to the density of water) of sample A before and after test divided by sub-samples of different sections

Figure 3.4.5 and Table 3.4.1 show that the percentage of fine particles below 75 µm is highest at the top section of the samples, followed by the middle and bottom sections. The percentages of fine particles after finishing the tests for sample A is 5.09%, 5.41%, and 5.74% from bottom to top respectively. The percentages of fine particles for sample B are 4.06%, 6.68%, and 7.63% from bottom to top, respectively. While the difference in the percentage of fine particles among different sections is minor for sample A (less than 1%), it is higher for sample B (around 3%).

Gs measurements are presented as a box plot in Figure 3.4.6. The box plots illustrate notable changes in the specific gravity of the sample in comparison to the original sample. The lowest *Gs* is found at the top section of sample A with the mean value of 2.65, followed by 2.67 in the middle section, and 2.70 at the bottom. As can be seen from Figure 3.4.6, the *Gs* of middle section of the sample is close to the *Gs* before the tests being around 2.67. In conclusion, the highest *Gs* is observed at the bottom section, with a slight increase in the middle section, and the lowest at the top, compared to the *Gs* of the sample before the test.

3.5. Discussion

Examining soil properties in the original sample before and after the constant head test reveals notable alterations in the soil characteristics. These changes directly impact the saturated hydraulic conductivity, highlighting the direct influence of the test on soil properties and subsequent hydraulic behaviour. For example, Figure 3.4.1(a & b) demonstrates a prevailing long-term decreasing trend in *Ks*. However, it is important to note that there are also intermittent shorter periods where *Ks* shows an increase. This observation highlights the dynamic nature of the system, wherein both long-term trends and shorter-term fluctuations in saturated hydraulic conductivity are evident.

There is a period of noticeable short increase in the *Ks* of both samples between days 35 and 40 (Figure 3.4.1). A similar temporary increase in the *Ks* was recorded by Vandevivere & Baveye (1992) and Du et al. (2018) during permeation of a sandy sample with an influent containing bacterial and chemical agents. However, they did not note the increase in their discussion. Subtle changes in the test set up can cause disturbance in the test and change *Ks*. In this research test set up was not changed during permeation. Additionally, the sudden increase of *Ks* occurs in both samples. The movement and accumulation of fine particles can block the drainable pores, and consequently, the blockage increases the pressure in the blocked zone. Then the pressure builds up and it reaches to a critical point that unblocks the pore and the fine particles move to another zone in the sample, and hence, *Ks* increases. Then the particles rearrange, and *Ks* keeps reducing. This effect might repeat if the test keeps running for a longer period.

The *Ks* tests on the coarse particles (sandy samples with less than 10% fines) are generally short because the variation of *Ks* is very marginal during the first few hours of the tests. For example, in sample *A*, the change of *Ks* during the first 5 hours from starting the test

was only 2%, which is negligible. However, after five days, the *Ks* dropped by 40%, and at the end of the test, the *Ks* dropped by around 96% from the beginning of the test.

The initial compaction moisture levels (8.1% for sample A and 11.8% for sample B) appear to have had limited influence on the extended-term variation of *Ks*. However, they might have played a role in the initial stages of permeation. As it can be seen from Figure 3.4.1, there is a relatively rapid period of spike in the *Ks* in sample B, which does not appear for sample A. There are marginal differences between sample A and B, including the PSD and dry bulk density. But the major difference is the initial compaction moisture, and the mentioned spike in sample B is related to the initial compaction moisture.

Also, throughout the head increase cycle, a notable pattern emerges: at the onset of each hydraulic head increment, there is a marginal uptick in *Ks*, which is subsequently followed by a sustained decrease. This minor elevation in *Ks* can be attributed to the abrupt rise in the hydraulic head.

Figure 3.4.2 clearly represents the dynamic nature of the samples' hydraulic gradient and pore pressure. These parameters undergo continuous fluctuations without exhibiting a consistent decreasing or increasing pattern. Even extending the test for a longer period (Figure 3.4.4 (a) and (b)) does not create a stable gradient in the sample. Therefore, it can be inferred that the connectivity of the drainable pores is constantly changing. This observation underscores the complex behaviour of the hydraulic system within the samples, emphasising the need to consider the temporal variations in pore pressure when analysing the overall hydraulic response. Nevertheless, in Figure 3.4.3 (Phase 10), representing a relatively quick test, the sample exhibits predominantly linear behaviour. This underscores the limitations of quick tests in accurately assessing the *Ks*. It is essential to acknowledge, however, that Phase 10 commenced after Phase 9, during which all finer particles in preceding phases have undergone rearrangement.

The variations in the hydraulic gradient and discharge relation, and hence saturated hydraulic conductivity in the samples, can be attributed to several factors. According to the ASTM standard (ASTM D5856-15, 2015), air entrapment can potentially reduce saturated hydraulic conductivity. In this research, air entrapment in the sample was minimised during saturation. As a result, no visible evidence of air entrapment was observed during the test. The transparent acrylic test cell facilitated direct observation of the sample particles throughout the experiment. The absence of any noticeable formation

of air bubbles among the particles from the sides of the samples suggests that air entrapment is unlikely to contribute to the observed reduction in *Ks* in our study.

Another factor that can affect the continuous reduction of *Ks* is the blockage of drainable pores with fine particles (Jeong et al., 2018b), which restricts the flow of water and leads to a decrease in the *Ks*. Particle size distribution of the samples (Figure 3.4.5) and Table 3.4.1 show that the fine particles in all sections have decreased compared to the original sample prior to the test. This reduction is about 2% for sample A, and varies between 1% to 4.4% in sample B. Furthermore, there is a decrease in *Gs* in the top section and an increase in the bottom section (Figure 3.4.6). It can be concluded that mobile low-density fine particles (such as fine pumice) have displaced from the bottom of the sample to the top. Another reason for the reduction in the *Ks* can be related to the continuous blockage of the drainable pores with fine particles with rough surfaces (such as glass shards) or the simultaneous impact of blockage by glass shards and mobilisation and blockage by low-density particles. The SEM image of the sample in Figure 3.5.1 shows a noticeable amount of glass shards and pumice in the small section of the sample. Continuous mobilisation or re-deposition of these particles can change the connection of the drainable pores and reduce *Ks*.

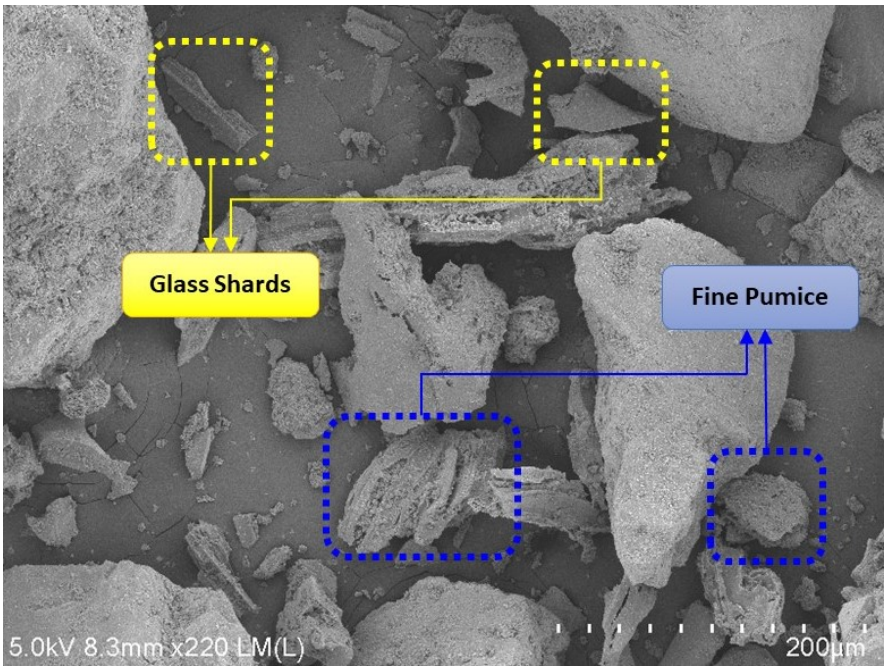

Figure 3.5.1. 220x magnification of the sample using SEM providing a closer view of the fine particles in the sample

The ASTM standard for granular soils (ASTM D2434-19, 2019) explains the procedure of estimating the *Ks* without mentioning the period of carrying out each test. Laboratory tests aimed at determining the *Ks* should account for the duration required for the specimen to attain a stable *Ks*. The standard cannot stipulate a fixed timeframe for achieving stable *Ks*, as each sample exhibits a distinct time requirement to reach this equilibrium. The mid to long-term *Ks* results in Figure 3.4.2 show a noticeable drop in the *Ks*, and if the test is terminated in a few hours, the resulting *Ks* will be 96% higher than the final one. Similar results were reported by Du et al. (2018) and Vanderzalm et al. (2020), when they permeated the sample with a solution containing *Fe (III)* or water with suspended solids. In our research, there was no *Fe (III)* contamination source, and the water used was drinking water from a tap. Figure 3.4.3 demonstrates a robust linear relationship between *Q* and *i* during the increasing and decreasing head phases during short-term testing. However, when comparing this figure to the long-term tests illustrated in Figure 3.4.2, it becomes evident that the *Q-i* relationship varies over time.

The long-term variability of saturated hydraulic conductivity holds significant importance for systems enduring extended saturation periods. The accurate estimation of *Ks* over the long-term plays a crucial role in modelling various hydrological processes, including infiltration, surface water runoff, soil erosion, and the design of drainage systems. Insight into *Ks* is essential for understanding and predicting the movement of water within soil systems, thereby informing effective management and engineering practices in these contexts. The findings of this investigation may serve as an initial reference for reevaluating the specification of saturated hydraulic conductivity in projects involving the backfilling of sandy materials subjected to prolonged saturation. Notably, this pertains to the substantial utilization of backfilled granular material in the construction of embankment dams (Tatone et al., 2009). These materials concurrently experience saturated conditions during reservoir water storage. Both the overestimation and underestimation of the saturated hydraulic conductivity of these materials can cause dam failure or incur additional expenses for backfilling and compaction. Additionally, sandy backfilled materials serve as filter components around subsurface drainage pipes and stormwater devices. Overestimating the saturated hydraulic conductivity of such filter materials may lead to reduced flow within the drainage system and increase surface ponding. Artificial soakage basins and soak pits are frequently recommended in the context of stormwater management in new urban developments (Shaver, 2020). These systems gather runoff from urban areas and gradually infiltrate the water into the ground.

A crucial factor in designing these soakage systems is the saturated hydraulic conductivity. However, it's important to note that the testing duration commonly used to assess the *Ks* rate is often short and may not accurately represent the long-term behaviour of saturated hydraulic conductivity. Consequently, it's wise to account for the long-term variation of Ks when reporting *Ks* values for applications involving soil saturation, such as soakage basins or drainage pipes. This precaution is essential as overestimation could lead to erroneous calculations.

Moreover, an array of studies has been conducted on pedotransfer functions, which establish relationships between soil properties, including void ratio, grain size, and pore size distribution, for the estimation of the *Ks* (Boadu, 2000; Daneshian et al., 2021; Jabro, 1992; Tanaka et al., 2003; Wang et al., 2017). The pedotransfer functions were generally developed to estimate the *Ks* of non-plastic and sandy soils (Breyer, 1964; Hazen, 1892; Kenney et al., 1984; Kozeny, 1927a), however there are few pedotransfer functions developed for plastic soil, as well (Mbonimpa et al., 2002). As these functions are usually developed based on *Ks* tests in the laboratory (Mbonimpa et al., 2002; Slichter, 1898; C. Terzaghi, 1925), comparing the variations of the Ks from this research with prediction of pedotransfer functions will reveal whether these functions are able to account for long-term changes of *Ks*.

3.6. Conclusion

This study provides valuable insights into the variation of saturated hydraulic conductivity in sandy samples through a long-term constant head experiment. To the knowledge of the authors, this is the first study that specifically focuses on the changes of the *Ks* over an extended period of time in the laboratory on sandy soils. The results demonstrate a significant reduction in *Ks*, primarily due to physical clogging caused by fines and pumice particles. The increased concentration of pumice particles in the top section indicates their mobility and potential blockage of drainable pore sections, affecting *Ks*. These changes were not observed in short-term tests, highlighting the importance of longer-term investigations. The findings stress the need for extended constant head tests to accurately assess and report *Ks* in sandy samples, enhancing our understanding of their hydraulic behaviour.

Given that sand mixtures are employed for various construction purposes as backfill materials, which may remain saturated for extended periods, this study highlights the necessity of conducting extended constant head laboratory tests to accurately report the *Ks*. This research specifically investigates the variations in *Ks* for non-plastic sand containing less than 10% fine material, thereby limiting the generalizability of the findings to sandy soils of different origins. Consequently, it is recommended that extended constant head tests be performed on other soil types to explore the variations in *Ks*. Additionally, the pattern of changes in *Ks* can be further examined through the use of advanced technologies such as x-ray computed tomography (CT) during testing. CT scanning has the potential to elucidate particle movement within the sample, offering valuable insights into the migration of fine particles during testing, the changes in the connectivity of drainable pores within the specimen, and the subsequent impact of these changes on *Ks*.

3.7. Acknowledgment

This research was supported by the University of Waikato Doctoral Scholarship.

3.8. Data Availability Statement

All data used and generated by this study, including hydraulic head and flow measurements, can be found in ZENODO repository (Ashouri, 2024).

Chapter 4. Range of variations in the saturated hydraulic conductivity of sand and gravel samples in the laboratory by constant head method in a rigid wall cell and comparison of results from Darcy's equation with predictive methods

Saeed Nikghalb Ashouri[1], Adrian Pittari[2], Ali Shokri[1]

1. School of Engineering, University of Waikato, Hamilton, New Zealand
2. School of Science, University of Waikato, Hamilton, New Zealand

Abstract

Saturated hydraulic conductivity (Ks) of the soil is one of the most important parameters that defines the rate of water flow in the soil. Most studies on determining Ks in the laboratory fail to investigate the variations of Ks within the test. The laboratory analysis involved the determination of Ks for 10 sandy samples using the constant head method within a transparent rigid wall cell. Two distinct groups of samples were subjected to testing: 1) with hydraulic heads varying from low to high levels; 2) at a consistent low hydraulic head. The results highlighted the presence of two discernible phases characterized by low and high Ks values, denoted as phase 1 and phase 3 respectively, with an intermediary phase designated as phase 2. These observations underscored the necessity of considering a spectrum of low and high Ks values for sand and gravel samples. Additionally, pedotransfer functions (PTFs) have been used for a long time for estimation of Ks. Subsequently, the experimental Ks data were compared against various PTFs to evaluate their efficacy in estimating Ks without the need for extensive laboratory testing. Innovative correction coefficients were proposed to refine one of the most accurate predictive models specific to the sand type under examination, with the aim of enhancing the agreement between predicted and observed Ks values. The correction coefficients relate Mbonimpa's pedotransfer function constants to the void ratio (e) and coefficient of uniformity (C_U). The study revealed that the revised correction coefficients derived from C_U and e, yielded Ks estimates ranging from 0.7 to 1.3 times the measured Ks values during constant head tests in both phase 1 and phase 3. These updated correction factors can be

effectively applied to predict the hydraulic conductivity (Ks) of clean river sand and non-plastic sands containing gravel mixes akin to those utilized in this particular investigation.

Key Words: saturated hydraulic conductivity, constant head test, non-plastic sand and gravel soils, pedotransfer functions, coefficient of uniformity, void ratio

THE UNIVERSITY OF WAIKATO
Te Whare Wānanga o Waikato

Co-Authorship Form

School of Graduate Research
The University of Waikato
Private Bag 3105
Hamilton 3240, New Zealand
Phone +64 7 838 5096
Email: SGR@waikato.ac.nz
Website: http://www.waikato.ac.nz/students/research-degre

This form is to accompany the submission of any PhD that contains research reported in published or unpublished co-authored work. **Please include one copy of this form for each co-authored work.** Completed forms should be included in your appendices for all the copies of your thesis submitted for examination and library deposit (including digital deposit).

Please indicate the chapter/section/pages of this thesis that are extracted from a co-authored work and give the title and publication details or details of submission of the co-authored work.
Thesis chapter 4: Nikghalb Ashouri. S., Pittari. A., Shokri. A. (Revised and ready for submission to a journal). Range of variations in the saturated hydraulic conductivity of sand and gravel samples in the laboratory by constant head method in a rigid wall cell and comparison of results from Darcy's equation with pedotransfer functions

Nature of contribution by PhD candidate	Experimental setup- data collection and analysis- writing and editing of the manuscript
Extent of contribution by PhD candidate (%)	90%

CO-AUTHORS

Name	Nature of Contribution
Ali Shokri	Provided input during experimental setup, study design, data interpretation, and revision of the manuscript
Adrian Pittari	Provided consultation and input during data interpretation, and reviewing the manuscript

Certification by Co-Authors

The undersigned hereby certify that:

- the above statement correctly reflects the nature and extent of the PhD candidate's contribution to this work, and the nature of the contribution of each of the co-authors; and
- that the candidate wrote all or the majority of the text.

Name	Signature	Date
Ali Shokri		21/06/2024
Adrian Pittari	Adrian Pittari	21/06/2024

List of Notation

Ks	Saturated hydraulic conductivity (cm/min)
i	Hydraulic gradient (m/m)
Q	flow rate (cm^3/s)
A	Cross sectional area of the specimen (cm^2)
e	Void ratio (-)
n	Porosity (-)
d_e	Effective grain size of the specimen (mm)
d_{10}	10% particles are finer than the size (mm)
d_{60}	60% particles are finer than the size (mm)
d_{90}	90% particles are finer than the size (mm)
C_U	Coefficient of uniformity (-) (d_{60}/d_{10})
C_C	Coefficient of curvature (-)
G_S	Specific gravity of solid particles (-)
C_G	A constant encompassing media attributes like tortuosity, particle shape, and specific surface area
x	A constant determined by the specimen's void ratio
g	Acceleration due to gravity (9.81 m/s^2)
ν	Kinematic viscosity of water (m^2/s)
γ_w	Unit weight of water (kN/m^3)
μ_w	Dynamic viscosity of water (Pa.s)

4.1. Introduction

The saturated hydraulic conductivity (K_s) serves as a crucial parameter for assessing the flow of water within the saturated soil zone. Precise determination of Ks is essential for aiding hydraulic modelers, designers, and water resource managers in evaluating surface and groundwater volumes. The hydraulic conductivity (Ks) can be determined through laboratory or field testing using either disturbed or undisturbed samples and destructive or non-destructive tests, or approximated through PTFs.

Although the determination of Ks in the laboratory or field can be resource-intensive in terms of time and budget, the resulting Ks values are founded on direct measurements of factors influencing Ks, including pore pressure and flow rate within the soil.

In contrast to the laboratory and field methods for determining Ks, PTFs offer a straightforward and efficient means of estimating Ks by correlating indirect soil attributes—such as void ratio (e) or effective grain size distribution (GSD)—with Ks (Adjuik et al., 2023; Chapuis, 2012).

In laboratory settings, the Ks of sandy samples is typically assessed using a constant head test arrangement within a rigid wall permeability cell (Sadeghi & AliPanahi, 2020). The Ks of clayey samples can be estimated during a consolidation test as well. Terzaghi's consolidation theory (Terzaghi, 1922) can be used, together with Casagrande or Taylor's methods (Taylor, 1948) to estimate the rate of consolidation from settlement time curve at each loading step (Su et al., 2020). However, this method can also be inaccurate (Su et al., 2020) and gives poor results for Ks (Chapuis, 2012). Within this study, the term 'soil' pertains to particle mixtures utilized for engineering or construction aims, characterized by a minimal presence of organic material. It is important to note that this interpretation of soil differs from the definitions found in disciplines such as soil science or agriculture.

A primary challenge in determining Ks of sandy samples in laboratory settings is the typically rapid nature of the tests, often concluding within a few hours of initiation. Additionally, Ks values are sometimes reported as an average over time without explicit reference to the test duration (Cabalar & Akbulut, 2016; Cherif Taiba et al., 2019; Rodgers & Mulqueen, 2004; Sarki et al., 2014; Wietsma et al., 2009). Given that the pores within the soil are in a state of dynamic saturation and that the connectivity of drainable pores undergoes continual shifts owing to particle movements and possible internal clogging,

uncertainties may arise concerning the stability of a sample during a short-term hydraulic conductivity test conducted in the laboratory.

A study concentrating on alterations in Ks resulting from pore clogging or bacterial growth has demonstrated that even in samples not exposed to bacterial infiltration, a decline in Ks can still occur (Chen et al., 2021a). The study highlighted a noteworthy 19% decrease in Ks during the constant head test conducted on the Malan loess of China over a duration of 101 hours. Furthermore, the reduction, albeit at a slower pace, persisted even beyond the stationary and death phases of bacterial activity. This decline in Ks might have endured further had the test been extended over a longer timeframe.

Studies examining variations in Ks resulting from bacterial proliferation often lead to the conclusion that the decrease predominantly occurs within the layer near flow or effluent inlet, while the Ks values of the remaining layers remain unaltered (Chen et al., 2021; Vandevivere & Baveye, 1992). Nevertheless, the decline in hydraulic head attributed to clogging influences the water pressure in adjacent layers, thereby contributing to the decrease in Ks throughout the sample.

In a study conducted by Mavis & Wilsey (1936) constant head tests were conducted on Iowa and Ottawa sands under very low hydraulic gradients ranging from 0.009 to 0.02 m/m, in the absence of bacterial growth. One of the samples was subjected to repeated cycles of constant head tests over a 5-day period, revealing a daily decline in Ks from 15.66 cm/min to 9.61 cm/min. The researchers attributed this reduction to clogging within the sample, offering it as the rationale for the alteration in Ks values. Pillsbury & Appleman (1945) observed a period of decrease and increase in Ks of Placentia loam and related it to air entrapment in the specimens. The incorporation of a range of Ks variations, rather than relying on a single value, appears to address the issue of potentially reporting an excessively low or high Ks value, thus offering a more comprehensive perspective on the variability within the data.

Conversely, to mitigate the expenses and labour associated with conducting field or laboratory tests to determine Ks and to facilitate quicker estimations, numerous PTFs have been formulated by researchers. A review of several PTFs can be found in Mavis & Wilsey (1936) and Chapuis (2012). The basis of all PTFs involves establishing a connection between Ks and properties of soils that can be measured with relative ease or rapidity, encompassing porosity or void ratio, effective grain size, specific surface area of the particles, and the coefficient of uniformity.

Some equations (Hazen, 1892; Kenney et al., 1984; Vuković & Soro, 1992) relate the Ks to effective grain size (d_{10} and d_5 respectively). Some other methods (Breyer, 1964; Kozeny, 1927; Slichter, 1898; Terzaghi, 1925) consider other soil properties as important factors on Ks. There are modifications to Kozeny's (Kozeny, 1927a) equation, with the most prominent being the adjustment introduced by Carman (1939). This modification, known as the Kozeny-Carman equation, incorporates the specific surface area of the particles alongside the void ratio in the estimation of Ks. Measuring the specific surface area of particles is typically challenging and is seldom conducted in practice (Chapuis, 2012). Theoretical equations exist that estimate the specific surface area by relating it to the liquid limit, particle density, or the coefficient of uniformity of the particles (Ren et al., 2016). Imprecise estimation of the specific surface area may result in the overestimation or underestimation of Ks when compared to the Ks values obtained through measurements (Aubertin et al., 2005; Sanzeni et al., 2013).

Modifications to Hazen's equation have been developed, yielding acceptable estimates of Ks. Among those, Chapuis (2004) and Mbonimpa et al. (2002) provide noticeable improvements on Hazen's equation. Chapuis (2004) adjusts Hazen's equations to be applicable to all ranges of porosity of sands and gravels by considering the maximum void ratio and specific surface area in the equation. Mbonimpa et al. (2002) proposed another predictive formula, which is a modification of Hazen's equation. This revised equation is simple to utilize and has the capability to predict Ks with considerable accuracy in comparison to empirically measured data (Yin, 2009). Mbonimpa's equation also bears similarity to the Kozeny-Carman equation. It considers that the specific surface area can be estimated based on particle size; hence, Mbonimpa's equation inherently accounts for the specific surface area factor within its formulation (Aubertin et al., 2005).

PTFs serve as valuable resources for estimating Ks in projects where constraints exist in budgeting for field or laboratory assessments of Ks. Nonetheless, it is imperative to verify the application of PTFs across diverse soil types. Currently, research that integrates a comparative analysis of PTFs with laboratory determination of Ks in a prolonged constant head test remains scarce. The majority of synthesis and empirical research papers utilizing Ks databases from previous studies often overlook the significance of test duration and test head variation on the outcomes of Ks results (Chapuis, 2004). Researchers who do acknowledge the duration of Ks tests either have not extended the tests over longer periods (Chapuis et al., 1989; Krumbein & Monk, 1942; Loudon, 1952), or have not addressed the fluctuation in Ks as a point of inquiry (Mavis & Wilsey, 1936).

This study investigates the fluctuations in Ks within a selection of sand and gravel specimens, subjected to different heads in a rigid wall cell. The study illustrates the varying patterns of Ks across different materials. Subsequently, data derived from a series of Ks tests on various samples are employed to evaluate the reliability of seven most commonly used (Khaja et al., 2022) predictive Ks methods. An adjustment is then introduced to enhance the predictive capabilities of one of the accurate equations. The span of Ks variations observed in this study highlights the significance of reporting Ks data with meticulous attention about the range of variations rather than a single number.

4.2. Materials

In this research, two distinct soil varieties were utilized. The initial variety is known as pit sand, typically sourced from the excavation of riverbanks. Characterized by its non-cohesive nature, pit sand is predominantly composed of quartz and feldspars, as revealed by X-ray diffraction (XRD) analysis. Microscopic examination of the pit sand discloses the presence of pumice (around 11%) and is amorphous to XRD. Pumice particles, due to vesicular nature, contribute to the relatively low dry bulk density of the pit sand, measured between 1.2 and 1.4 g/cm^3 in this study. The size of the pumice particles spans a spectrum from fine to coarse, with a notably loose texture, making them susceptible to fragmentation upon application of pressure between fingers. The identification of pit sand is further facilitated by its distinctive yellow and golden colour. The XRD analysis, microscopic examination for particle counting, and pumice content of the particles are derived from Nikghalb Ashouri et al. (2023) who did a previous research on the same materials.

The second category of sand employed in this study is known as washed sand, or riverbed sand, distinguished by its lack of fine particles smaller than 0.005 mm. Analogous to pit sand, washed sand primarily consists of quartz and feldspar particles. Contrasting with pit sand, however, washed sand contains no pumice, leading to a naturally higher dry bulk density, recorded at 1.55 g/cm^3 for samples used in this research. Moreover, washed sand exhibits a darker hue in comparison to pit sand.

4.3. Methods

4.3.1. Sample preparation

The primary objective of this study was to investigate the variabilities in K_s across diverse mixes of sand and gravel. The preparation of the mixtures was meticulously designed to encompass a broad spectrum of sand and gravel combinations. For the purpose of this research, particle sizes were delineated based on the American Association of State Highway and Transportation Officials (AASHTO) classification system. According to this system, particles measuring less than 0.075 mm are categorized as silt and clay (referred to herein as fine particles), those ranging from 0.075 to 2 mm are classified as sand, and particles exceeding 2 mm are identified as gravel or stone (herein referred to as gravels). The characteristics of these mixtures are detailed in Table 4.3.1.

The initial subset of the mixtures, which varied in the ratio of fine particles and gravels, was designated as 'C'. Within this group, the hydraulic head was adjusted in accordance with a constant head test to evaluate Ks under different hydraulic pressures. In mixtures C1 through C4, the proportion of fine particles was systematically increased from 8.3% to 15.1% by weight to assess the impact of increased fine particle content on Ks. Mixtures C5 and C6 were specifically formulated to examine the effects of incorporating gravel into the sand (13% and 20%, respectively) and the resultant changes in Ks.

The second group of mixtures (C7) utilized washed sand and aimed to explore the temporal variations of Ks in a sample with a minimal presence of fine particles. This facet of the study was intended to ascertain whether Ks fluctuations were attributable to the presence of fine particles.

Lastly, the series labelled 'S' (S1-S2-S3), entailed the use of original pit sand from which particles larger than 2 mm had been removed. This set was deployed to monitor Ks changes at a consistent hydraulic head over a prolonged duration (approximately 50 hours), to determine if Ks variations were linked to alterations in the testing hydraulic head.

In the preparatory phase of the constant head experiments, two additional mixtures of pit sand were assessed to validate the experimental setup's efficacy. These preliminary tests were tagged as 'T1' and 'T2.' The properties of these trial mixtures, akin to those of the original pit sand (S group), are not enumerated in Table 4.3.1. However, details concerning

the constant head tests conducted on these samples are outlined in section 4.3.3 dedicated to these tests.

The characteristics of the mixtures and specimens are delineated in Table 4.3.1. Additionally, Figure 4.3.1 features a flowchart summarizing the mixtures and specimens, offering an overview of the rationale for the preparation of each mixture.

To prepare the mixtures, the pit sand batch was initially dried in an oven at a temperature of 106°C for a duration of 12 hours. After drying, the sand was sieved using 2 mm and 5 mm sieves placed on a vibrating table, allowing for the segregation of particles larger than 5 mm and the differentiation of particles between 2 mm and 5 mm from those smaller than 2 mm. For the extraction of fine particles, the sand that remained was subjected to a wet sieving process using a sieve with a mesh size of 0.075 mm. The particles that passed through this sieve were collected in water, subsequently oven-dried. The wet sand obtained post-sieving was also dried in an oven, preparing it for inclusion in the mixtures. The dried fine particles were further reduced to a powder using a pestle and mortar, readying them for addition to the mixtures. This process yielded particles in three distinct categories: fine particles smaller than 0.075 mm, sand ranging from 0.075 mm to 2 mm, and gravels ranging from 2 mm to 5 mm. These materials were then employed in the preparation of mixtures C1, C3, C4, C5, and C6. Mixtures S1 to S3, and C2 were similar in composition, whereas C7 consisted of the original washed sand, exclusively with gravels removed. The mixing ratios were carefully calculated to incrementally increase the proportion of fine particles in mixtures C1, C3, and C4, and similarly to increase the gravel content in mixtures C5 and C6. The specific percentages of fine particles, sand, and gravel in the mixtures are detailed in Table 4.3.1. According to ASTM D2434-19 (2019) the ratio of cell diameter (76.2 mm in this research) to the largest particle size in the mixture should not be more than 8-10. Otherwise, it could induce preferential leakage from cell wall. Consequently, the maximum gravel size permissible in the mixtures was restricted to 5 mm.

The particle size distribution (PSD) of the mixtures was determined using a laser diffractometer (Malvern Mastersizer 3000 manufactured by Malvern Panalytical). Due to the instrument's limitation in measuring particles larger than 2 mm, the gravel content was quantified by weight prior to being incorporated into the mixtures. This gravel percentage was then proportionally integrated into the grain size distribution graph (illustrated in Figure 4.3.2). Additionally, the total dry weight of each mixture was

meticulously recorded for subsequent analyses, which include computations of the bulk dry density, void ratio, and evaluation of the saturation degree. The specific gravity of the solid particles (G_s), which is reported relative to the density of water, for each mixture was measured using a gas pycnometer (the Quantachrome Ultrapycnometer 1000). To ensure reliability, the determination of both PSD and G_s was conducted in five replicates for each type of mixture.

To ensure consistent compaction across the specimens, the moist tamping method was applied (Ladd, 1978). This process involved moistening the mixtures with water constituting 12% of their weight to facilitate the compaction process. Subsequently, the mixtures were covered and left for 24 hours to achieve moisture equilibrium. Special care was taken during handling to prevent any loss of particles, as such losses could complicate the assessment of saturation levels. After the 24-hour period, the mixtures were compacted into the Ks measurement acrylic cell in layers, each measuring 12 mm in thickness. The dimensions of the cell were specified as 292 mm in length and 76.2 mm in diameter. The cell, once compacted, was weighed to calculate the bulk density of the sample, which is documented in Table 4.3.1. With the known dry weight of the sample, the weight of water added, and the specific gravity (G_s) of the particles, it was possible to compute both the void ratio (e) and the dry bulk density of the compacted material.

Following the compaction of the samples, a set procedure was adopted to remove trapped air from the pores. Initially, the samples were subjected to a vacuum pump for one hour to evacuate any air pockets. Subsequently, deaired water was slowly permeated from the base of the cell to prevent air entrapment. Once the water level had ascended to the top of the cell for each specimen, the permeation was halted, and the cell with the specimen was left undisturbed overnight to allow for complete saturation and minimize any residual air bubble entrapment within the specimens.

It was observed that the water level in the cell dropped by a few millimetres overnight. This phenomenon, attributed to trapped air bubbles within the specimens, did not impede the saturation process, provided that the water level at the top did not fall below the specimen's surface. The following day, each saturated specimen in the cell was weighed to confirm full saturation, in accordance with the method outlined by Chapuis (2004). It was noted that all specimens achieved a saturation level of 95% or higher.

The saturation evaluation method described in Chapuis (2004) may necessitate modifications to assess the saturation degree during the test. The procedure allows the

researcher to temporarily halt the test, close the cell valves, weigh the cell, and resume the test seamlessly, without compromising the final Ks results. However, it is important to note that disrupting the continuous head gradient in the specimen could potentially prompt rearrangement of the drainable pores, influencing subsequent Ks values. Notably, extended or repeated Ks tests on the same sample, as highlighted by Snehota et al. (2015), may yield different Ks values due to pore rearrangements resulting from handling or perturbations.

Furthermore, any minor movements or displacements of the test cell during the experiment, such as transferring it between surfaces, can induce alterations in the specimen's pore structure, consequently affecting Ks measurements. Therefore, it is advisable to limit cell repositioning and only assess the saturation degree before and after the tests. The subsequent section on results and discussion will delve into the impact of interrupting and recommencing the test on specimens T1 and T2.

Table 4.3.1. Properties of the mixtures prepared and compacted specimens (samples S1 to C6 used pitsand, but sample C7 was prepared with washed sand)

Parameter	Specimen Name									
	S1	S2	S3	C1	C2	C3	C4	C5	C6	C7
Particles below 0.075 mm (%)	9.8	9.8	9.8	8.3	9.8	10.5	15.1	7.2	7.7	0.9
Particles between 0.075-2 mm (%)	90.2	90.2	90.2	91.7	90.2	89.5	84.9	79.7	72.3	99.1
Particles above 2 mm (%)	0.0	0.0	0.0	0.0	0.0	0.0	0.0	13.1	20.0	0.0
d_{10} (mm)	0.075	0.075	0.075	0.091	0.075	0.068	0.034	0.105	0.099	0.223
d_{30} (mm)	0.202	0.202	0.202	0.222	0.184	0.221	0.167	0.245	0.266	0.362
d_{60} (mm)	0.390	0.390	0.390	0.401	0.332	0.429	0.325	0.476	0.537	0.570
d_{90} (mm)	0.827	0.827	0.827	0.788	0.636	0.924	0.701	2.703	3.500	0.978
C_U	5.17	5.17	5.17	4.39	4.41	6.25	9.60	4.52	5.41	2.56
C_C	1.38	1.38	1.38	1.35	1.36	1.66	2.53	1.20	1.33	1.03
G_S	2.68	2.68	2.68	2.68	2.69	2.67	2.68	2.74	2.72	2.86
e	1.12	1.14	1.12	1.12	1.07	1.03	1.04	0.93	0.90	0.85
Bulk density (gr/cm^3)	1.42	1.40	1.41	1.41	1.45	1.47	1.47	1.59	1.60	1.73
Dry bulk density (gr/cm^3)	1.26	1.25	1.26	1.26	1.30	1.32	1.31	1.42	1.43	1.55

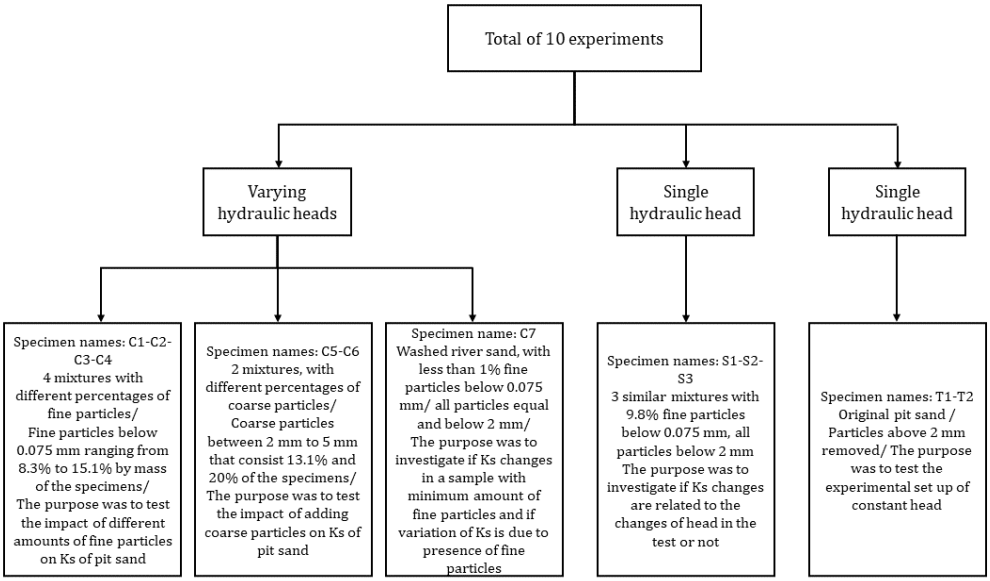

Figure 4.3.2. Flow chart of test specimens and purpose of making each mixture

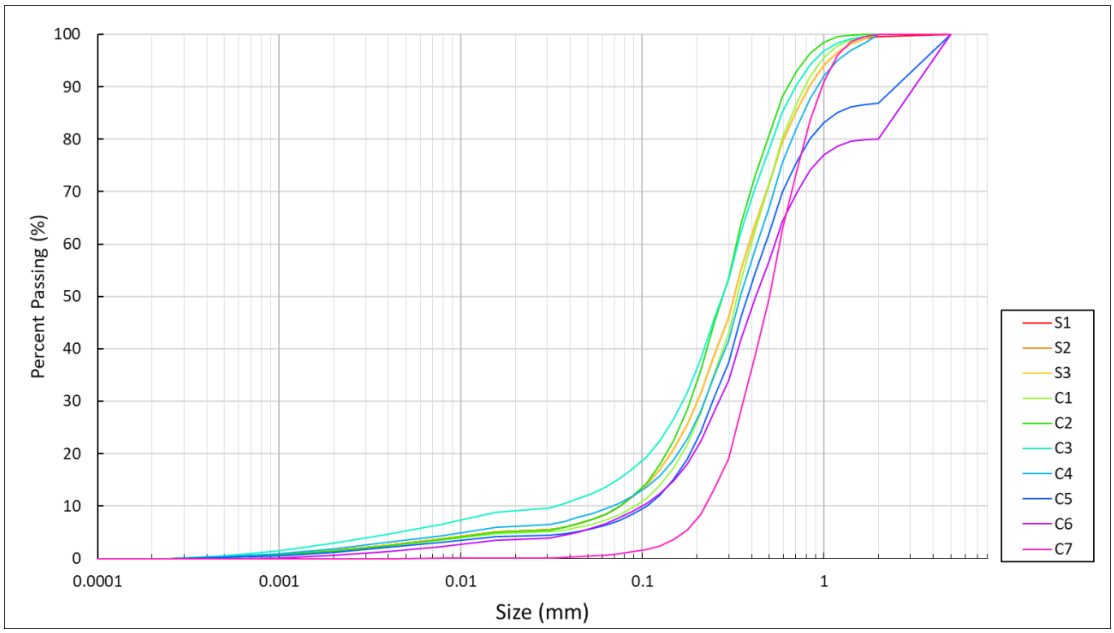

Figure 4.3.3. Grain size distribution of the specimens

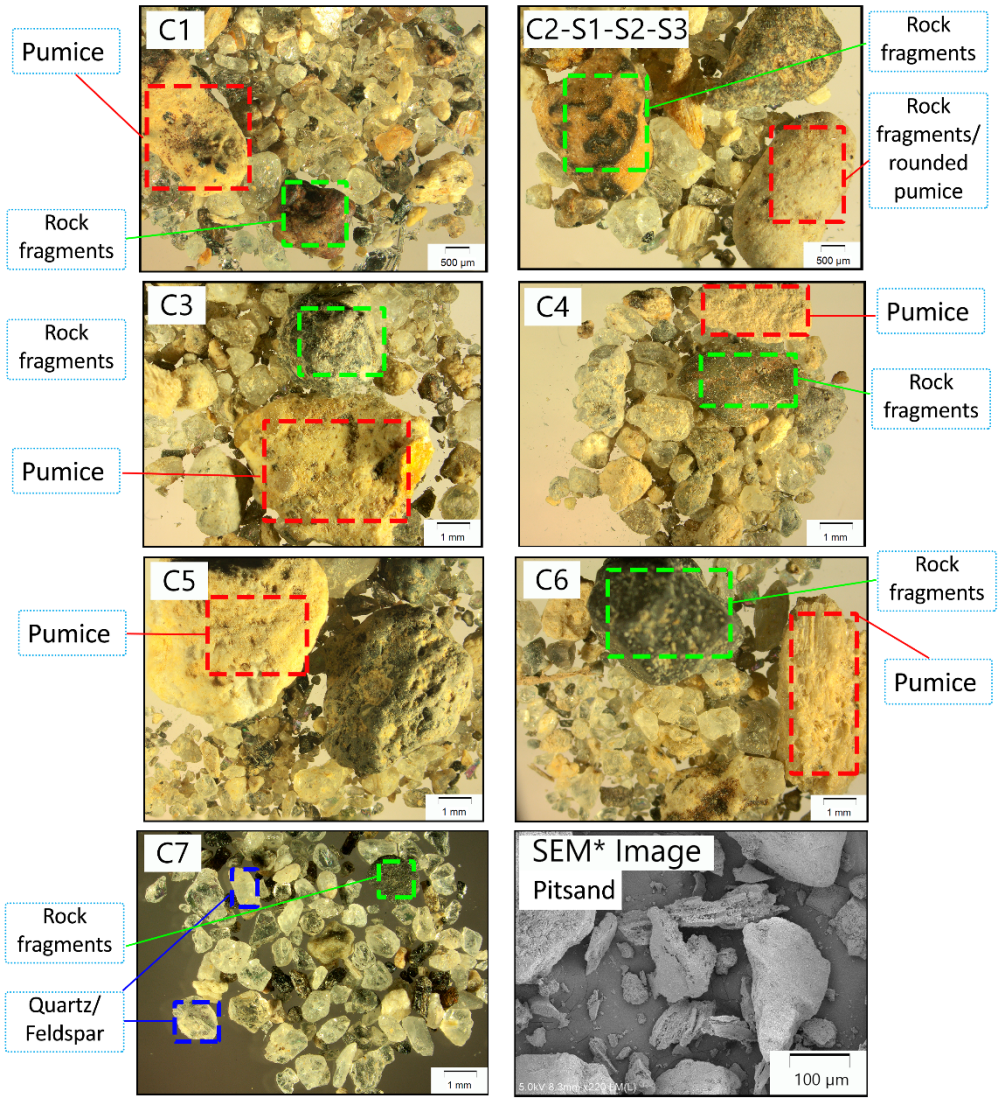

Figure 4.3.4. Composition of all specimens under microscope- The clear glassy looking grains are mostly quartz, and the translucent white grains are mostly feldspar, and the colorful particles are mostly rock fragments (ferromagnesian minerals)

** SEM: Scanning electron microscope*

4.3.2. Constant head saturated hydraulic conductivity tests

The constant head apparatus employed in this study featured an adjustable screw mechanism to position the water bucket at various desired levels. The hydraulic heads utilized in the experiments spanned from very low to high values, with a detailed breakdown provided in Table 4.3.2. The hydraulic head adjustments were made in increments ranging from 10 cm to 15 cm. Notably, all hydraulic head measurements were conducted with reference to the bottom of the test cell as the datum point for accuracy and consistency.

For each hydraulic head setting, a period was allocated to allow the specimen to acclimate to the new water level before recording the flow rate and head variance once a stable flow rate had been achieved. This stabilization period ensured accurate measurements of both flow rate and head difference. Measurements of flow rate and head difference were taken twice at each hydraulic head setting, with intervals of approximately half an hour between recordings. The water levels were monitored using gauged piezometers installed within the specimen, while the flow rate was calculated by tracking the weight of the outflow over time.

In the case of the "C" series experiments with fluctuating hydraulic heads, the total duration ranged from 6 to 8 hours. Conversely, for the "S" series experiments with a constant hydraulic head, the duration extended to approximately 53 hours.

While it is advisable to utilize deaired water for Ks tests to minimize air entrapment, the practical challenges posed by sand and gravel specimens, which inherently exhibit high Ks values, often make it arduous to supply deaired water for the whole period of the test and on large specimens. Consequently, tap water was employed for these Ks tests, acknowledging the presence of dissolved air within the tap water. Despite the dissolved air content in tap water, it is worth noting that any potential impact on Ks results would likely be negligible, particularly within the context of relatively shorter test durations spanning 6 to 8 hours, except for specimens S1 to S3 which were evaluated over an extended period.

Given that the experiments were conducted in a laboratory environment with controlled temperature settings, any potential influence of temperature fluctuations on Ks results can be considered negligible.

The Ks at each recording of flow rate and hydraulic head was calculated according to Darcy's equation:

$$K_s = \frac{Q}{i \times A}$$

Where "Ks" is the saturated hydraulic conductivity of the specimen at each reading (m/s), "Q" is the rate of outflow from specimen, "i" is the head gradient (m/m) and is defined as the difference between the water heads in piezometer tubes inside the specimen divided by the height of the specimen, and A is the cross sectional area of the specimen (m^2).

Table 4.3.1. The hydraulic heads applied in the experiments

Specimen name	**Selected hydraulic heads (mm)**
C1- C2 - C3 - C4 - C5 - C6 - C7	591 – 697 – 805 – 911 – 1018 – 1127 – 1231 – 1339 – 1527 – 1624 – 1758
S1 - S2 - S3	964

4.3.3. Test experiments on T1 and T2 specimens

Before proceeding with the tests on the samples outlined in Figure 4.3.1 and Table 4.3.1, preliminary trial tests were conducted to validate the effectiveness of the sample saturation method, confirm the water-tight integrity of the test setup, and ensure uninterrupted test runs. Interestingly, these trial tests yielded valuable insights regarding the Ks, which will be elaborated upon in the results section and subsequently discussed in detail in the discussion section.

In the test experiments conducted on specimens T1 and T2, the hydraulic gradients were not documented as it was a preliminary assessment. However, flow rates were recorded over time, and the tests were structured in multiple cycles of permeation under a consistent hydraulic head. These cycles aligned with the sample saturation approach proposed by Chapuis (2004) and aimed to investigate the potential for air entrapment in the samples when utilizing tap water. Each cycle spanned a duration ranging from 32 to 72 hours.

At the conclusion of each cycle, the inflow valve was sealed, and the cell was detached from the piezometer connectors for weighing. Following the weighing process, the sample was

reattached to the inflow valve and piezometers to continue the test under the same hydraulic head. Specimen T2 followed a comparable test procedure to T1, albeit with two permeation cycles under a single low hydraulic head. The duration of the tests for T2 exceeded that of T1, with the initial cycle lasting 164 hours and the subsequent cycle extending to 194 hours.

Although the hydraulic gradient data were not recorded for these specimens, precluding the calculation of Ks, it was observed that there was no variance in the saturated weights of the specimens. This consistency indicated that running the constant head tests with tap water for the specified durations did not lead to air entrapment in the samples, provided they were fully saturated beforehand.

4.3.4. Pedotransfer functions

The PTFs utilized in this study are detailed in Table 4.3.1, with the parameters expressed in metric units. These equations represent some of the most widely cited predictive models in the existing literature, drawing on research by Yin (2009), Chapuis & Aubertin (2010), Chapuis (2012), and Águila et al. (2023). Each equation is accompanied by specific conditions pertaining to the selection of parameters such as effective grain size (d_e), coefficient of uniformity (C_U), and void ratio (e) or porosity (n). The influencing factors on Ks can be classified into three main categories: properties of the permeating fluid, pore characteristics, and attributes of the solid particles (Yin, 2009). While certain equations incorporate all these factors, others focus on specific aspects. For instance, the USBR equation (Cheng & Chen, 2007) accounts for only the effective grain size (d_{20}) and properties of the permeating fluid, while Kozeny's equation utilizes d_{10} as the effective grain size and includes porosity as a determining factor for Ks.

The specimens used in this study generally satisfy the criteria outlined for the equations detailed in Table 4.3.3. Notably, for the Hazen and USBR equations, the coefficient of uniformity (C_U) of some samples slightly exceeds 5 (specimens S1, S2, S3, C3, and C6). However, in the case of specimen C4, C_U is approximately 9, significantly higher than the specified criteria for the Hazen and USBR equations. Despite these discrepancies, Ks calculations were conducted for all samples, even those not meeting the specific conditions, with the aim of evaluating the sensitivity of these equations when the criteria are not fully met.

Table 4.3.1. List of PTFs used and the conditions of using each equation

Method	**Equation**	**Conditions**
Hazen	$k=6\times 10^{-4}\times\frac{g}{\nu}(1+10\,(n\text{-}0.26))\,d_{10}^2$	$0.1\ mm < d_{10} < 3\ mm$ $C_u < 5$
Kozeny	$k=8.3\times 10^{-3}\times\frac{g}{\nu}(\frac{n^3}{(1\text{-}n)^2})\,d_{10}^2$	*Large size sand*
Slitcher	$k=10^{-2}\times\frac{g}{\nu}(n^{3.287})\,d_{10}^2$	$0.01\ mm < d_{10} < 5\ mm$
Terzaghi	$k=8.4\times 10^{-3}\times\frac{g}{\nu}(\frac{n\text{-}0.13}{\sqrt[3]{1\text{-}n}})^2\,d_{10}^2$	*Large size sand*
Breyer	$k=6\times 10^{-4}\times\frac{g}{\nu}\log(\frac{500}{C_u})\,d_{10}^2$	$0.06\ mm < d_{10} < 0.6\ mm$ $1 < C_u < 20$
USBR	$k=4.8\times 10^{-4}\times\frac{g}{\nu}d_{20}^{0.3}$	$C_u < 5$ *Medium size sand*
Mbonimpa	$k=C_G\times\frac{\gamma_w}{\mu_w}(\frac{e^{3+x}}{1+e})\,C_u^{1/3}\,d_{10}^2$	$10^{-9}\ mm^2 < \frac{d_{10}^2 e^3}{1+e} < 10^2\ mm^2$ *Non-plastic soils*

Mbonimpa's equation, developed as a modification of Hazen's equation, has been tailored to accommodate a broader spectrum of non-plastic materials. Mbonimpa et al. (2002) identified C_U, C_G, and x as critical factors influencing Ks. C_G is a constant encompassing media attributes like tortuosity, particle shape, and specific surface area, while x is a constant determined by the specimen's void ratio. The values of x and C_G in Mbonimpa's equation are conventionally set at 2 and 0.1 based on numerous sample tests. However, the appropriateness of these specific values may come into question, particularly when dealing with soils exhibiting diverse particle shapes and void ratios compared to those examined in the original study.

To steer clear of assuming a universal constant, this research ventured to explore the relationship between x and void ratio, as well as C_G and C_U, to refine Mbonimpa's equation parameters. By linking x and C_G to specific soil properties, this approach aimed to tailor the equation parameters to the unique characteristics of the soils under investigation, enhancing the accuracy and applicability of Mbonimpa's equation across varying soil compositions.

Adjustments were made to the values of x and C_G in Mbonimpa's equation to minimize the discrepancy between predicted and average measured Ks values. Upon determining the optimal equation parameters for the individual specimens, the next step involved establishing the relationship between x and C_G with pertinent soil properties such as void ratio, d_{10}, and C_U. By identifying the most suitable correlations between the equation parameters and specific soil characteristics, it became feasible to replace the generic values of x and C_G in Mbonimpa's equation with specimen-specific parameters. This process, aimed at tailoring the equation to the specific properties of each soil sample, sought to enhance the precision and reliability of Ks predictions for the diverse range of specimens under examination.

4.4. Results

4.4.1. Impact of interruption and re-initiation of the test

Samples T1 and T2 were fully saturated and subjected to tests under very slight hydraulic gradients. Both saturated samples T1 and T2 were weighed before and after testing, revealing marginal difference in weight. This minor weight variance was deemed negligible and not considered a significant indicator of air entrapment within the samples, and so unlikely to introduce variations in Ks values. The flow rate versus time graphs for T1 and T2 are depicted in Figure 4.4.1. It is noteworthy that specimen T1 underwent 4 cycles of permeation under a single head, while specimen T2 underwent 2 cycles, with these cycles highlighted accordingly in the figures. Interestingly, the graphs illustrate that the flow rates inside the specimens varied at each interval of test interruption and re-initiation, denoting fluctuations in the permeation dynamics.

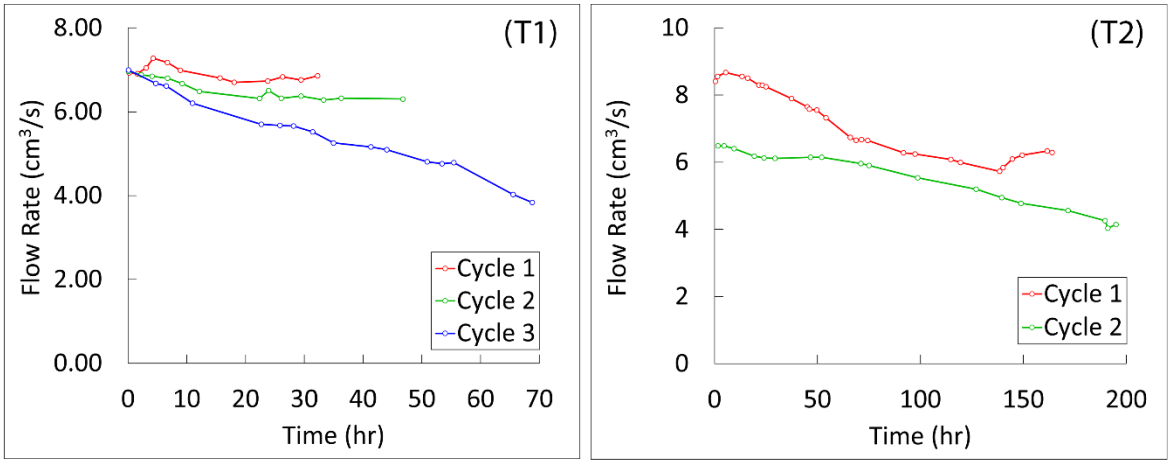

Figure 4.4.1. Flow rate of specimens T1 and T2 under single hydraulic heads with cycles of interruption and re-initiation of the test

4.4.2. Saturated hydraulic conductivity

The results of the Ks tests for the seven specimens with varying heads and the three specimens with a single hydraulic head are depicted in Figure 4.4.2. Each specimen, ranging from C1 to C7 and S1 to S3, is represented in distinct graphs to showcase the diversity in Ks values resulting from differing percentages of fine and coarse particles.

In Table 4.4.1, a statistical analysis of the Ks values for all specimens is provided, highlighting three discernible phases based on data variance. In phases 1 and 3, Ks values are closely clustered around the average with minimal variance, while phase 2 exhibits a pronounced increase in Ks over time, following a linear trajectory.

Phases 1 and 3 are visualized in different colours as indicated in the legend of Figure 4.4.2. For specimens with varying heads (C1 to C6), phase 1 Ks ranges between 1.2 to 2.8 cm/min, climbing in phase 2 to peak values between 5 to 7 cm/min in phase 3. Specimen C4 deviates slightly with a lower Ks of 3.65 cm/min, attributed to its elevated fine particle content per Table 4.3.1.

Notably, specimens S1 to S3 with a single hydraulic head, tested for approximately 50 hours, exhibit Ks values within a similar range as the specimens with varying heads. While Ks remains stable for the initial 5 hours before escalating steeply around the 25-hour mark and stabilizing once more.

A comparison across the specimens highlights the impact of varying fine and coarse particle percentages on Ks. For instance, increasing the fine particles from 8.3% in C1 to 15% in C4 results in a notable decrease in average phase 1 and 3 Ks values. On the other hand, specimens C5 and C6 demonstrate that augmenting gravels doesn't noticeably alter phase 1 and phase 3 Ks values. Moreover, the addition of aggregates to C5 and C6 leads to even lower Ks compared to samples with higher fine particle content, barring C4 due to its distinctive elevated fine percentage.

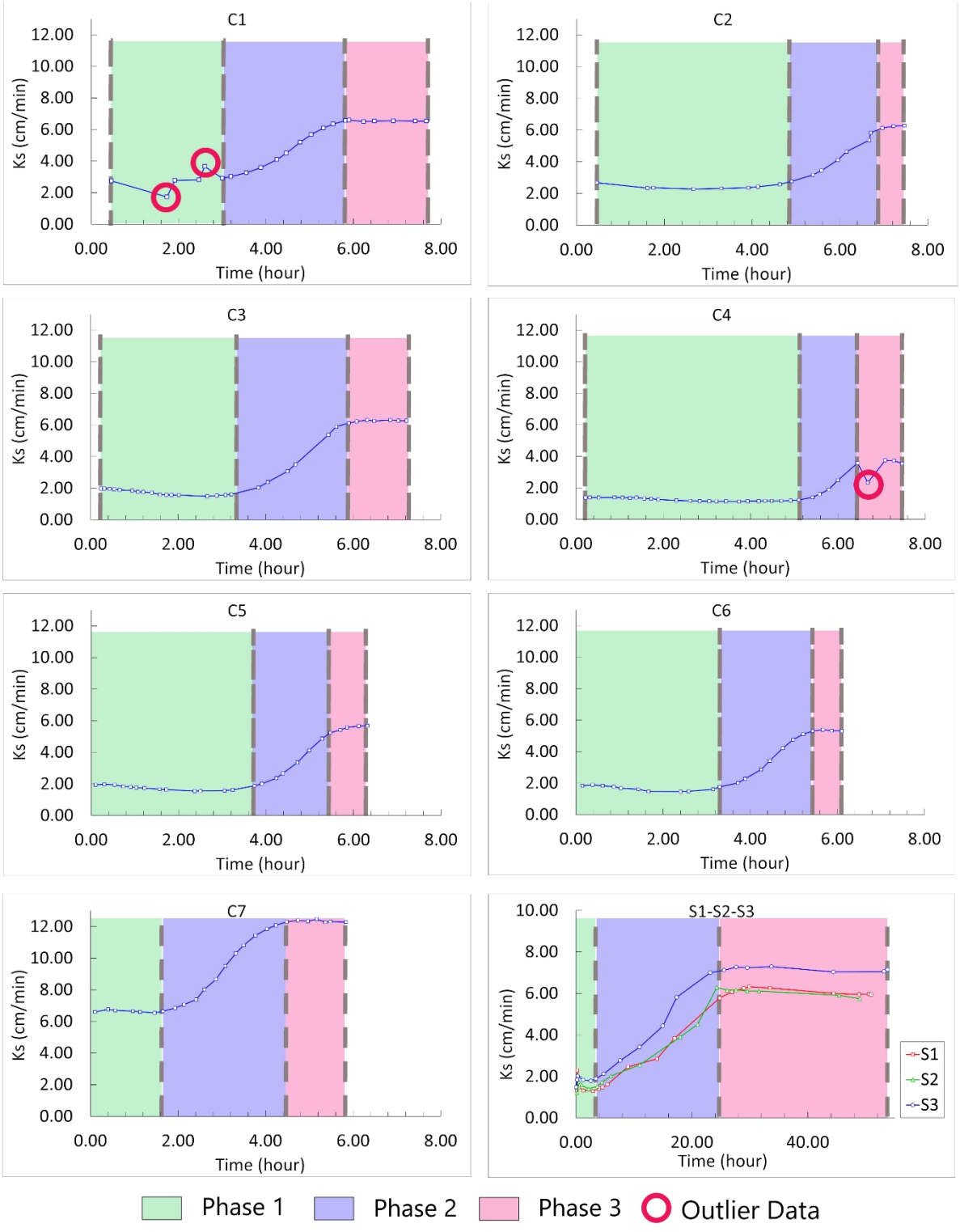

Figure 4.4.1. Changes of Ks over time in the specimens. Three phases of Ks are noticeable in the experiments and they are divided by different colour

Table 4.4.1. Average Ks and variance of the data in phase 1 and 3

Specimen	Phase 1		Phase 3	
	Average Ks (cm/min)	Variance	Average Ks (cm/min)	Variance
S1	1.43	0.01	6.10	0.02
S2	1.60	0.06	6.07	0.03
S3	1.85	0.04	7.13	0.01
C1	2.86	0.01	6.47	0.01
C2	2.42	0.02	6.24	0.01
C3	1.75	0.03	6.25	0.01
C4	1.25	0.01	3.65	0.01
C5	1.77	0.03	5.51	0.03
C6	1.70	0.03	5.30	0.01
C7	6.72	0.03	12.25	0.03

4.4.3. Relation of flow (Q) and head gradient (i)

Figure 4.4.3 demonstrates the shifts in flow rate (Q) and hydraulic gradient (i) within the specimens, showcasing a notable linearity in the Q-i relationship during Phases 1 and 3, aligning with the principles of Darcy's law and ASTM guidelines. While the ASTM guidelines do not explicitly address the three-phase behaviour observed in the soils, the linear trend in flow rate relative to hydraulic gradient is observable, indicating that an increase in hydraulic gradient leads to a corresponding rise in flow rate within the specimens. This linear trend is prevalent in both Phase 1 and Phase 3 of specimens with varying heads, reflecting a correlation with the average Ks values outlined in Table 4.4.1, with a higher correlation coefficient observed in Phase 3 compared to Phase 1.

The delineation of flow rate and hydraulic gradient into the 3 identified phases mirrors the categorization established for Ks. The transitions between these phases occur at varying hydraulic heads for different specimens. Specifically, in specimens C1, C2, C3, and C7, the shift from Phase 1 to Phase 2 commences around a hydraulic head gradient of approximately 2, whereas for specimen C4, this transition initiates at a gradient of around 3.

Conversely, in samples subjected to tests with single heads (S1, S2, and S3), there is a declining trend in the head gradient over time. Phase 1 commences at a head gradient of approximately 3 and transitions to Phase 2 around a gradient of 2. Phase 3 maintains a relatively stable head gradient of 1 to 1.5, despite displaying an increase in flow rate.

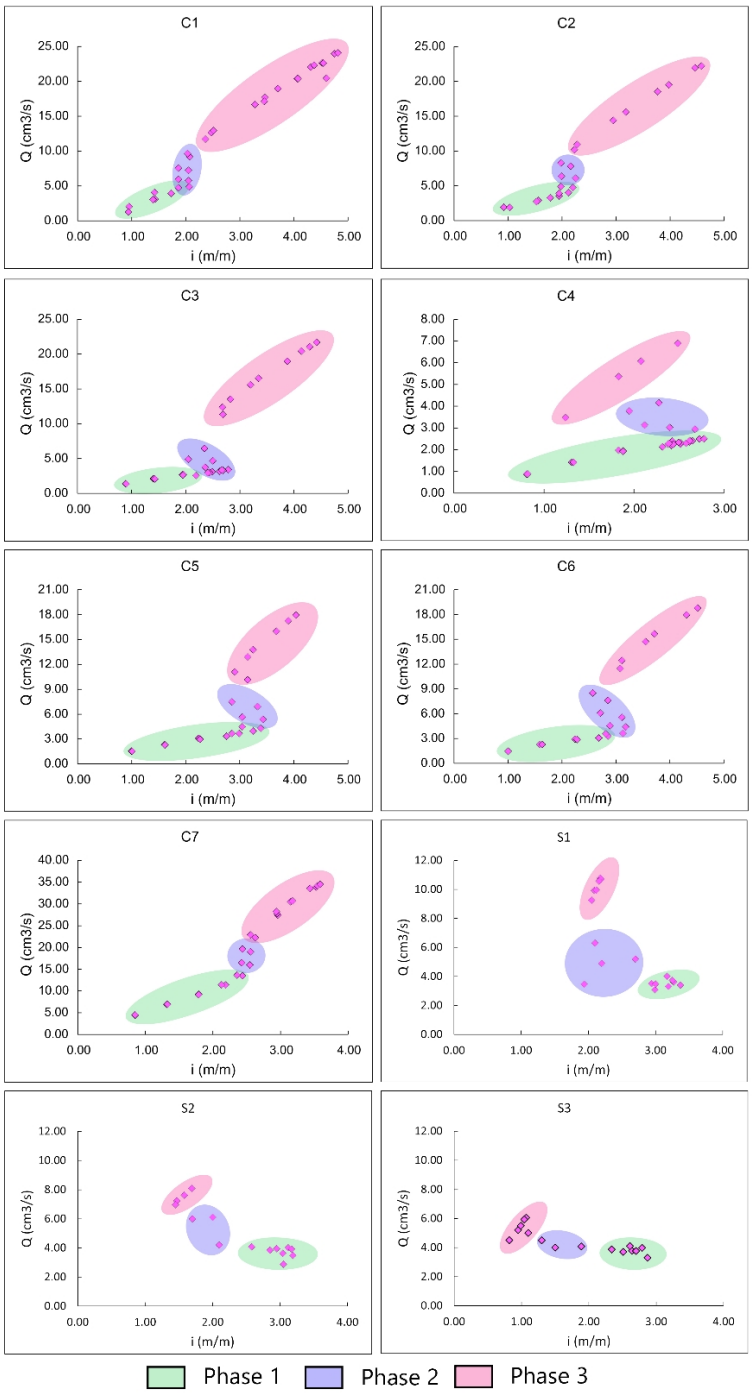

Figure 4.4.1. Q-i relationship in experiments with varying hydraulic heads

4.4.4. Pedotransfer functions

The detailed analysis and observations from Figure 4.4.4 showcase the comparison of predicted Ks values from various PTFs with measured experimental data in Phases 1 and 3 for different specimens. Noteworthy trends include the disparities between predicted Ks values and the horizontal lines representing measured Ks in Phases 1 and 3. Notably, the USBR equation, lacking considerations for void ratio and uniformity coefficient, produces the lowest predictions.

Across the spectrum of specimens, predictions from Hazen, Slitcher, Terzaghi, and Breyer exhibit considerable underestimations of Ks values compared to the measured Ks in samples with varied fine particle content (S1 to S3 and C1 to C4). Conversely, predictions align more closely with measured Ks for specimens with lower fine particle percentages (C5 to C7). Kozeny's equation demonstrates better congruence with measured Phase 1 Ks values, with Mbonimpa's equation showcasing greater alignment with Phase 3 measured data. Notably, Mbonimpa's equation provides the best predictions overall, offering estimates that straddle the measured Ks values across Phases 1 and 3 for various specimens.

Further refinements in Mbonimpa's equation involved fitting parameters 'x' and 'C_G' with soil properties like void ratio (e), coefficient of uniformity (C_U), and effective grain size (d_{10}). The optimization process highlighted the range of 'x' defined based on e and 'C_G' defined based on C_U. Visualization through Figure 4.4.5 elucidates the relationships between x-e and C_G-C_U in Phases 1 and 3, demonstrating a clearer association between 'x' and e, and 'C_G' and C_U.

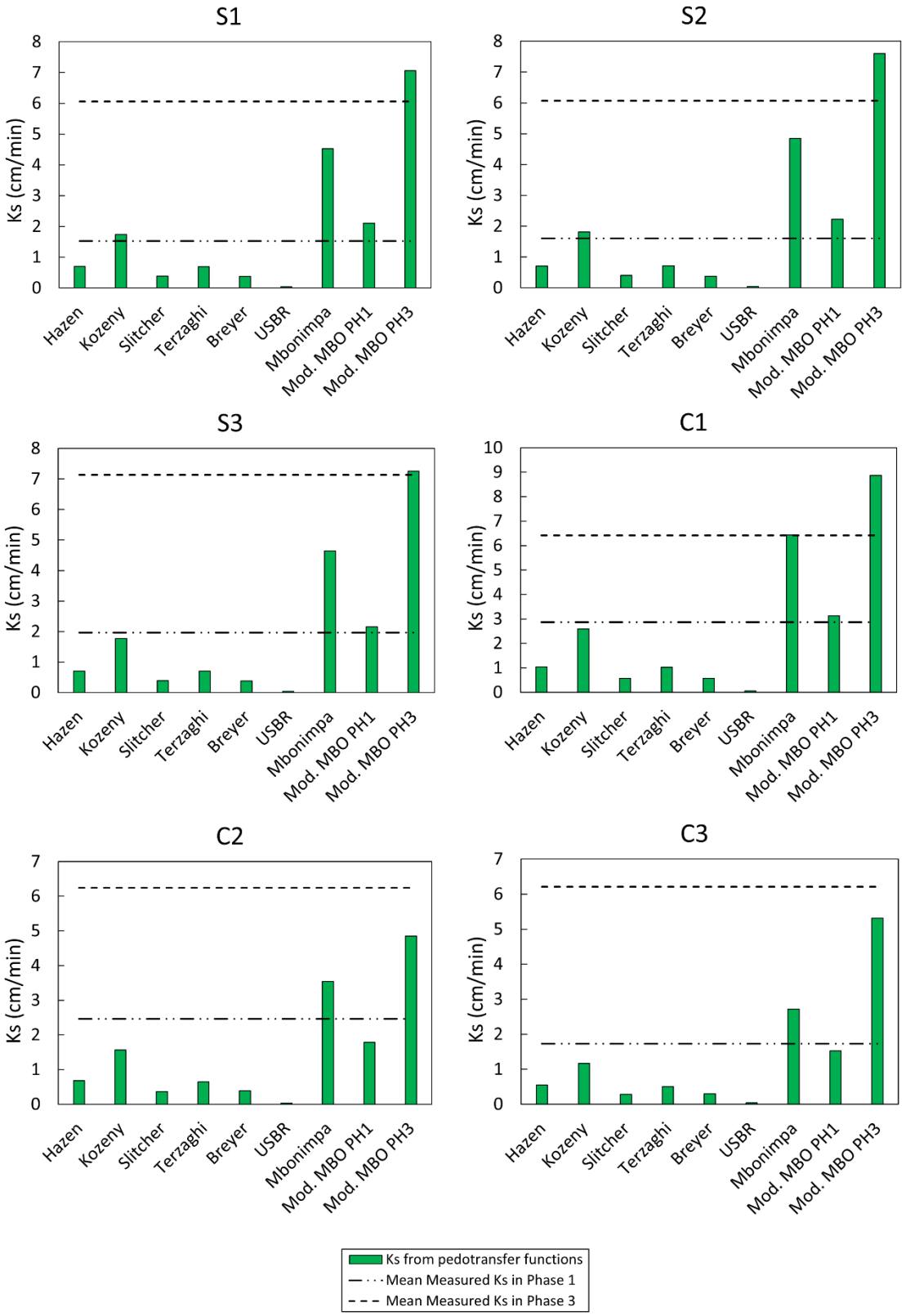

Figure 4.4.1. Comparison of PTFs and measured Ks

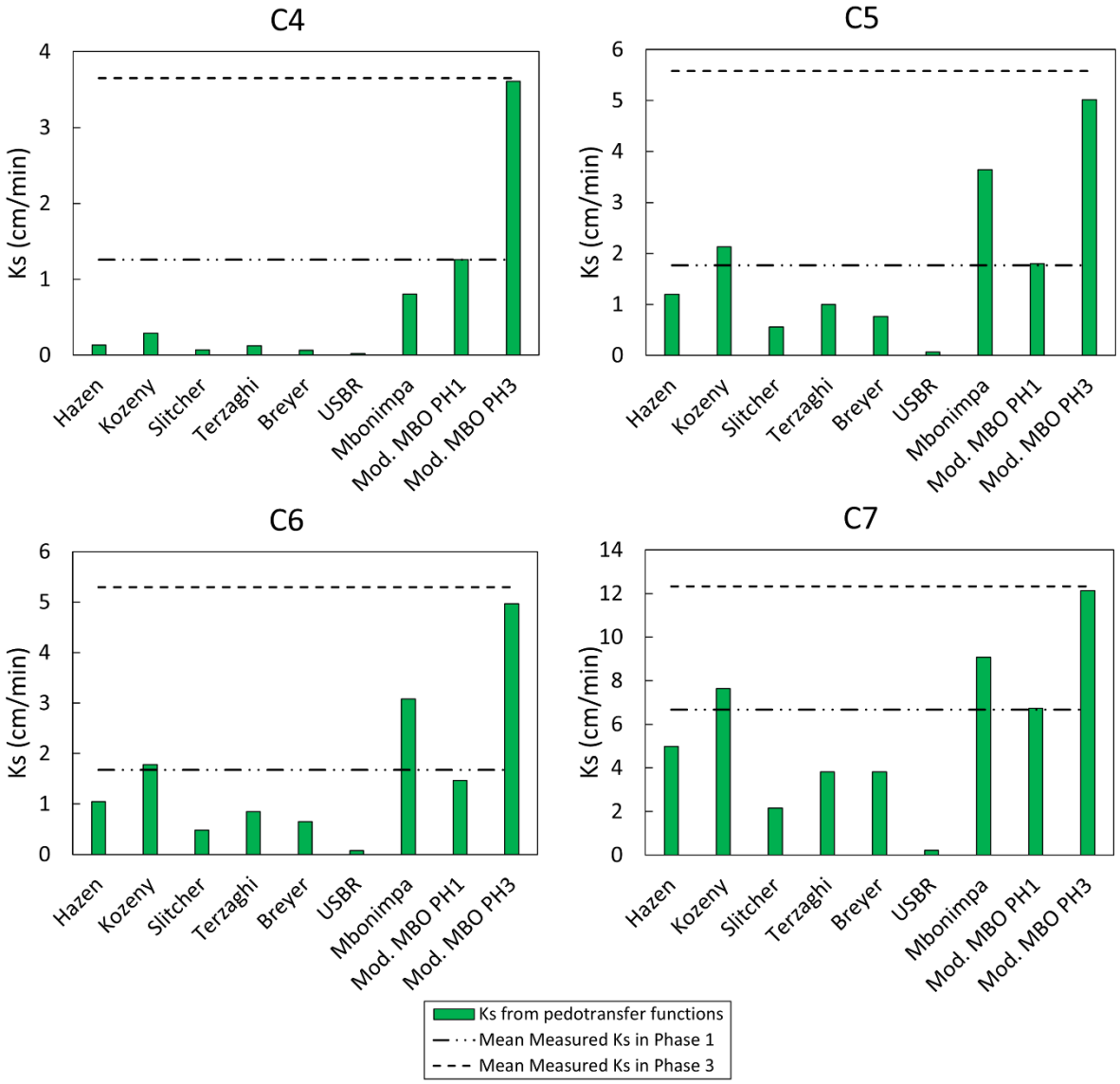

Figure 4.4.4. Comparison of PTFs and measured Ks- continued

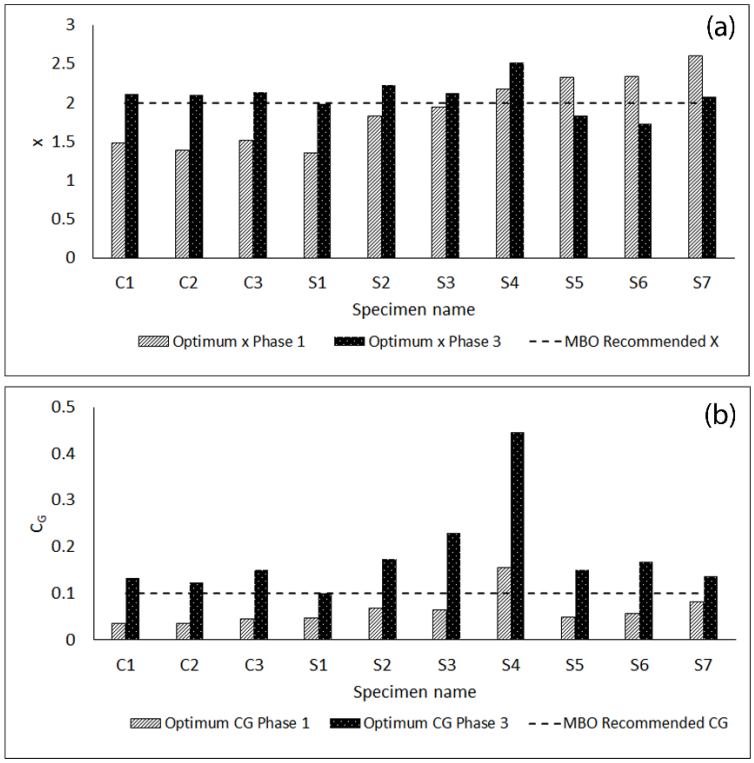

Figure 4.4.2. Comparison of optimum Mbonimpa equation parameters, x and CG, with recommended values in phases 1 and 3

4.5. Discussion

4.5.1. Saturated hydraulic conductivity tests

Sandy soils have widespread applications in various civil engineering projects and are commonly employed as filters to aid in water movement. Ensuring an accurate evaluation of the Ks of these materials, both prior to and following their utilization in construction projects, holds considerable importance. Such assessments are crucial for assuring the efficiency and functionality of backfilled sand in hydraulic and filtration applications, providing valuable insights into the performance and viability of these materials within the project environment.

As outlined in the methodology section, achieving complete saturation of specimens is a critical aspect of the testing procedure. The methodology detailed is designed to ensure a high level of sample saturation for accurate and reliable test results. It is imperative that the test setup remains undisturbed and stable throughout the testing process. Any inadvertent movement or alteration of the setup, whether for assessing saturation levels during the test or adjusting hydraulic heads, can impact the test outcomes (Chapuis, 2004). The observations from tests on specimens T1 and T2 underscore the importance of test setup stability, highlighting that each interruption and restart of the test can lead to variances in flow rates, underscoring the sensitivity of the testing environment to disruptions.

As depicted in Figure 4.4.2, the Ks values for all samples typically commence around 2 cm/min, maintaining stability at specific hydraulic heads before witnessing a marked increase characterized by a steep slope, followed by a return to stability where Ks ceases to fluctuate despite further hydraulic gradient increments. The notably lower Ks of specimen C6 can be attributed to its elevated percentage of fine particles compared to other samples.

In Phase 1, the impact of an increase in fine particles on Ks is minimal, with the specific percentages influencing Ks numbers. The observations from Figure 4.4.2 reveal that the fine particles present in the specimens primarily consist of fractures from larger pumice particles, which inherently possess high porosity. Notably, the rise in fine particles exerts a more pronounced effect on Phase 3 Ks values than Phase 1. Specimen C5, which boasts the highest fine particle percentage, exhibits the lowest final Ks compared to the other

specimens, suggesting that fine particles may impede a portion of the drainable pores, resulting in a decrease in Ks values across all phases.

Overall, it can be deduced that the presence of fine particles contributes to pore blockage, leading to reduced Ks values across all phases. However, this blocking effect is more pronounced in Phase 3, signifying a greater impact on hydraulic conductivity as hydraulic gradients increase.

The analysis of specimens S1 to S3, characterized by similar particle size distribution and subjected to comparable testing conditions under a single hydraulic head for approximately 50 hours, reveals distinct phases in the behaviour of Ks. The initial phase, Phase 1, is observed to last for about 5 hours, followed by an extended Phase 2 lasting for approximately 20 hours. This elongated Phase 2 period can be interpreted as a duration necessary for the rearrangement of drainable pores within the specimens, signifying the time required for these structural adjustments to occur under the single low head conditions.

Subsequently, after around 25 hours into the experiments, the specimens reach a state of stability, indicating the completion of the rearrangement process of drainable pores. This trend suggests that each alteration in the hydraulic head triggers a series of pore rearrangements that necessitate a distinct timeframe to achieve pore stability. The phased nature of these adjustments highlights the intricate interplay between hydraulic conditions and pore structure, underscoring the dynamic nature of hydraulic conductivity behaviour in response to varying hydraulic gradients and durations.

A notable example cited by Mavis & Wilsey (1936) demonstrates a 50% reduction in Ks over a five-day constant head test on a sandy sample. They attributed this decrease to potential sand blockages, despite using washed river sand with no fine particles to initiate these blockages. Additionally, employing very small hydraulic heads minimizes the likelihood of internal particle movement. In a similar vein, Chen et al. (2021) witnessed Ks reductions as their testing period advanced, suggesting evolving behaviours within the sandy samples over time.

Chapuis (2012) highlights the significant influence of saturation degree on Ks in sandy samples during constant head tests, emphasizing the critical need for ensuring total sample saturation. His recommendation includes the use of deaired water, flowing gradually from the bottom to the top of the cell, accompanied by vacuum pressure application during the saturation process, conditions that were adhered to in this research.

It is practical to acknowledge that continuous use of deaired water throughout the testing might be unfeasible, particularly for specimens with high Ks values, considering the challenges posed by such procedures on an ongoing basis.

The observed changes in Ks across three distinct phases may be interpreted as follows: Phase 1 represents a stage characterized by minimal Ks values associated with low hydraulic heads. Phase 2 serves as a transitional phase marked by rapid fluctuations in Ks, while Phase 3 witnesses a stabilization of Ks values.

The increase in hydraulic head may prompt the rearrangement of drainable pores or the removal of fine particles from the specimen, leading to a subsequent equilibrium in Ks. However, the Ks results from specimens such as C7, possessing a low percentage of fine particles, or specimens S1 to S3 under low hydraulic heads, continue to display multi-phase behaviour, indicating complex changes in Ks as the experiments progress. This suggests that the connectivity of drainable pores within the samples undergoes alterations over the course of the experiments, underscoring that pore connectivity may not be solely contingent upon the presence of fines or coarse particles in the specimens.

The incorporation of fine particles typically leads to a modest reduction in Phase 1 and Phase 3 Ks, reflecting a potential hindrance to overall permeability. Contrarily, the addition of coarse particles does not consistently bolster Ks values. Notably, a substantial percentage of coarse aggregates, likely exceeding 20%, appears necessary to enhance the total connectivity within the specimens. It seems that coarse particle content below 20% reduces Ks values, implying a nuanced relationship between particle size distribution and hydraulic conductivity. This underscores the intricate balance required in optimizing the particle composition of soil specimens to achieve ideal pore connectivity.

The observations from Figure 4.4.3 highlight how mixture differences among specimens influence their progression through the phases of Ks. Specifically, specimens C1, C2, C3, and C7, characterized by a lower content of fine particles, transition to phase 2 at a lower hydraulic gradient when compared to specimen C4, which contains a higher percentage of fine particles. This suggests that the presence of fine particles in the mixture may delay the onset of phase 2, requiring a higher hydraulic gradient to initiate considerable changes in Ks.

Interestingly, the behaviour exhibited by specimens C5 and C6, which have gravels in the mixture, stands out as these specimens transition to phase 2 at a higher hydraulic gradient than their counterparts. Despite the addition of coarse materials (13.1% and 20%), this

does not facilitate better connectivity among drainable pores. Instead, the evidence suggests that the incorporation of coarse particles at these proportions may obstruct water flow within the sample, thus reducing Ks.

This phenomenon underlines the complexity of soil structures and the delicate balance required to enhance Ks through particle composition. Rather than straightforwardly improving water flow, the addition of coarse material beyond certain thresholds might inadvertently hinder the efficiency of pore connectivity, demonstrating the complex interplay between particle size distribution, hydraulic gradients, and the resultant hydraulic conductivity in soil specimens.

The differential increase in Ks observed between the groups of experiments with single and varying hydraulic head conditions, despite their superficial similarities, underscores the intricate dynamics governing water flow through soil specimens. According to the Ks equation, which establishes Ks's direct proportionality with flow rate and inverse proportionality with hydraulic gradient, the underlying mechanisms driving Ks changes vary fundamentally between these experimental setups.

In the case of specimens C1 to C7, subjected to varying hydraulic head conditions, the observed increase in flow rate corresponds directly to elevations in the hydraulic gradient due to the incrementally raised water head during the tests. This scenario leads to an overall increase in Ks primarily because the rate of increase in Ks surpasses the rate of hydraulic gradient increase, making the flow more efficient through the specimen's porous medium.

Conversely, for experiments S1 to S3, where the water head remains constant, the Ks increase results from a different phenomenon: a decline in the internal hydraulic gradient alongside a rise in flow rate. This suggests a reconfiguration of the soil's internal structure, possibly through the formation of new connected pores or drainable channels, which effectively reduces the internal hydraulic resistance and facilitates an improved flow rate. This reconfiguration reaches a point where it minimizes the internal hydraulic gradient, essentially enhancing the soil's Ks under stable, unchanging external conditions.

This latter effect, observed predominantly in samples exposed to prolonged single-head conditions, hints at a natural process wherein water flow tends to reorganize the soil's microstructure towards optimizing flow paths, reducing internal resistance, and thus achieving a more efficient hydraulic system. This insight might reflect a broader

hydrological principle, suggesting that water flow within the earth operates in a manner that naturally seeks to minimize internal gradients while maximizing flow efficiency.

4.5.2. Pedotransfer functions of saturated hydraulic conductivity

The efficacy of PTFs in estimating Ks highly depends on the diversity and number of samples subjected to analysis. It is essential to evaluate the adjustment parameters derived from this research across a broader spectrum of samples and mixtures to authenticate the reliability and applicability of the suggested parameters. The relationship between C_G (a constant that encapsulates media characteristics such as tortuosity and shape) and C_u (coefficient of uniformity) in Phase 1, which has been fitted with a polynomial function exhibiting a correlation coefficient exceeding 0.9, points to a strong predictive potential. However, the absence of sufficient data for void ratios greater than 6 underscores a gap in the robustness of this fit across the entire possible range of soil characteristics.

Drawing comparisons between Ks values derived from PTFs and those measured empirically, it becomes evident that equations lacking inclusion of parameters such as d_{10} as effective grain size, C_u, and the degree of sample compaction, typically represented through void ratio (e) or porosity (n), tend to yield inferior predictions. This discrepancy underscores the importance of incorporating comprehensive soil parameters into predictive models to accurately reflect the hydraulic properties of the soil. Specifically, the pronounced underestimation attributable to the USBR equation underlines the limitations of using d_{20} alone as a predictive index for Ks, suggesting that a more multifaceted approach is necessary to capture the nuanced effects of soil texture and structure on water percolation.

This analysis highlights a critical path forward: the need for expansive testing and refinement of current predictive models to incorporate a wider range of soil characteristics, particularly those that directly influence fluid mobility through soils, such as grain size distribution, uniformity, and compaction state. By doing so, researchers and engineers can noticeably improve the accuracy of Ks predictions, enhancing the utility of these models in design, analysis, and management of geotechnical and hydrological systems.

The comparative analysis of the performance of various PTFs, including those of Hazen, Slitcher, Terzaghi, and Breyer, in relation to the USBR equation reveals insights into their effectiveness in predicting Ks across different soil types. While these equations outperform

the USBR equation, their predictive values still fall below the measured Ks values during Phase 1, indicating certain limitations in their applicability.

The varying degree of these equations' effectiveness is particularly noticeable when examining their performance across specimens with differing fine particle content. Notably, the equations perform relatively better for samples C5 to C7, which contain minimal percentages of particles below 0.075 mm. This suggests that Hazen, Slitcher, Terzaghi, and Breyer equations are more appropriate for soils with scarce fine particles, aligning with their original design considerations.

Despite the widespread use of Hazen's equation for Ks prediction in engineering practices, it is crucial to acknowledge its original development context aimed at clean sands with a d_{10} range of 0.1 to 3 mm. Even in cases where specimens meet the criteria set by Hazen's equation, such as specimens C1, C5, C6, and C7, discrepancies in prediction accuracy persist. This outcome emphasizes the complexities involved in Ks estimation and the influence of soil characteristics, particularly fine particle content, on the performance of PTFs.

Kozeny's equation stands out for its improved performance in predicting Ks values, particularly close to those observed in Phase 1 of the measurement spectrum. This accuracy, however, tends to diminish in samples C2 to C4 where a higher content of fine particles is present. The impact of increased fine particle content introduces complexities like secondary porosity, which could potentially skew the predictive accuracy of Kozeny's equation. This phenomenon has been corroborated by studies such as those by Aubertin et al. (2005) and Carrier (2003), highlighting the challenges associated with accurately predicting Ks in presence of substantial fine particles.

Notably, Mbonimpa's equation exhibits a good comparison, providing predictions that align more closely with measured Ks values across both Phase 1 and Phase 3. This equation's inclusion of the coefficient of uniformity along with accounting for void ratio and d_{10}, plays a pivotal role in its superior predictive capability. The integration of these parameters facilitates a holistic consideration of the soil's physical attributes, enhancing the equation's predictive accuracy. This comprehensive approach is possibly why Mbonimpa's equation yields results that closely match empirical observations, as supported by Yin (2009).

Optimizing the parameters of Mbonimpa's equation, specifically x and C_G, through correlation with soil properties such as void ratio (e) and coefficient of uniformity (C_U),

represents a nuanced approach to enhancing the equation's applicability and accuracy. This strategy effectively avoids reliance on universal values for x and C_G, tailoring the equation more closely to the specific characteristics of the soil being studied.

Initial findings indicate a strong correlation between x and e as well as between C_G and C_U in Phase 1 of hydraulic conductivity testing. However, during Phase 3, the correlation between x and e weakens. Despite this, sensitivity analyses reveal that predicted Ks values exhibit less susceptibility to variations in x than in C_G. Even when x ranges from 1 to 3, representing a wide spectrum, the resultant changes in Ks predictions hover around ±20%. Given the inherent level of approximation enveloping all PTFs, such deviations in the fitting quality of x during Phase 3 are deemed within acceptable bounds. This insight underscores the criticality of C_G in influencing Ks predictions, indicating that adjustments to C_G based on soil properties may yield more noticeable impacts on the accuracy of hydraulic conductivity estimations.

Although the samples used in this research cover a relatively wide range of sands with different contents of fine and coarse particles, it is still needed to test the application of modified Mbonimpa equation for a wider range of specimens. The limited range of C_U covered in this research, specifically the gap for sands with C_U values between approximately 5.5 to 10 as suggested by the absence of data in Figure 4.4.5 (b) and (d), indicates the necessity for broader testing on a more diverse array of sand specimens. Expanding the range of tested sands is essential to verify the enhanced predictability of the modified Mbonimpa equation across a broader spectrum of sandy soils, ensuring its reliability and applicability.

The modifications have notably refined Ks predictions in phase 1, demonstrating the potential of targeted equation adjustments to align predicted values closely with empirical data. However, phase 3 presents challenges in prediction accuracy, particularly for specific specimens like C1. The high sensitivity of the modified Mbonimpa equation to variations in the C_G parameter has been identified as a contributing factor to discrepancies in predicted versus measured Ks values, thus affecting the equation's overall statistical robustness (lower R^2) in phase 3.

When compared to the Kozeny-Carman equation, which is renowned for its utility in predicting Ks (Huang et al., 2011) albeit with a broad possible range of 1/3 to 3 times the measured data (Aubertin et al., 2005; Chapuis, 2004; Chapuis, 2012; Sanzeni et al., 2013), the modified Mbonimpa equation in this study showcases a narrower and closer

prediction range of 0.7 to 1.3 times the measured Ks. This improvement underscores the efficacy of the adjustments made to the Mbonimpa equation, indicating a step forward in narrowing the prediction gap and enhancing the reliability of Ks estimations for sandy soils.

Achieving a predictive model that balances accuracy across all phases of saturated hydraulic conductivity testing is a complex endeavour, given the intricate and variable nature of soil properties. However, the progress illustrated by the modified Mbonimpa equation, particularly in providing tighter prediction ranges, highlights the value of continuous research and adaptation of existing models. Through further testing and analysis, particularly focusing on underserved C_U ranges and the variability of sandy soils, the predictive accuracy and applicability of such equations can be substantially improved, offering valuable tools for hydrological and geotechnical applications.

4.6. Conclusions

The comprehensive analysis of sandy soil characteristics and their impact on Ks within specified experimental conditions yields important insights into the behaviour of these materials under various hydraulic gradients and saturation levels. The study's analysis resulted in conclusions drawn from comparing the outcomes. The key findings are listed below:

- **Importance of complete saturation.** Ensuring complete saturation of sand specimens is crucial for obtaining accurate and reliable Ks measurements. The methodology adopted effectively achieves high levels of sample saturation, emphasizing the sensitivity of Ks outcomes to test setup stability and procedural integrity.
- **Impact of fine particles on Ks.** The presence of fine particles within sandy soils tends to reduce Ks values, particularly in Phase 3 where the blocking effect of fine particles is more pronounced.
- **Dynamic behaviour of Ks under different phases.** The study identifies distinct phases (Phase 1, Phase 2, and Phase 3) in the behaviour of Ks, highlighting the complex interplay between hydraulic conditions and pore structure. Each phase demonstrates varying Ks values corresponding to different hydraulic heads and specimen composition.

- **Influence of particle size distribution.** The particle size distribution, especially the presence and ratio of fine to coarse particles, plays a critical role in determining the hydraulic conductivity of sandy soils.
- **Predictive models and equations.** The study evaluates the effectiveness of various PTFs in estimating Ks values. It finds that equations incorporating comprehensive soil parameters, such as grain size distribution and void ratio, tend to offer more accurate predictions. Specifically, Mbonimpa's equation, with adjustments for soil properties, shows promise in closely aligning predicted Ks values with empirical observations.
- **Advancements in Understanding Soil Hydraulic Behaviour:** The study contributes to a deeper understanding of the factors influencing hydraulic conductivity in sandy soils and the complex dynamics governing water flow through these materials. It also highlights the relationship between soil texture, particle composition, and hydraulic performance, offering insights into optimizing soil conditions for civil engineering applications.

This study provides valuable contributions to the field of civil engineering, presenting an understanding of sandy soils' hydraulic properties. Future research focusing on the gaps identified, particularly in predictive model refinement and broader sample testing, has the potential to considerably advance the predictability and efficiency of hydraulic conductivity assessments in sandy soils. The analysis underscores the need for expansive testing and refinement of predictive models to include a broader range of soil characteristics. Expanding the tested range of sands and refining parameters within PTFs could enhance the accuracy and applicability of these models.

Chapter 5. Using Inverse Gaussian Distribution for Analysis of Breakthrough Curves in Tracer Tests for Sandy Samples in Rigid Wall Cell

Saeed Nikghalb Ashouri[1], Adrian Pittari[2], Ali Shokri[1]

1. School of engineering, University of Waikato, Hamilton, New Zealand
2. School of Science, University of Waikato, Hamilton, New Zealand

Abstract

Tracer tests conducted in aquifers and laboratory settings serve as essential methodologies for estimating the hydraulic properties of porous media. Nevertheless, the estimation of solute transport parameters, such as the dispersion coefficient and velocity, remains a challenge. In this research, a total of 94 tracer tests were performed on nine sandy mixtures packed in a rigid wall hydraulic conductivity cell using sodium chloride (NaCl). The electrical conductivity (EC) of the effluent was continuously monitored throughout the tests, yielding breakthrough curves for each experiment. These breakthrough curves were subsequently fitted using the inverse Gaussian distribution, which proved to be simpler, less complex, and less time- and computation-intensive compared to the classical advection-dispersion model. Furthermore, the application of the Inverse Gaussian distribution resulted in better fitting of the breakthrough curves compared to the advection-dispersion model, with the model efficiency exceeding 0.9 in the majority of cases. The Inverse Gaussian distribution has the potential to be related to the hydraulic properties of samples during tracer tests, that saves considerable amount of time for making initial estimates of dispersivity and pore velocity in the advection-dispersion models.

Keywords: Tracer test; solute transport; saturated hydraulic conductivity; inverse gaussian distribution; constant head test; Breakthrough curves; advection-dispersion model

THE UNIVERSITY OF WAIKATO
Te Whare Wānanga o Waikato

Co-Authorship Form

School of Graduate Research
The University of Waikato
Private Bag 3105
Hamilton 3240, New Zealand
Phone +64 7 838 5096
Email: SGR@waikato.ac.nz
Website: http://www.waikato.ac.nz/students/research-degre

This form is to accompany the submission of any PhD that contains research reported in published or unpublished co-authored work. **Please include one copy of this form for each co-authored work**. Completed forms should be included in your appendices for all the copies of your thesis submitted for examination and library deposit (including digital deposit).

Please indicate the chapter/section/pages of this thesis that are extracted from a co-authored work and give the title and publication details or details of submission of the co-authored work.
Thesis chapter 5: Nikghalb Ashouri. S., Pittari. A., Shokri. A. (Revised and ready to be submitted to a journal). Using inverse gaussian distribution for analysis of breakthrough curves in tracer tests for sandy samples in rigid wall cell

Nature of contribution by PhD candidate	Experimental setup- data collection and analysis- writing and editing of the manuscript
Extent of contribution by PhD candidate (%)	90%

CO-AUTHORS

Name	Nature of Contribution
Ali Shokri	Provided input during experimental setup, study design, data interpretation, and revision of the manuscript
Adrian Pittari	Provided consultation and reviewing the manuscript

Certification by Co-Authors

The undersigned hereby certify that:

- the above statement correctly reflects the nature and extent of the PhD candidate's contribution to this work, and the nature of the contribution of each of the co-authors; and
- that the candidate wrote all or the majority of the text.

Name	Signature	Date
Ali Shokri		21/06/2024
Adrian Pittari	Adrian Pittari	21/06/2024

5.1. Introduction

Tracer tests are invaluable tools in hydrological studies for estimating various hydraulic properties of aquifers and flow systems. By introducing a tracer into the system and monitoring its movement, these tests provide crucial data that aid in the understanding of subsurface and surface hydrological processes, such as estimation of hydraulic conductivity and dispersivity, and travel times in the river for hydrological assessments (Hess et al., 1992; Knöll & Scheytt, 2018; Leibundgut et al., 1993; Prych, 1999; Quinton et al., 2008; ROWIŃSKI et al., 2008; Vienken et al., 2017; Yeh et al., 2000). Tracer experiments may be conducted at various spatial scales, encompassing both field and laboratory settings (Ptak et al., 2004; Seifert & Engesgaard, 2007b). Through the execution of a series of tracer tests within an aquifer and subsequent development of a model tailored to that particular aquifer, scientists can anticipate parameters such as hydraulic conductivity (Ks), arrival times, groundwater flow velocities, and the heterogeneous nature of subsurface soil strata. Hence, meticulous planning and analysis of tracer test outcomes are vital in ensuring the fidelity of the derived model with respect to soil hydraulic characteristics.

Within field settings, tracer experiments typically entail the injection of a chosen tracer element (e.g., potassium bromide, sodium chloride, potassium chloride) into a borehole. Subsequently, the changes of the tracing element's concentration, electrical conductance, or electrical resistance is monitored temporally within horizontal galleries or observation wells (Beach et al., 2005; Hördt et al., 2007; Jardani et al., 2013; Pollock & Cirpka, 2010; Prych, 1999; Ranieri et al., 2013). Vienken et al. (2017) and Passos et al. (2018) utilized salt as a tracing element for the hydraulic characterization of sedimentary formations. Alternatively, thermal energy can serve as a tracer, whereby heat generation sources and sensor arrays function as key components for detection purposes (Sarris et al., 2018).

In laboratory settings, tracer experiments are conducted on soil columns to aid in the interpretation of tracer data particularly for hydraulic tomography (HT) applications related to aquifers. Yeh et al. (2000) conducted a comparative analysis between flow rate measurements and tracer techniques to assess Ks and effective porosity in saturated clays under minimal gradients. The study suggested that while the tracer method offers more accurate results for Ks estimation, it might lead to an overestimation of effective porosity. Zhao et al. (2022) employed tracer tests to identify soil layer heterogeneity within a sandbox environment. The insights gained from HT data are useful in constructing Ks fields for the aquifer under investigation, subsequently enabling the exploration of aquifer

heterogeneity (Minutti et al., 2020). Although dye tracers find application in laboratory settings, their utility is constrained by substantial adsorption by specimens and limited to single-use scenarios per sample, making them unsuitable for studying travel times (Bloem et al., 2012)

The application of tracer tests can be constrained by time and cost considerations, potentially impacting the interpretation of soil hydraulic behaviour based on the extent of observation wells or piezometers (Jardani et al., 2013). Given the often time-intensive nature of tracer experiments, attempts have been made to streamline the acquisition of soil hydraulic properties through shortened yet precise tracer tests (Vienken et al., 2017). Some scholars have turned to minimally invasive geophysical techniques for the estimation of soil hydraulic characteristics. These inverse methodologies establish connections between geoelectrical, geomagnetic, electromagnetic, or seismic attributes and aquifer hydraulics, although their accuracy remains a subject of scrutiny (Pollock & Cirpka, 2010; Ptak et al., 2004). Consequently, geophysical methods are frequently employed alongside tracers to enhance the precision of outcomes (Qiu et al., 2023).

The process of conducting a tracer test typically involves the injection of a tracer element into a soil layer and monitoring its concentration, electrical conductivity (EC), or heat energy at another point. The collected data can be represented as breakthrough curves (BTC), illustrating the evolution of the tracing element concentration over time along with travel times. Subsequently, parameters within solute transport models are fine-tuned to align the predicted concentration or EC with the observed BTC. Traditionally, tracer BTC data are fitted using advection, dispersion, and diffusion (Fickian) equations in one or two dimensions, which have long served as key indicators of solute transport mechanisms within porous media.

While moment analysis offers an alternative method for studying solute transport in porous media, equations grounded in dispersion tend to offer superior accuracy (Bloem et al., 2012). However, accurately estimating the parameters within dispersion-based equations to reflect actual tracer movement in porous media can pose challenges. As a result, BTC data are employed to calibrate parameters within solute transport equations through curve fitting (Bloem et al., 2012; Mojid, 2024). Jardani et al. (2013) and Pollock & Cirpka (2010) have employed an inverse approach, melding saline tracer data with electrical resistivity and electrical potential tomography to elucidate soil hydraulic behavior. Singha and Gorelick (2005) conducted moment analysis on EC data from saline

tracer tests to construct tomograms between two pumping wells. Ranieri et al. (2013) utilized potassium bromide (KBr) as a tracer to evaluate artificial wetland efficiency, modelling dispersivity within the COMSOL Multiphysics environment. Jimenez et al. (2015) utilized fluorescent tracers to calibrate tomograms derived from pumping tests. Qiu et al. (2023) used an inversion method based on travel time, solving the eikonal equation derived from groundwater flow equations.

While the majority of studies typically rely on advection-dispersion equations (ADE) for interpreting tracer tests due to their extensive numerical modelling requirements, statistical distributions have the potential to be utilized in tracer tests. This shift is motivated by the high accuracy and comparatively lower computational demands associated with statistical approaches (Fienen et al., 2006). In geothermal contexts, the relationship between tracer responses depicted through fractal Gaussian distributions and one-sided Gaussian distributions of permeability serves to illuminate connectivity between injection and production wells (Weir, 2018). Fienen et al. (2006) , on the other hand, employed a Bayesian geostatistical technique to deduce transfer functions for tracer tests.

For the analysis of positively skewed data like BTCs, the Inverse Gaussian distribution (IG) finds varied applications (Niu et al., 2014) owing to its theoretical resemblance to the normal distribution (Tian, 2006). The IG distribution finds utility across diverse fields such as the stock market, biology, hydrology, electronics, reliability, and generalized linear modelling (Punzo, 2019; Villaseñor et al., 2019; J. Wang et al., 2023). Extensive applications of the IG distribution can be explored in Chhikara (1988), showcasing its efficacy in transitioning from highly skewed to normal patterns (Tian, 2006). Originally developed for characterizing particle movement under Brownian motion processes (Nagatsuka & Balakrishnan, 2013), the IG distribution was used to describe particle movement in gases or liquids under free or externally influenced conditions in open space (J.-C. Wu et al., 2019). However, the capability of the IG distribution in analysing tracer tests within porous media remains unexplored.

In the current study, NaCl was employed as a tracer element, with EC measurements used to generate BTCs for sandy samples within a laboratory setting. A total of nine samples (comprising two long-term and seven short-term tests) underwent 94 different tracer injection experiments. Subsequently, the IG distribution was parameterized to fit the BTCs. An aim of this research is to demonstrate the promising potential of statistical methods in

describing solute transport within porous media and to compare prediction accuracy with classical ADE.

5.2. Materials and Methods

5.2.1. Specimens

The soil material initially utilized in the study is loose sandy material known commercially as pit sand, containing around 8% fine particles (below 0.075 mm) and sourced from riverbanks. This pit sand exhibits a characteristic yellow colour and X-ray diffraction (XRD) analysis indicated the dominant minerals present are quartz and feldspar. There are also pumice (11%) and rock fragments in the mixture. The detailed particle counting of the mixtures are presented in Nikghalb Ashouri et al. (2023) who used similar mixtures for the tests.

To capture a diverse range of tracer data across varying grain size mixtures, hydraulic heads, and Ks test durations, nine distinct samples were constructed from the original pit sand. The specifics of these samples are outlined in Table 5.2.1. Samples L1 and L2 corresponded to the original pit sands, while samples C1 to C7 featured varying proportions of fine and coarse particles. The particle size distributions (PSD) of these samples were assessed using a laser diffractometer (Malvern Mastersizer 3000 by Malvern Panalytical), and the specific gravity of particles was determined utilizing a gas pycnometer (Quantachrome Ultrapycnometer 1000).

Table 5.2.1. Properties of the specimens used in the experiments

Parameter	Specimen								
	L1	**L2**	**C1**	**C2**	**C3**	**C4**	**C5**	**C6**	**C7**
Particles below 0.075 mm (%)	7.36	8.43	8.3	9.8	10.5	15.1	7.2	7.7	0.9
Particles between 0.075-2 mm (%)	92.61	91.56	91.7	90.2	89.5	84.9	79.7	72.3	99.1
Particles above 2 mm (%)	0.0	0.0	0.0	0.0	0.0	0.0	13.1	20.0	0.0
G_S	2.67		2.68	2.69	2.67	2.68	2.74	2.72	2.86
Dry Bulk density (gr/cm^3)	1.289	1.261	1.26	1.30	1.32	1.31	1.42	1.43	1.55

5.2.2. Short and long-term constant head Ks tests

In this study, the terms "short-term" and "long-term" are employed to differentiate between 1-day and multi-day Ks experiments. While it is understood that the determination of Ks and tracer tests may typically extend beyond the test periods in this research, the use of "long-term" for tracer tests on highly permeable samples in a laboratory setting is deemed appropriate.

The constant head Ks tests were conducted using a setup featuring an adjustable height for the inlet pressure head. These tests were conducted continuously for each specimen, with alterations in head height not disrupting water permeation. Specimens C1 to C7 were subjected to permanently increasing hydraulic head levels, whereas the hydraulic heads for specimens L1 and L2 followed an order of increase followed by decrease. The specific hydraulic head values utilized for each specimen are detailed in Table 5.2.2.

Table 5.2.1. Hydraulic heads used in the constant head tests for each specimen

Specimen	**Hydraulic heads**
C1 to C7	591 – 697 – 805 – 911 – 1018 – 1127 – 1231 – 1339 – 1527 – 1624 – 1758
L1 and L2	963 – 1163 – 1365 – 1558 – 1765 – 1558 – 1365 – 1163 – 963

5.2.3. Calibration of tracer probe

In the research, the EC of the effluent was measured using an EC probe (ProQuatro Multiparameter Meter by YSI). The probe underwent calibration using reference solutions of varying NaCl concentrations to establish the EC-concentration relationship. The resulting EC-concentration graph was utilized to convert EC readings to concentration values during the experiments. Notably, Figure 5.2.1 demonstrates a coefficient of determination (R^2) close to 1, indicating a strong correlation between EC and concentration. This correlation was achieved by fitting the calibration data using a power function. However, it is observed that at high salt concentrations (exceeding 80,000 mg/lit), the data begins to deviate from the fitted line. Consequently, in all tracer tests, the saline solution was prepared to ensure concentrations within the specimens remained below 80,000 mg/lit.

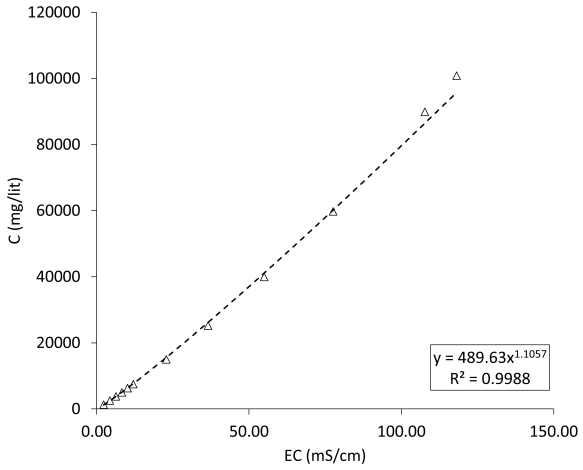

Figure 5.2.1. Correlation of EC measured by ProQuatro probe and reference concentration solutions

5.2.4. Tracer tests

NaCl is a commonly employed tracer compound in various studies focusing on solute transport within porous media (Chabokpour, 2020; Mitrinović et al., 2019; Seifert & Engesgaard, 2007b). Its popularity stems from its cost-effectiveness and the ease with which it can be continuously and automatically detected by EC probes. The assumption was made that NaCl exerts minimal impact on the hydraulic properties of the specimens, and its sorption effects are negligible, given that tracer tests are allowed to run until all salt is recovered in the effluent. In most experiments, tracer data was recorded until the

EC of the outflow returned to the EC value before each test to confirm complete salt recovery from the specimen.

During the experiments, the tracer was injected into the flow carrying tube using a small injection syringe as a sudden short pulse or Dirac pulse (Fienen et al., 2006). Subsequently, EC measurements in the effluent were continuously monitored using an EC probe until the readings reverted to the initial value, indicating complete salt recovery. In cases where the Ks was low, salt recovery took an extended period beyond the probe's memory capacity, leading to incomplete recovery in some tracer test EC measurement graphs.

Given the multiple tracer tests conducted, a systematic naming convention was adopted to differentiate between experiments. The first part of the tracer test name identifies the specimen, the second part indicates the hydraulic head in millimetres, and the third part denotes the day since the commencement of continuous Ks testing. The day designation is solely relevant for long-term Ks tests that extended over multiple days. Also, the “R” suffix at the end of some long-term tests indicates the head reducing phase of multiple day tests. For example, L1-1558R-D3 signifies the tracer test conducted on specimen L1, at a hydraulic head of 1558 mm during a head reduction (R), on the third day of continuous Ks testing on the specimen.

5.2.5. Inverse Gaussian

The IG distribution serves as a statistical tool with diverse applications, particularly in models involving stochastic processes (Johnson et al., 1994) where data deviates from a normal distribution. IG distribution finds utility in scenarios where data exhibit positive skewness (Leiva et al., 2008). In the context of expressing the movement of a particle along a linear pathway, the IG distribution can be expressed by (Johnson et al., 1994; Tian, 2006):

$$f\left(t;\mu,\lambda\right) = \left\{\frac{\lambda}{2\pi t^3}\right\}^{1/2} exp\left[-\frac{\lambda\{t-\mu\}^2}{2\mu^2 t}\right], \qquad t,\ \mu,\ \lambda>0 \tag{1}$$

where μ and λ are the shape and scale parameters respectively, and t is the time.

A scaling factor "c" is necessary as a multiplier to align the tracer data with the IG distribution. This parameter serves as a tracer concentration scale factor, dictated by the concentration of the tracer solution introduced into the sample.

The accuracy of the IG distribution was evaluated by calculating the root mean squared error (RMSE) and Nash-Sutcliffe efficiency (NSE) for both the measured and simulated BTCs. RMSE serves as a metric to assess how well a model predicts quantitative data. It is computed as the square root of the average of the squared errors between the predicted and observed values. RMSE is a key performance indicator for regression models, offering insight into the model's predictive capability.

On the other hand, NSE functions as an indicator of goodness of fit, representing the ratio of the mean squared error of the model to the variance of the observed data. An unbiased model will yield an NSE value ranging between 0 and 1 (McCuen et al., 2006). A value of NSE close to 1 indicates highly reliable predictions, while an NSE close to 0 shows that the mean of the observations is a better predictor than the model. An NSE below 0 signifies an unreliable model (Tian et al., 2024). The calculations for RMSE and NSE (Nash & Sutcliffe, 1970) are as follows:

$$RMSE = \sqrt{\frac{\sum (C_m - C_p)}{n}} \tag{2}$$

$$NSE = 1 - \frac{\sum (C_m - C_p)^2}{\sum (C_m - \overline{C_m})^2} \tag{3}$$

Where C_m is the measured concentration and C_p is the predicted concentration, $\overline{C_m}$ is the average of the measured concentrations, and n is the number of recorded concentrations.

To determine the parameters of the IG distribution, Microsoft Excel Solver was employed with the objective of minimizing the root mean squared error (RMSE) between the measured and predicted concentrations.

5.2.6. Comparison of accuracy and usability of IG distribution

In order to assess and compare the efficacy, precision, complexity, and computational requirements of fitting BTCs using an IG distribution against models based on conventional ADE, two distinct methodologies were employed. ADE models utilize parameters such as pore water velocity and dispersion coefficient to align observed and anticipated BTC data. The initial approach involved contrasting the outcomes of curve

fitting utilizing IG with an ADE model, while the second approach applied the IG distribution to additional datasets sourced from other studies (Ani et al., 2009; Zhao et al., 2022).

A specific dataset (C7-697) was arbitrarily selected for BTC fitting using an ADE model, with the intention of potentially replicating this process across other datasets within the same study. The parameters of the solute transport model were fine-tuned to minimize deviations between observed and predicted normal concentrations for C7-697. Calibration of these parameters was executed using the STANMOD toolbox (Simunek et al., 1999) and the CXFIT module (Torride et al., 1999) within the software environment. CXFIT, a Microsoft Windows-based package, provides functionality for assessing solute transport parameters under various groundwater flow conditions using the classical ADE (van Genuchten, Simunek, Leij, Toride, et al., 2012).

Within the CXFIT toolkit, a deterministic equilibrium model was employed in conjunction with resident concentration mode to accommodate continuous monitoring of NaCl EC in outflow, alongside a Dirac pulse representing the abrupt tracer injection. The ADE parameters, encompassing dispersion coefficient and pore water velocity, were calibrated to align the observed and predicted BTCs. While the CXFIT module includes an inverse problem option for estimating ADE parameters from BTC data, it was deliberately not utilized due to concerns about potentially unreliable determinations of dispersion coefficient and pore water velocity (van Genuchten et al., 2012).

The selection of a single BTC dataset was based on the research focus of evaluating the IG distribution's capabilities rather than delving into solute transport parameters using ADE models. The intent was to highlight methodological comparisons within a single dataset as adequate for the research scope. Notably, estimation of solute transport parameters for individual datasets using ADE models in CXFIT is time-intensive and challenging.

As the next step, the BTC data were extracted from two additional studies that involved calibrating ADE models. In one study, Zhao et al. (2022) employed the classical ADE to predict the Ks in sandbox tracer tests, enhancing predictions through hydraulic tomography. Hydraulic tomography measurements were conducted across multiple ports (measurement points), with specific emphasis placed on data from four selected ports for comparison. In separate research, Ani et al. (2009) utilized tracer tests to evaluate ADE model parameters in four reaches of a river.

5.3. Results

5.3.1. Saturated hydraulic conductivity

The Ks values for all specimens are visualized in Figure 5.3.1. The time axis on Figure 5.3.1 has been normalized relative to the total duration of each test to include all experiments into a single graph, thus eliminating the differences in test durations.

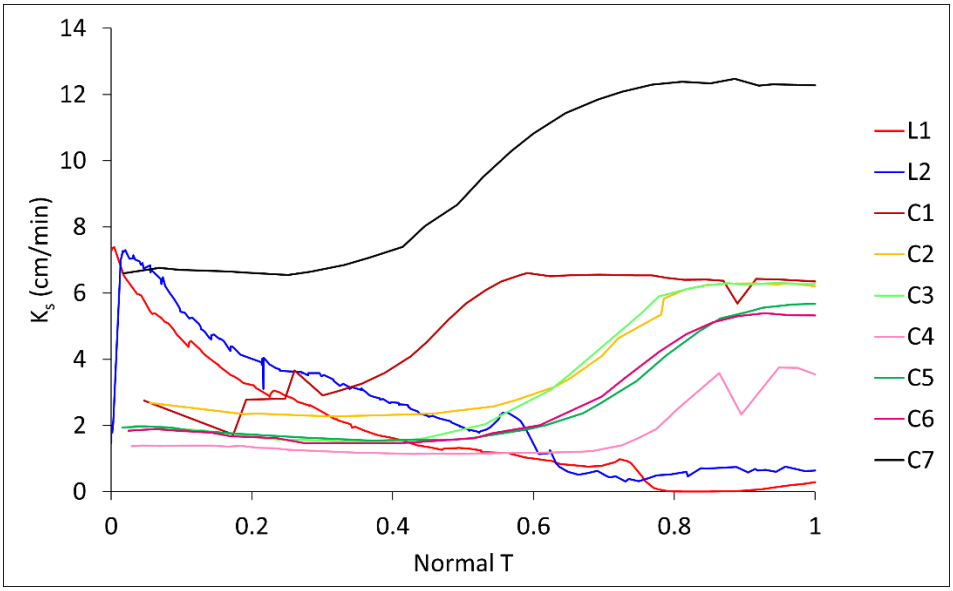

Figure 5.3.1. Saturated hydraulic conductivity (Ks) of all specimens- The time is normalized based on the total duration of each test

5.3.2. Tracer experiments on long and short Ks tests and BTCs

In Figures 5.3.2 to 5.3.10, BTCs are referenced. Within these BTCs, tracer experiments are designated by numbers in black circles, organized to illustrate the sequence of peak arrival times in a coherent manner from left to right, with the corresponding experiment number indicated next to it. An example within Figure 5.3.2 highlights that the peak arrival time of the first tracer experiment, L1-963, surpasses that of experiment L1-1163-D3, the third in sequence.

In the concentration versus time graph, certain peak arrival times were notably prolonged due to the lower Ks of the relevant phases. Specifically, in L1-1163R and L1-963R, concentration peaks manifest after 4452 and 2249 seconds. This delayed peak occurrence

is limited to these two cases and is omitted from the graph to prevent obscuring other peaks by extending the horizontal axis.

Observing the short-term Ks tests reveals a consistent decrease in peak arrival time with increasing hydraulic head, conversely, this pattern is not universal in long-term experiments. Examining the arrangement of numbers in the black circles in Figures 5.3.2 and 5.3.3, it becomes evident that for specimens L1 and L2, an elevation in hydraulic head does not invariably result in faster peak arrival times. For instance, in Figure 5.3.2, experiment 11 (L1-1765-D6) at the highest hydraulic head exhibits a considerably slower peak arrival time compared to experiment 2 (L1-1163-D1) with a lower head. Similarly, in Figure 5.3.3, the peak arrival time of experiment 14 (L2-1365-D1) is swifter than that of experiment 15 (L2-1765-D5).

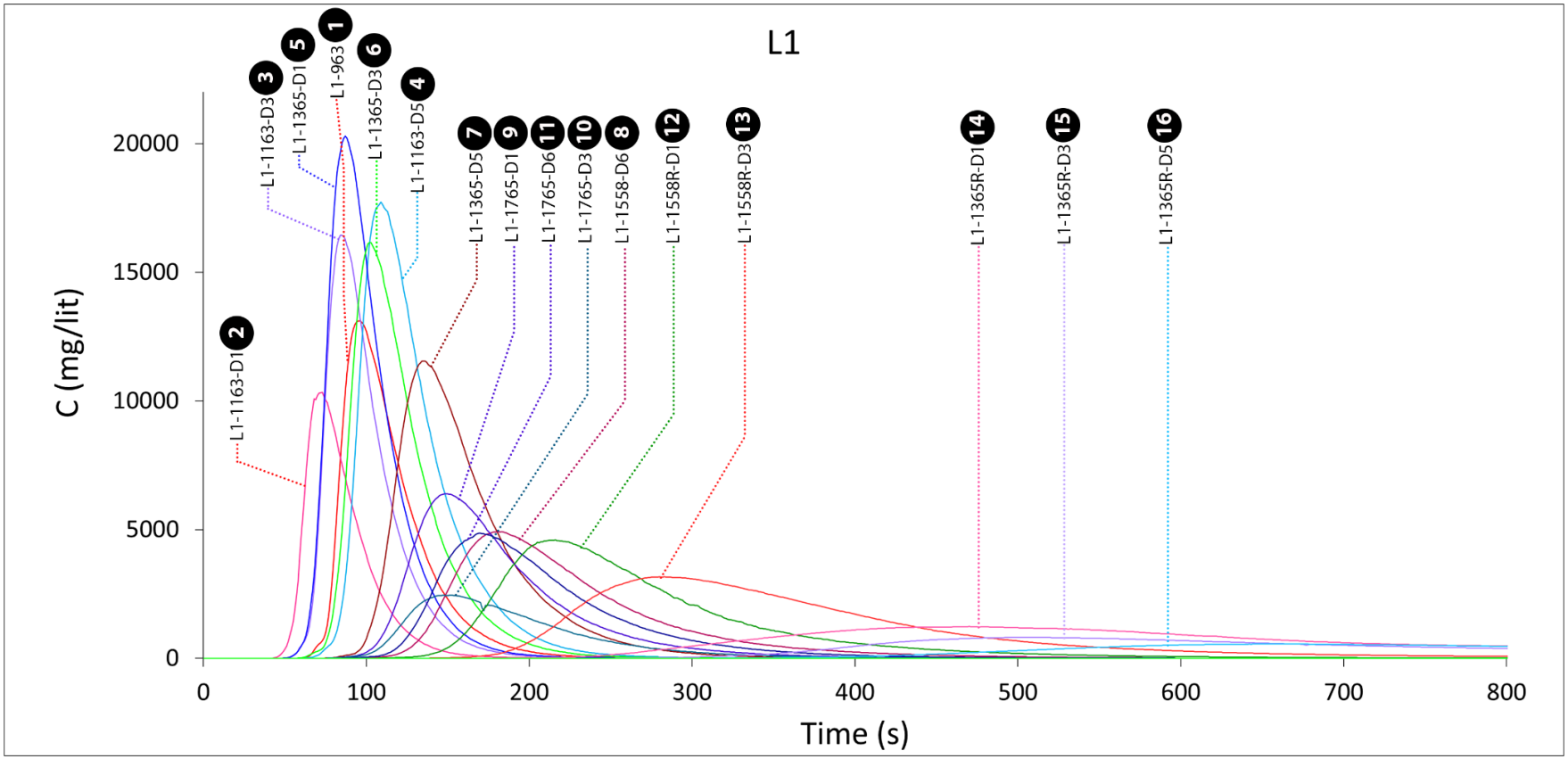

Figure 5.3.1. Breakthrough curves for specimen L1 in different hydraulic heads. The numbers in circles show the order of experiments

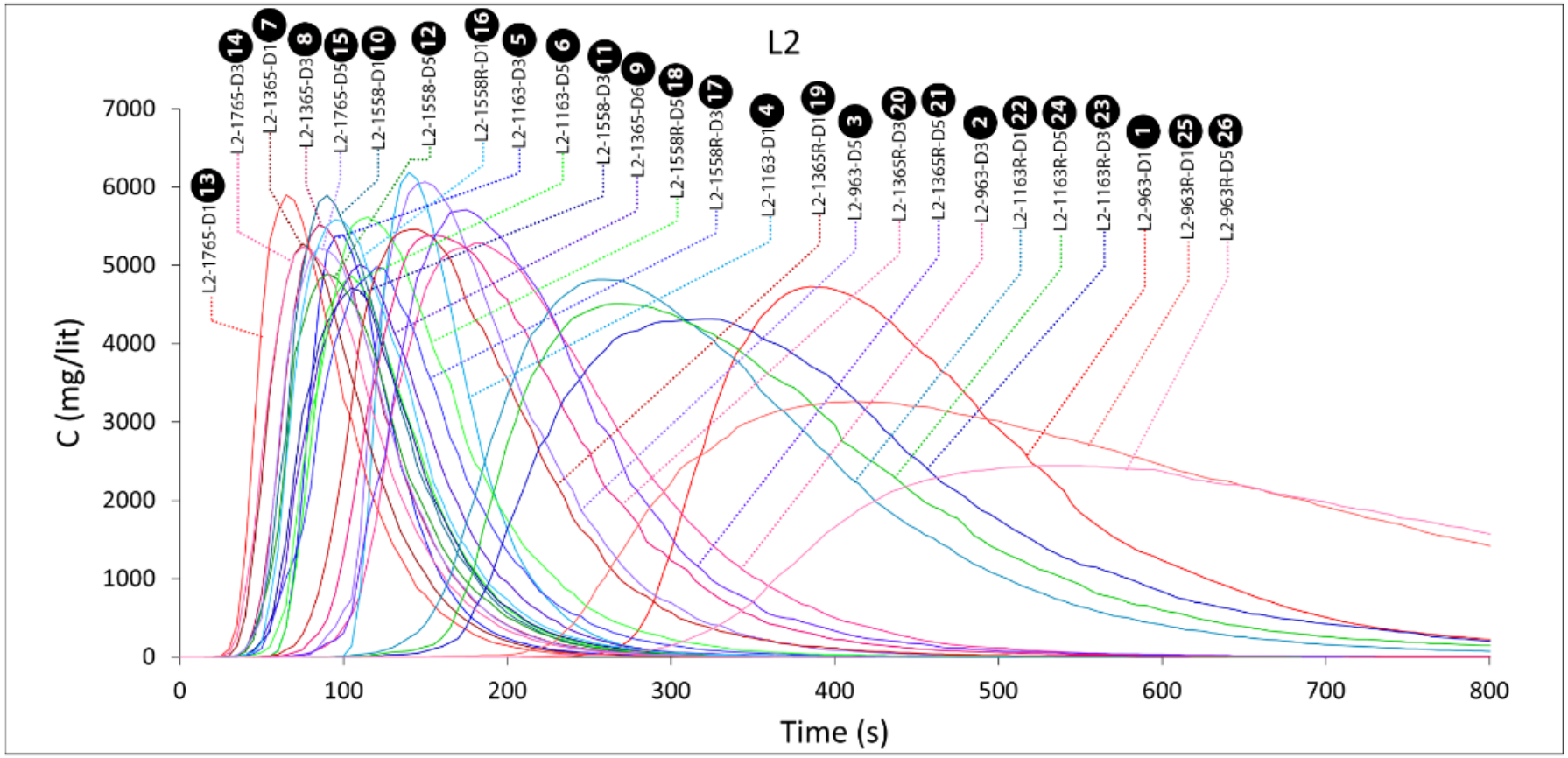

Figure 5.3.2. Breakthrough curves for specimen L2 in different hydraulic heads. The numbers in circles show the order of experiments

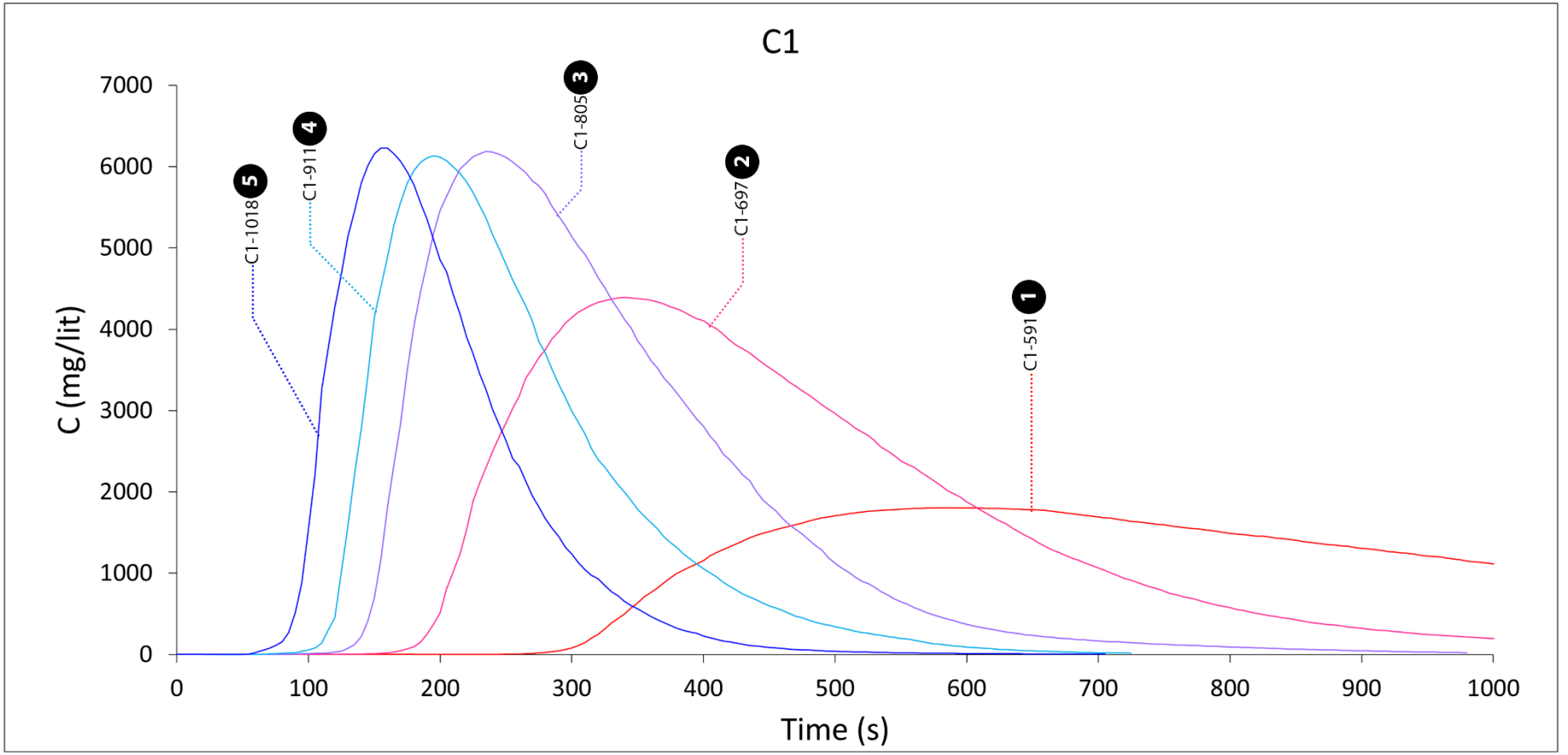

Figure 5.3.3. Breakthrough curves for specimen C1 in different hydraulic heads. The numbers in circles show the order of experiments

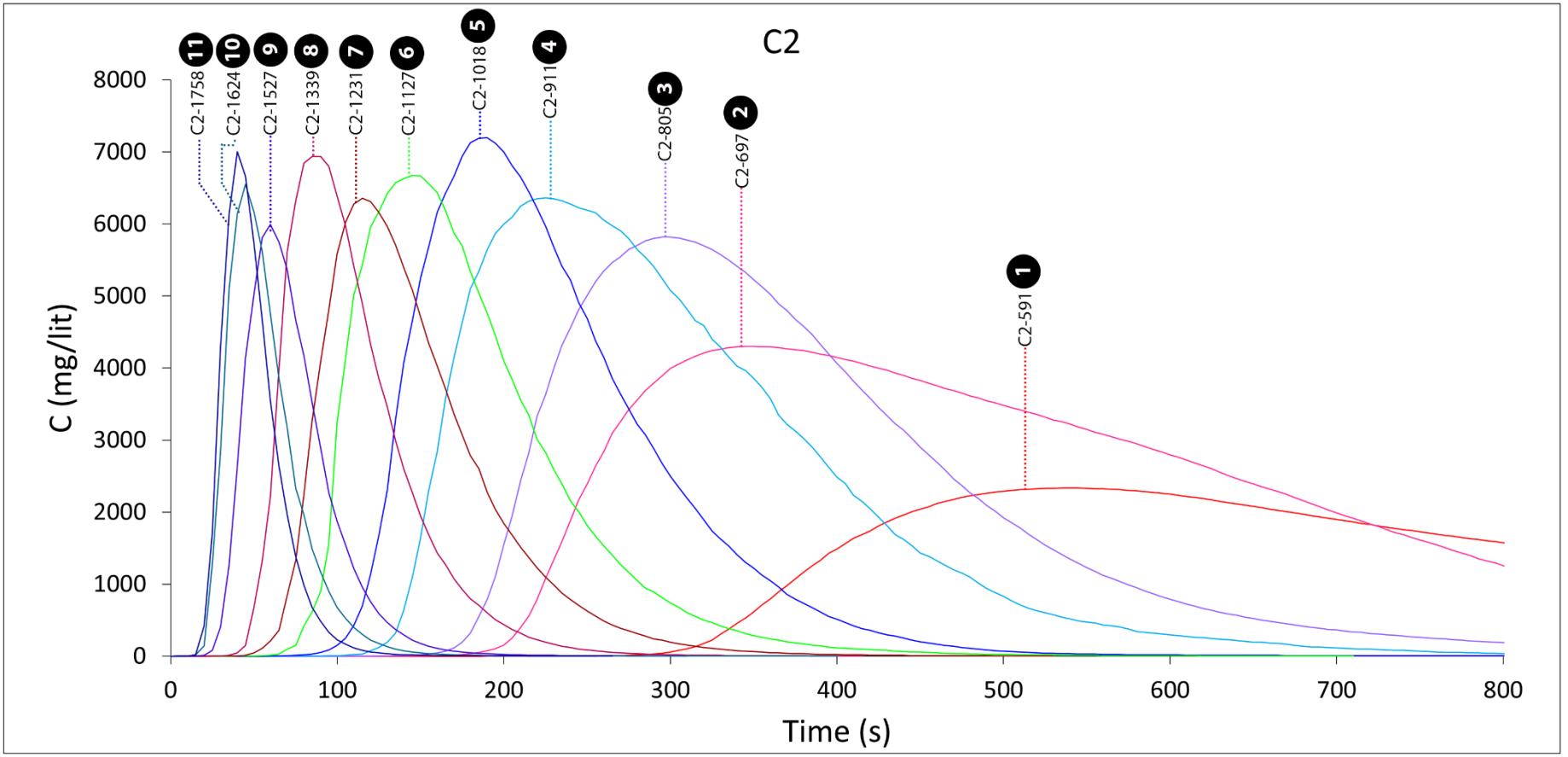

Figure 5.3.4. Breakthrough curves for specimen C2 in different hydraulic heads. The numbers in circles show the order of experiments

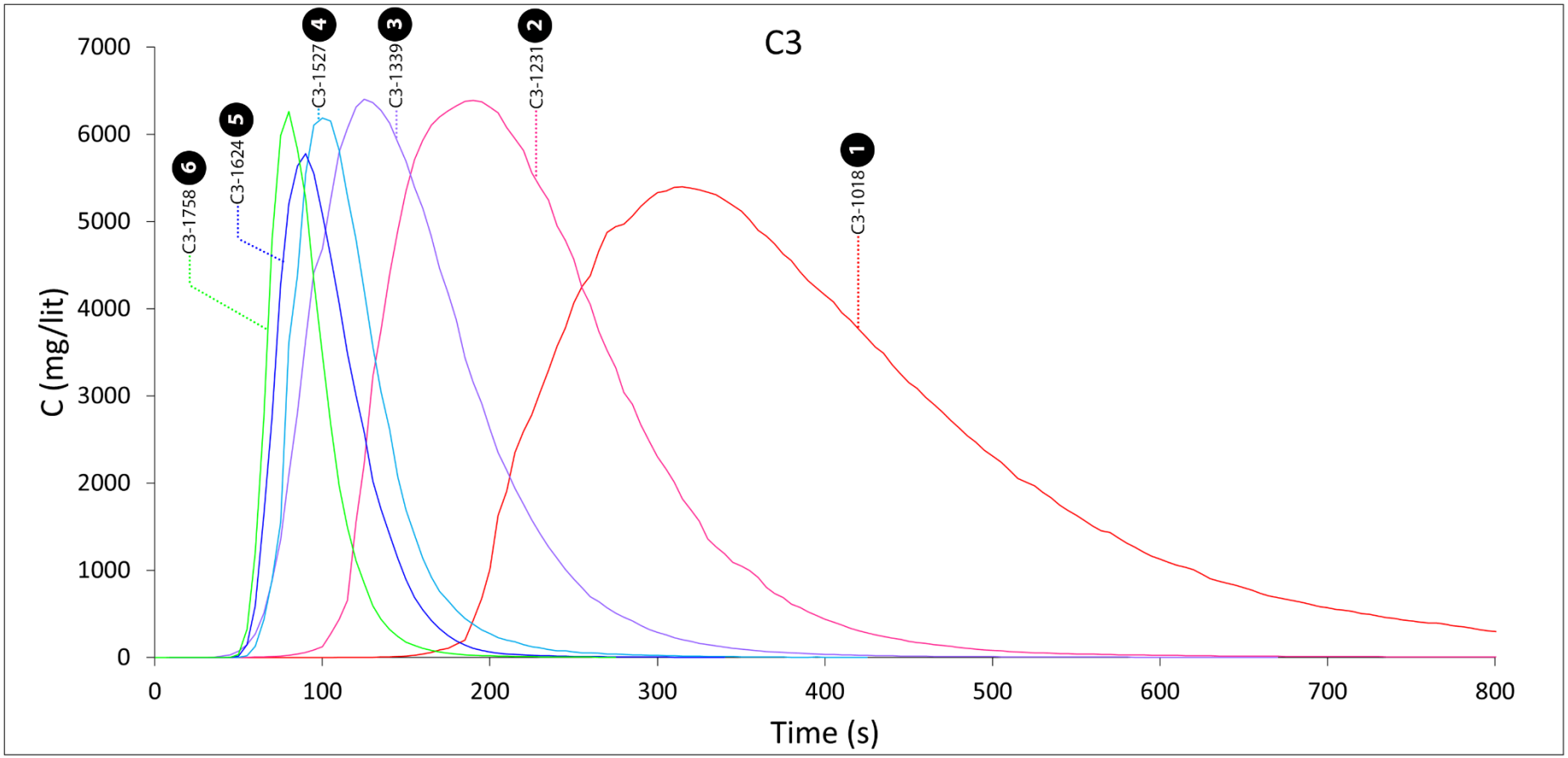

Figure 5.3.5. Breakthrough curves for specimen C3 in different hydraulic heads. The numbers in circles show the order of experiments

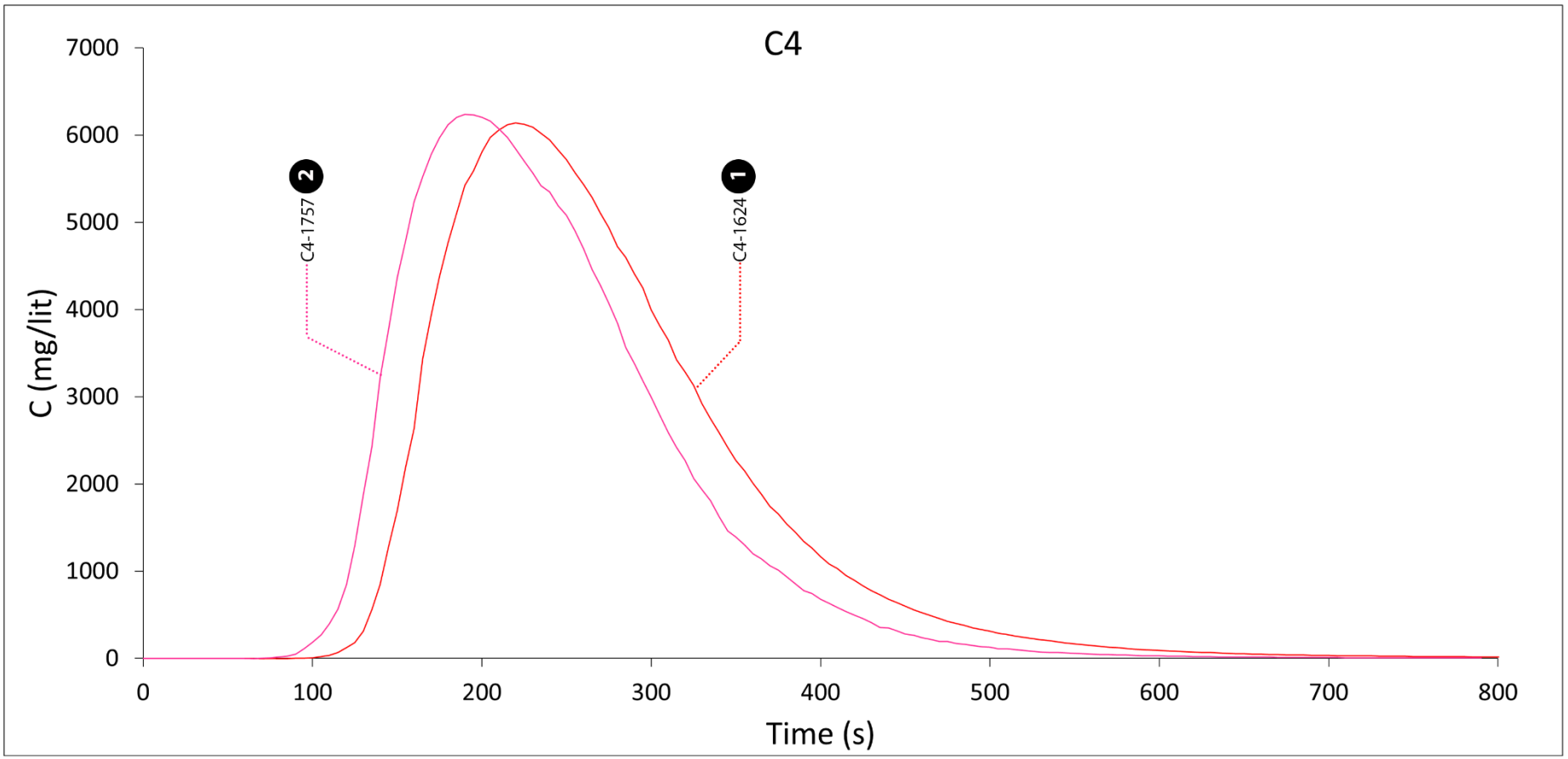

Figure 5.3.6. Breakthrough curves for specimen C4 in different hydraulic heads. The numbers in circles show the order of experiments

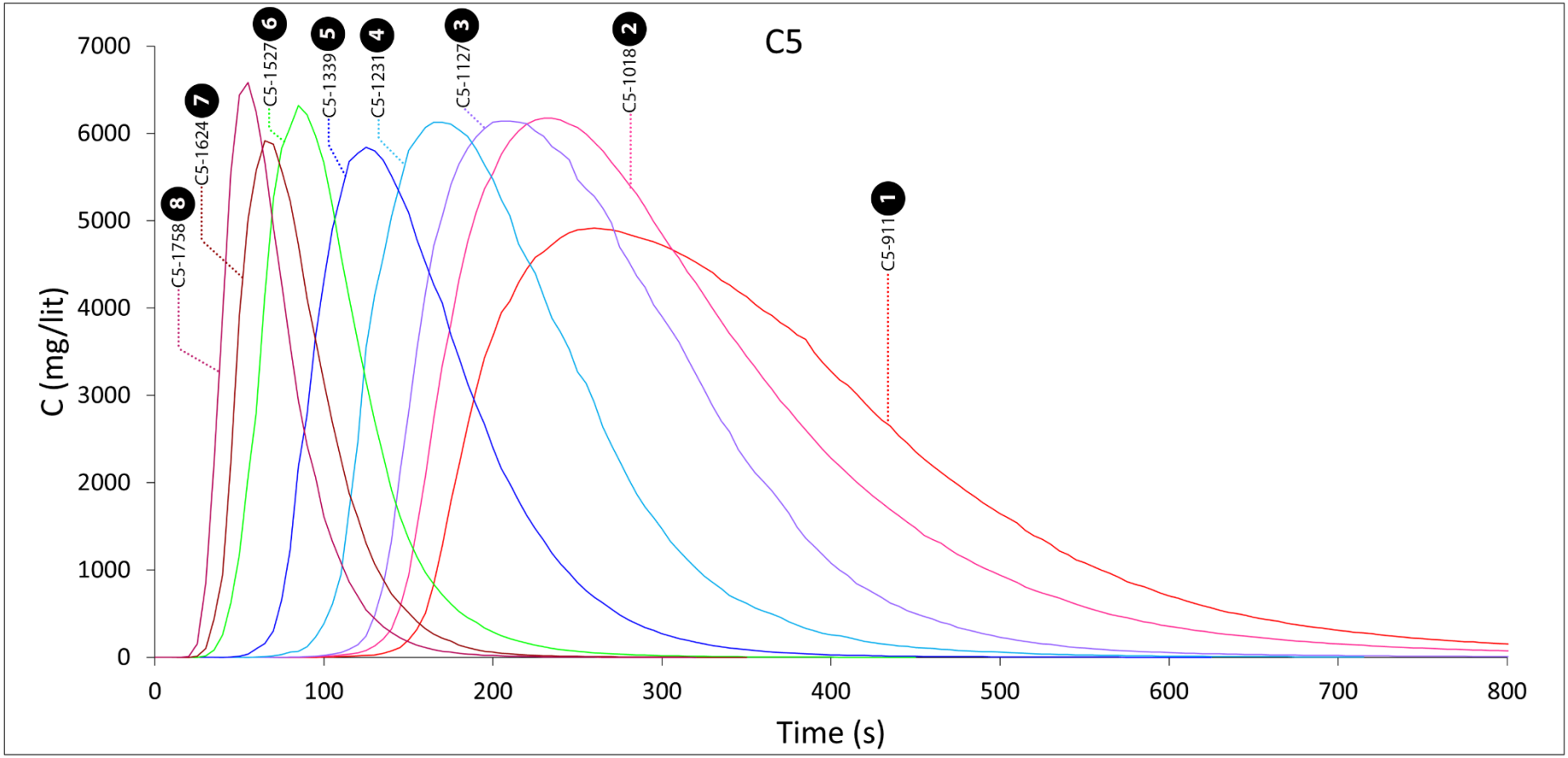

Figure 5.3.7. Breakthrough curves for specimen C5 in different hydraulic heads. The numbers in circles show the order of experiments

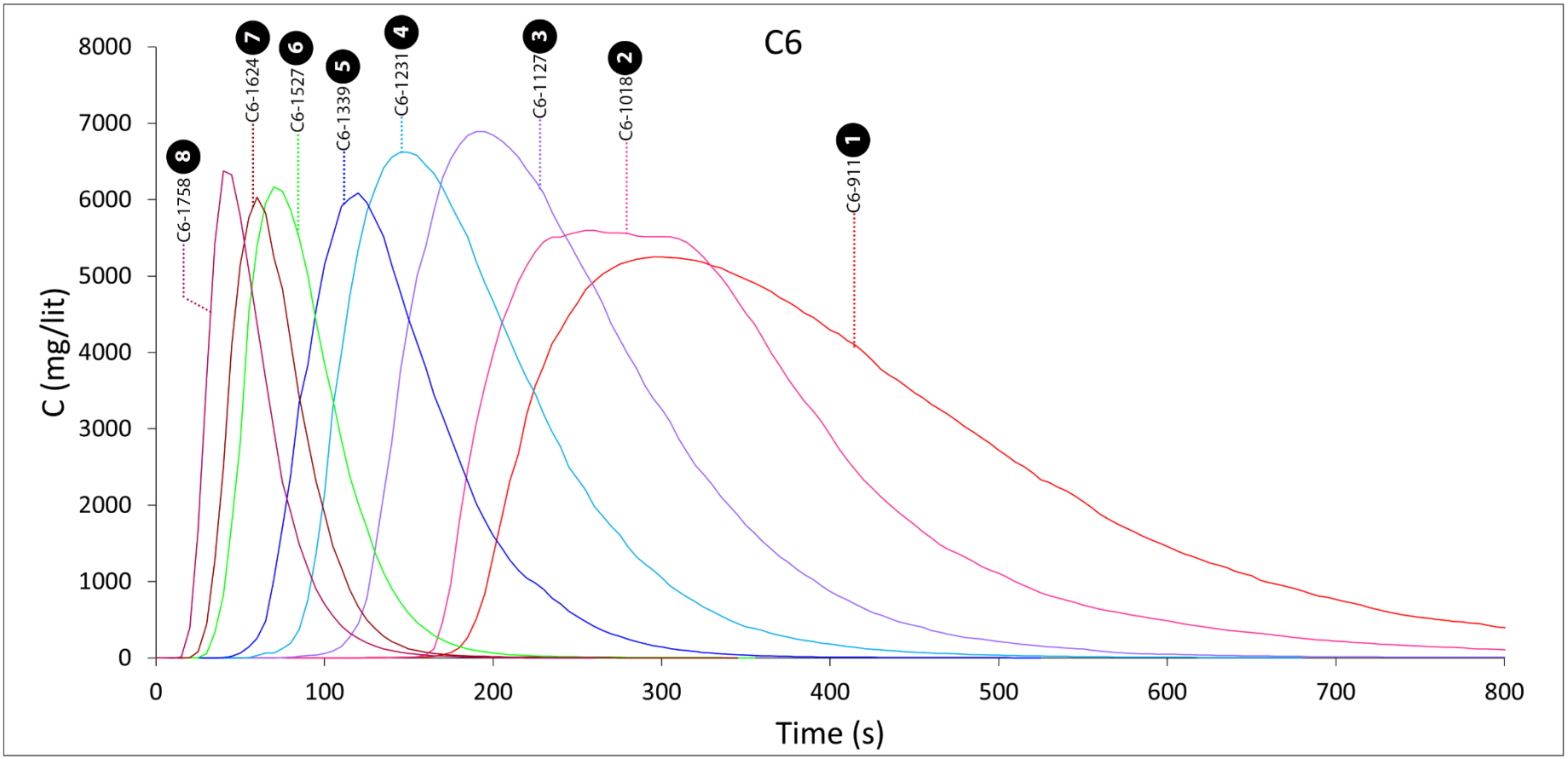

Figure 5.3.8. Breakthrough curves for specimen C6 in different hydraulic heads. The numbers in circles show the order of experiments

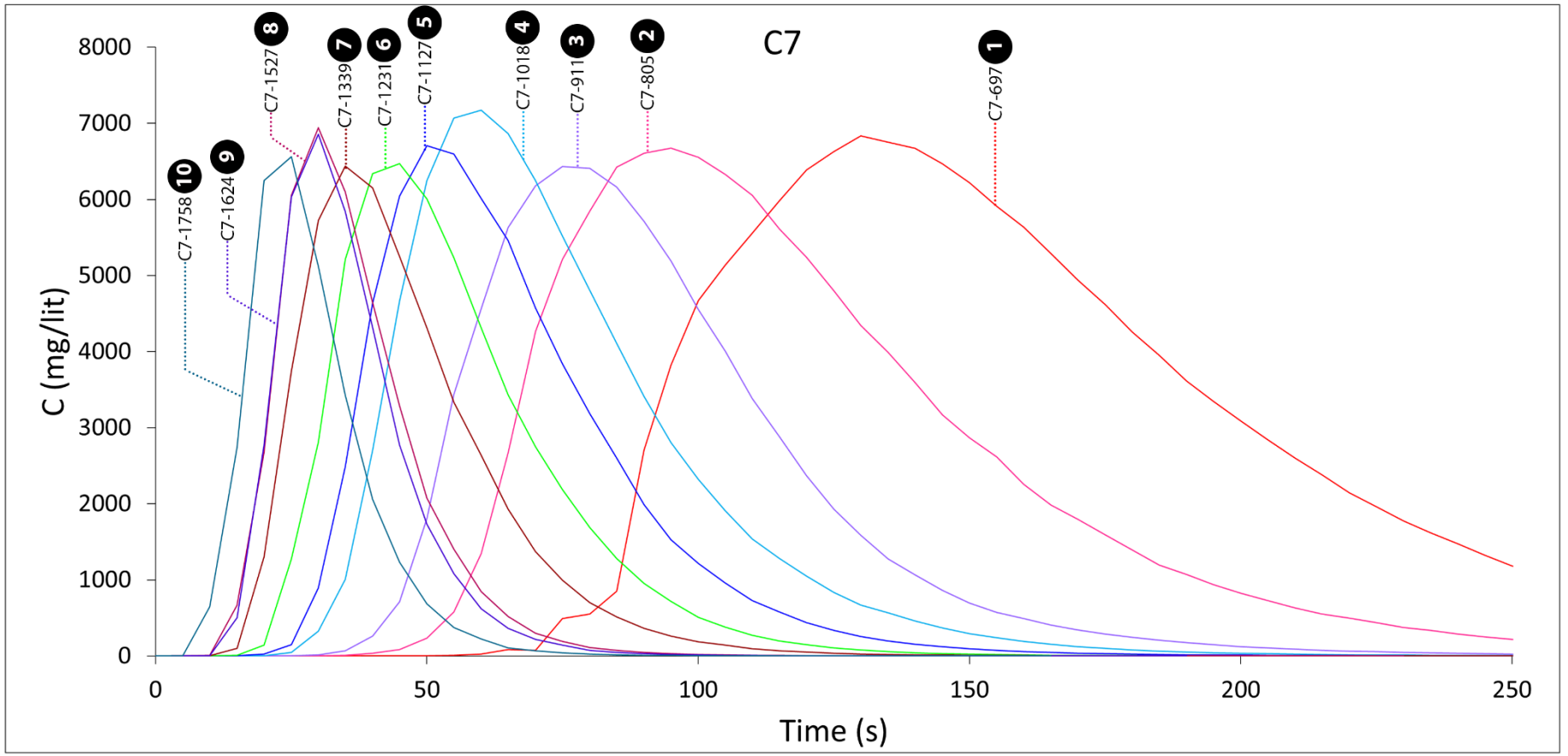

Figure 5.3.9.Breakthrough curves for specimen C7 in different hydraulic heads. The numbers in circles show the order of experiments

5.3.3. Parametrization of IG distribution with BTC data

Figure 5.3.11 illustrates the correlation between measured and predicted concentrations (C) for all experiments. The BTCs are provided in Appendix 1, along with the fitted curves for each tracer experiment using the IG distribution. The data points in Figure 5.3.11 for specimen L1 are denser than the other specimens. This is attributed to the fact that readings for L1 were captured at 1-second intervals, whereas readings for the other experiments were recorded every 5 seconds due to the less noticeable variations in concentration.

The figures are labelled continuously and it can be seen that the Nash-Sutcliffe Efficiency (NSE) in the majority of experiments exceeds 0.9 for all IG fittings and approaches 1 in some instances. This overall trend indicates that tracer experiments can be reliably fitted using the IG distribution. Notably, the experiments "n, o, p, q, r, ar, and as" exhibit lower NSE values as depicted in Figure 5.3.11. Examination of the appendix BTCs reveals that during these specific tracer experiments, the BTCs exhibit multiple peaks in the recorded data (Appendix 1: L1-1365R-D1, L1-1365R-D3, L1-1365R-D5, L1-1163R-D1, L1-963R-D7). Detailed IG parameters for individual experiments are provided in Appendix 2.

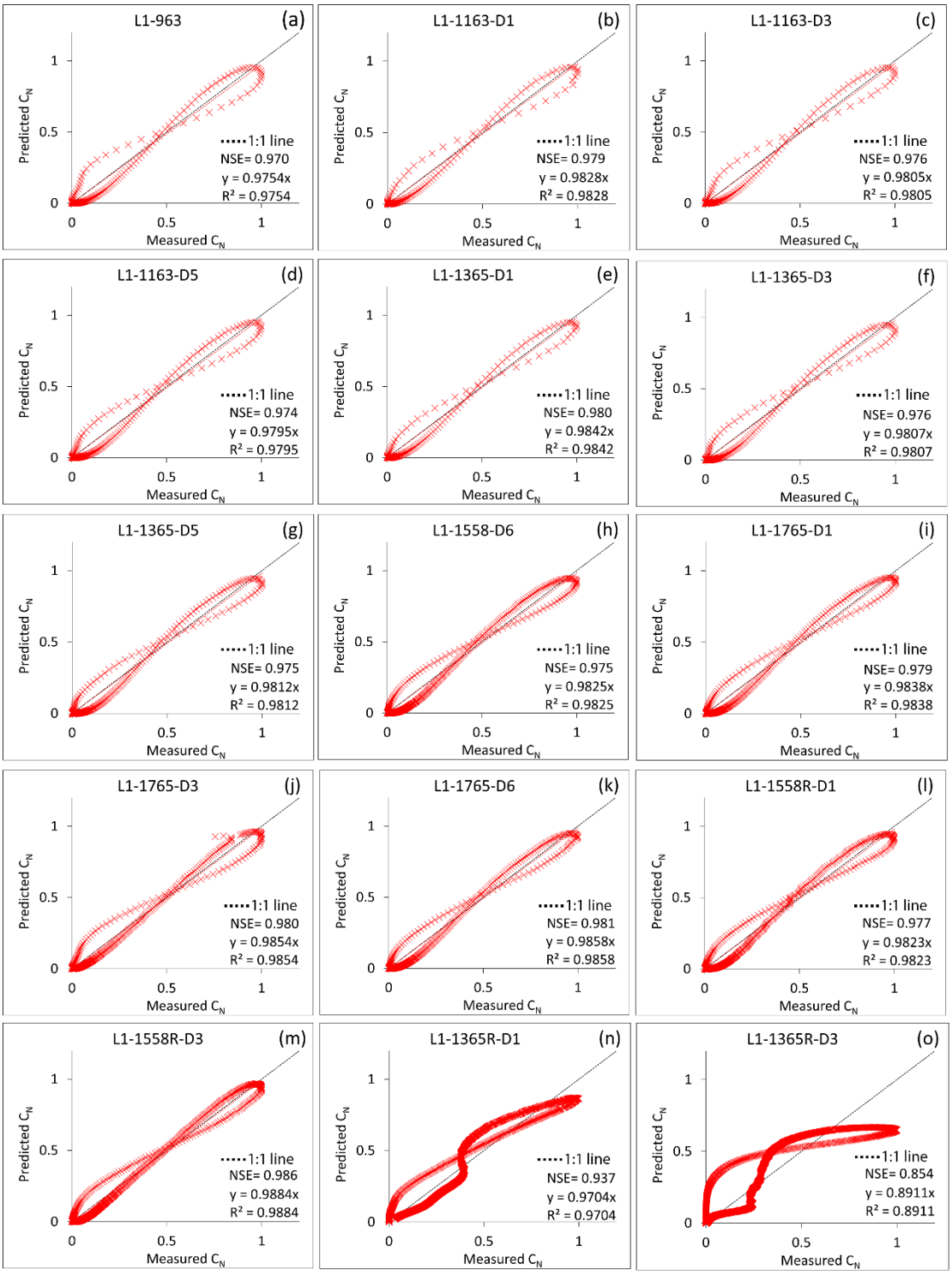

Figure 5.3.1.Measured C_N values versus predicted C_N using IG for all tracer experiments- As can be seen the NSE value for most of the predicted concentrations is more than 0.9

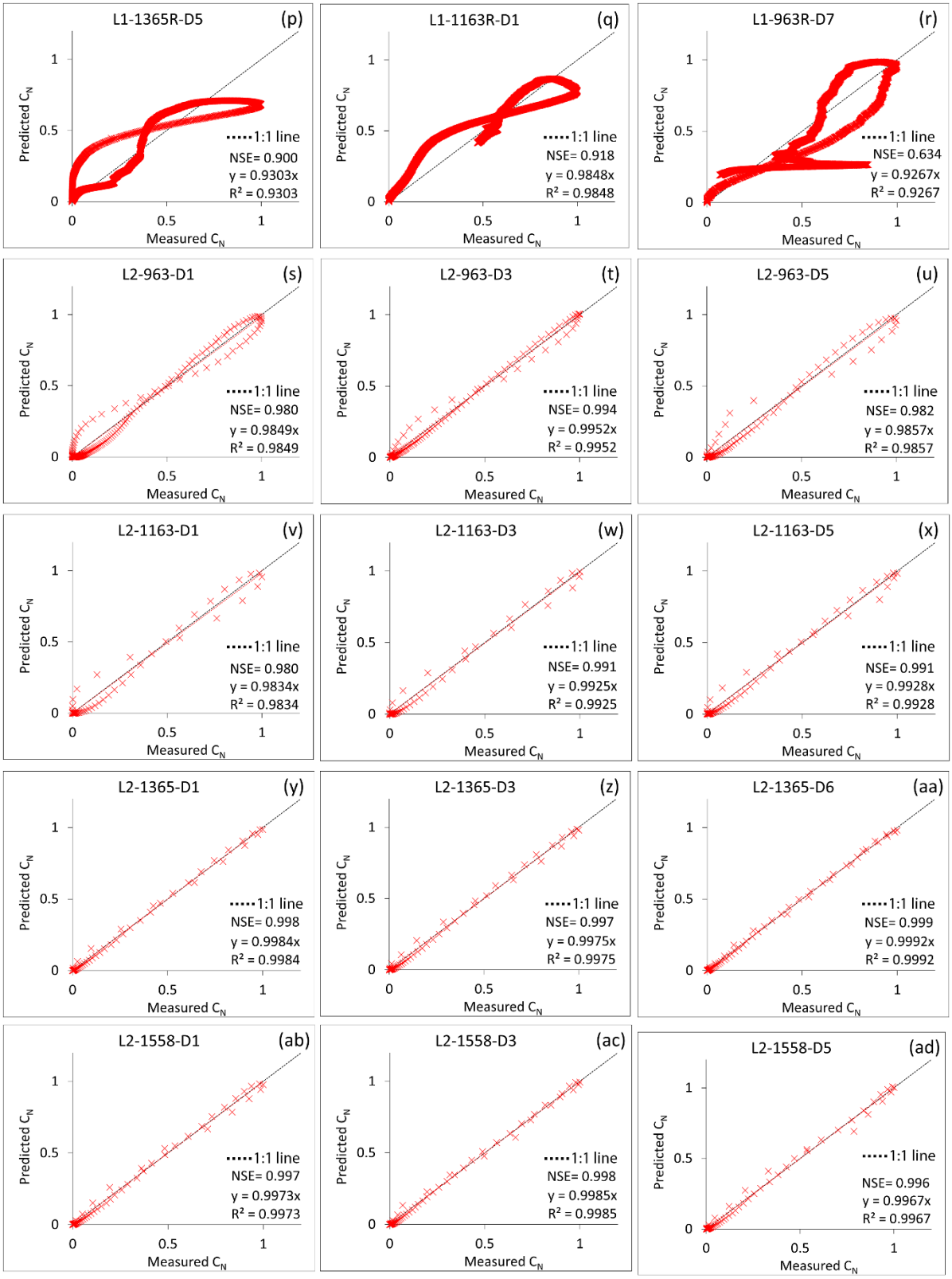

Figure 5.3.11. (Continued)

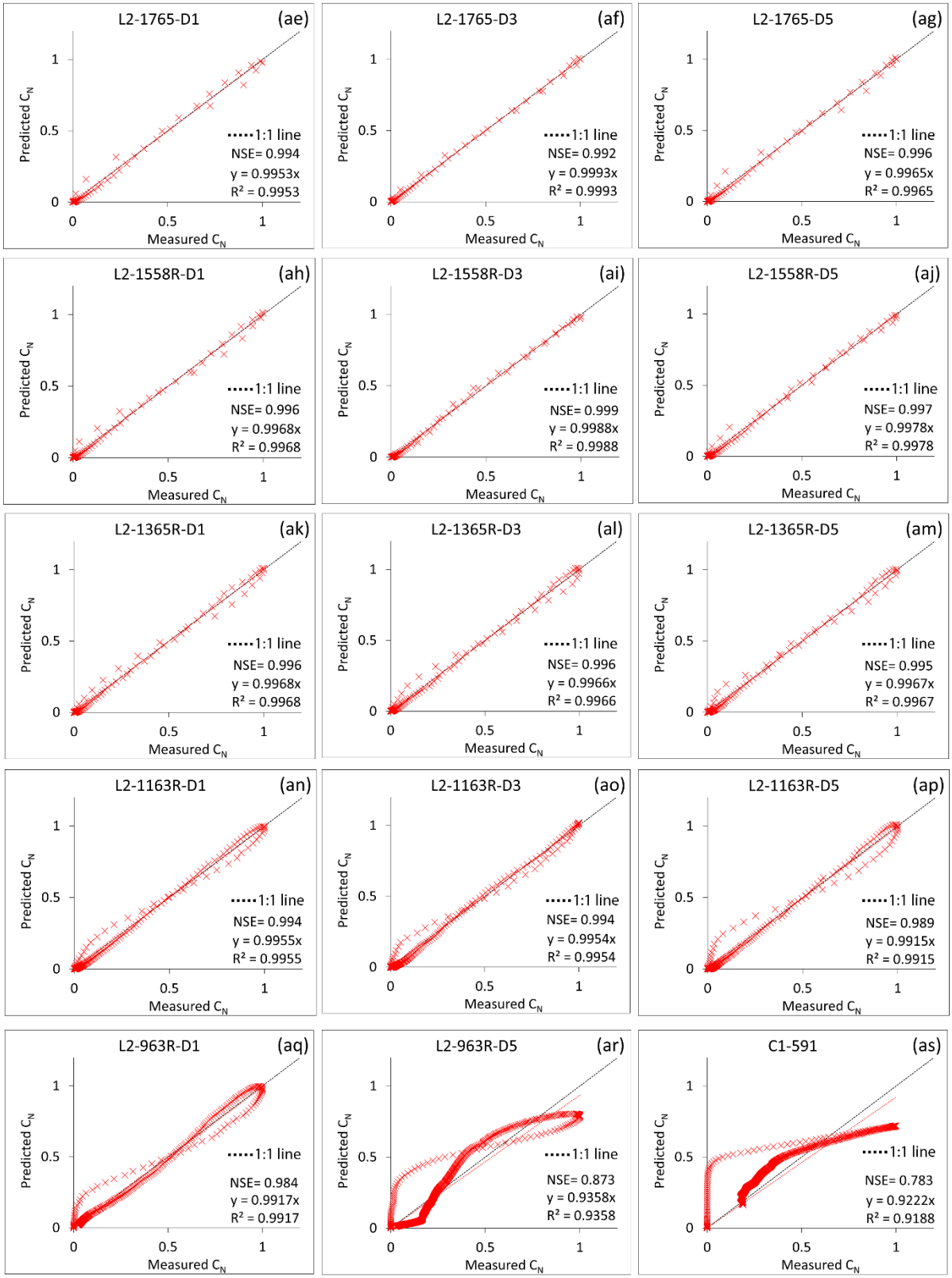

Figure 5.3.11. (Continued)

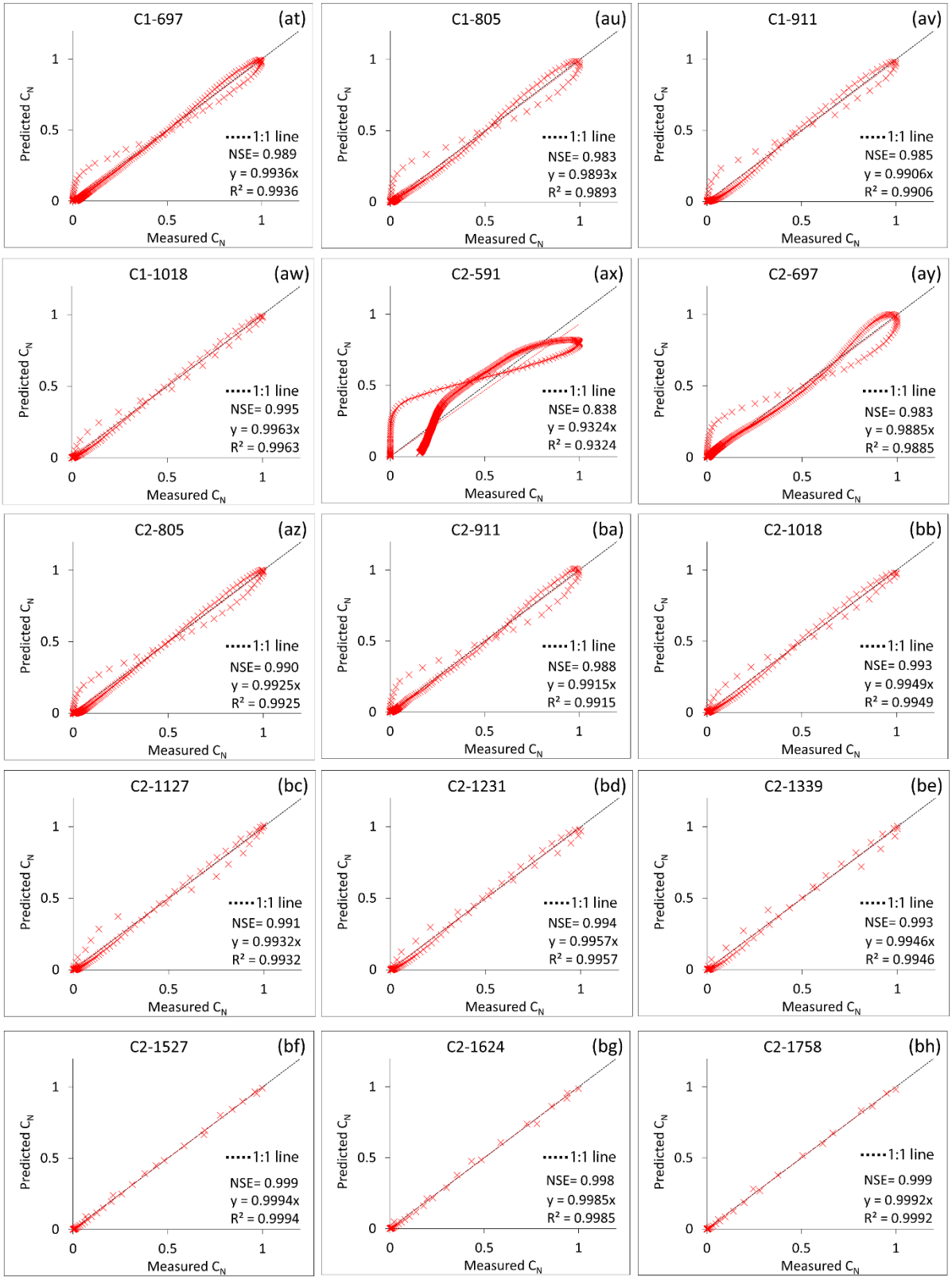

Figure 5.3.11. (Continued)

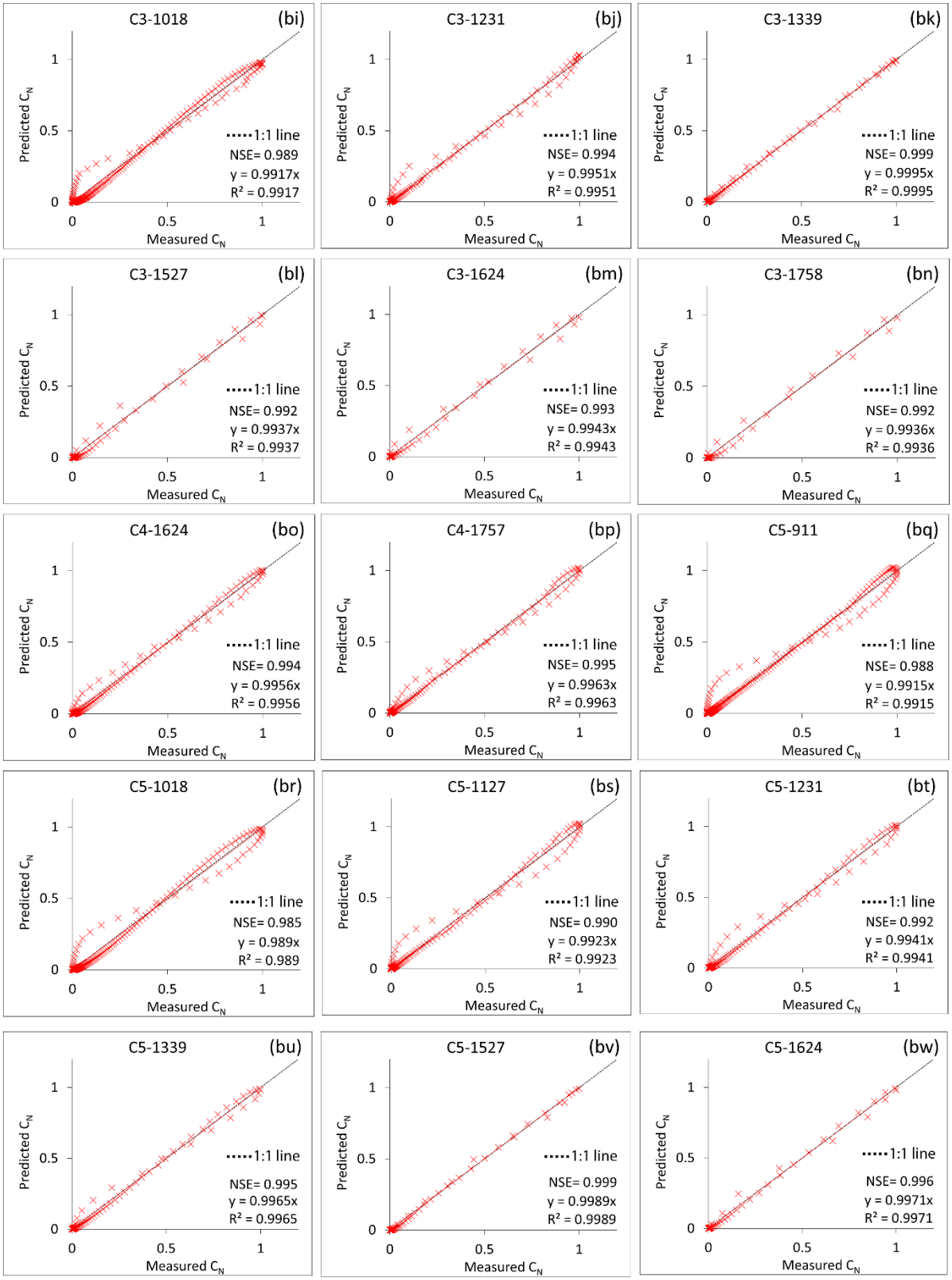

Figure 5.3.11. (Continued)

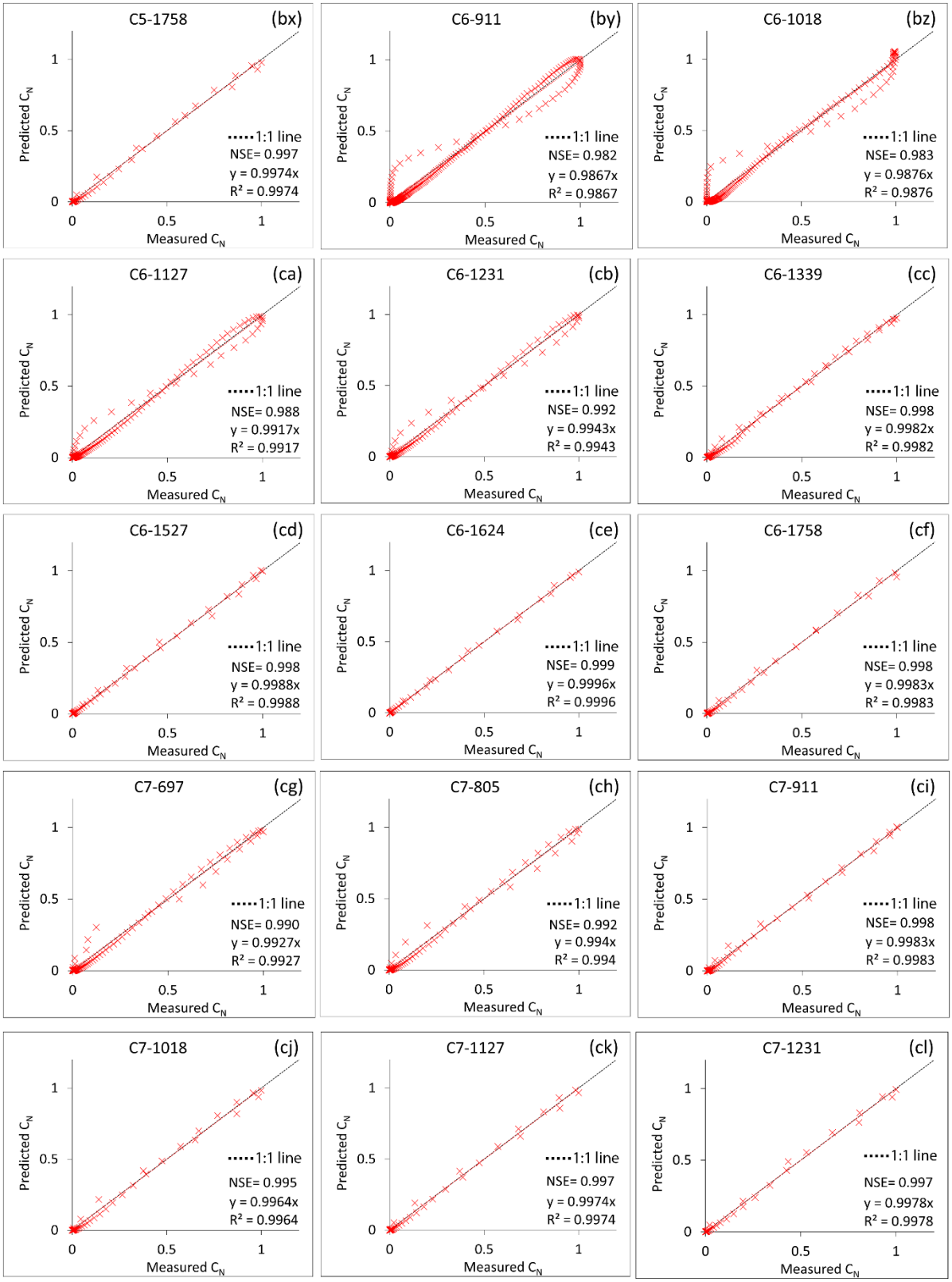

Figure 5.3.11. (Continued)

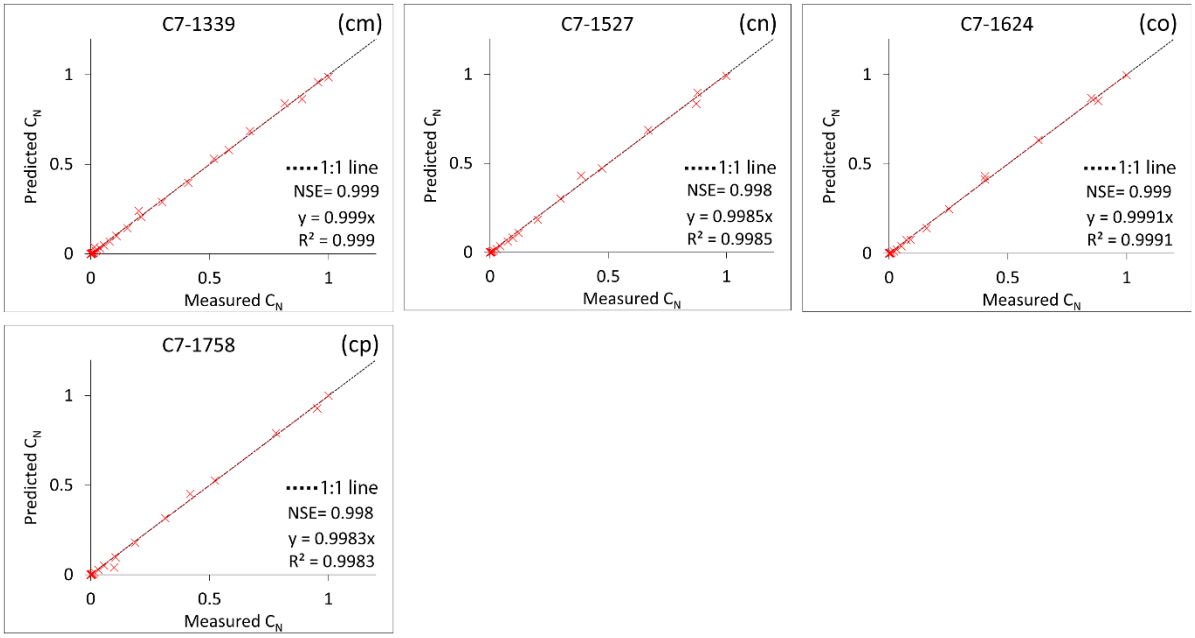

Figure 5.3.11. (Continued)

5.3.4. Comparison of IG distribution with ADE models

In the analysis comparing the predictions of the IG distribution and the ADE model using the BTC of experiment C7-697, it is evident from Figure 5.3.12 that the Nash-Sutcliffe Efficiency (NSE) of the IG distribution surpasses that of the ADE model. Furthermore, the simulation results of both the IG distribution and ADE closely align with the measured BTC on the left limb of the plot. However, noticeable deviation occurs on the right limb, where the ADE model diverges more from the measured concentration profile compared to the IG distribution. The final calibrated value of pore water velocity (v) necessary to match the measured and predicted BTC was determined to be 0.00140 m/s, marginally lower than the calculated Darcy velocity obtained through head difference and discharge measurements (0.00147 m/s). Additionally, the calibrated dispersion coefficient was calculated to be 6×10-6 m^2/s.

Comparison of fitting of BTCs by IG distribution and ADE model from the research of Zhao et al. (2022) and Ani et al. (2009) are shown in Figures 5.3.13 and 5.3.14 respectively. As can be seen from Figure 5.3.13, in all cases the NSE of IG has been higher than the ADE models. Looking at Figure 5.3.13 shows the ADE model has not predicted the BTCs efficiently, with the minimum and maximum NSEs being -0.28 for Port 28 and 0.84 for port 9. However, IG distribution shows excellent prediction of TBCs with all NSEs being more

than 0.97. Comparison of ADE model of Ani et al. (2009) with IG distribution in Figure 5.3.14 also shows better performance of IG distribution. The minimum and maximum NSEs of the ADE model are 0.8 and 0.94 respectively. But minimum and maximum NSEs of IG distribution of the same data are 0.99 and 1.

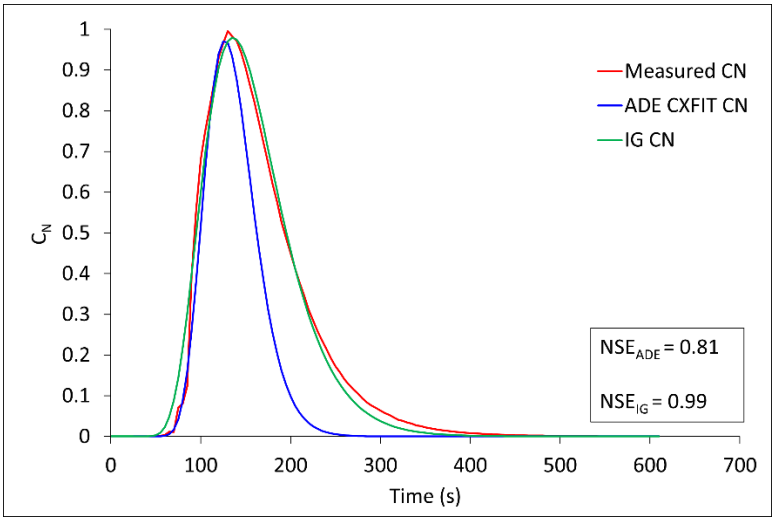

Figure 5.3.1.Comparison of the ADE model and IG distribution to fit the measured BTC for experiment C7-697

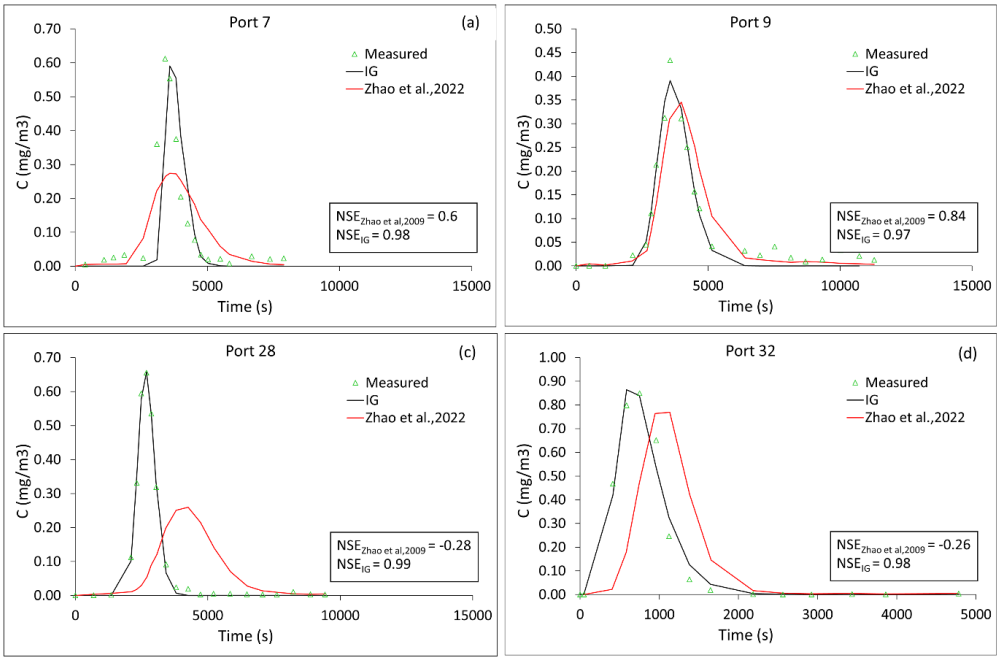

Figure 5.3.2.Comparison of fitting BTCs using IG and method recommended by Zhao et al. (2022)*using BTC measurements by* Zhao et al. (2022)

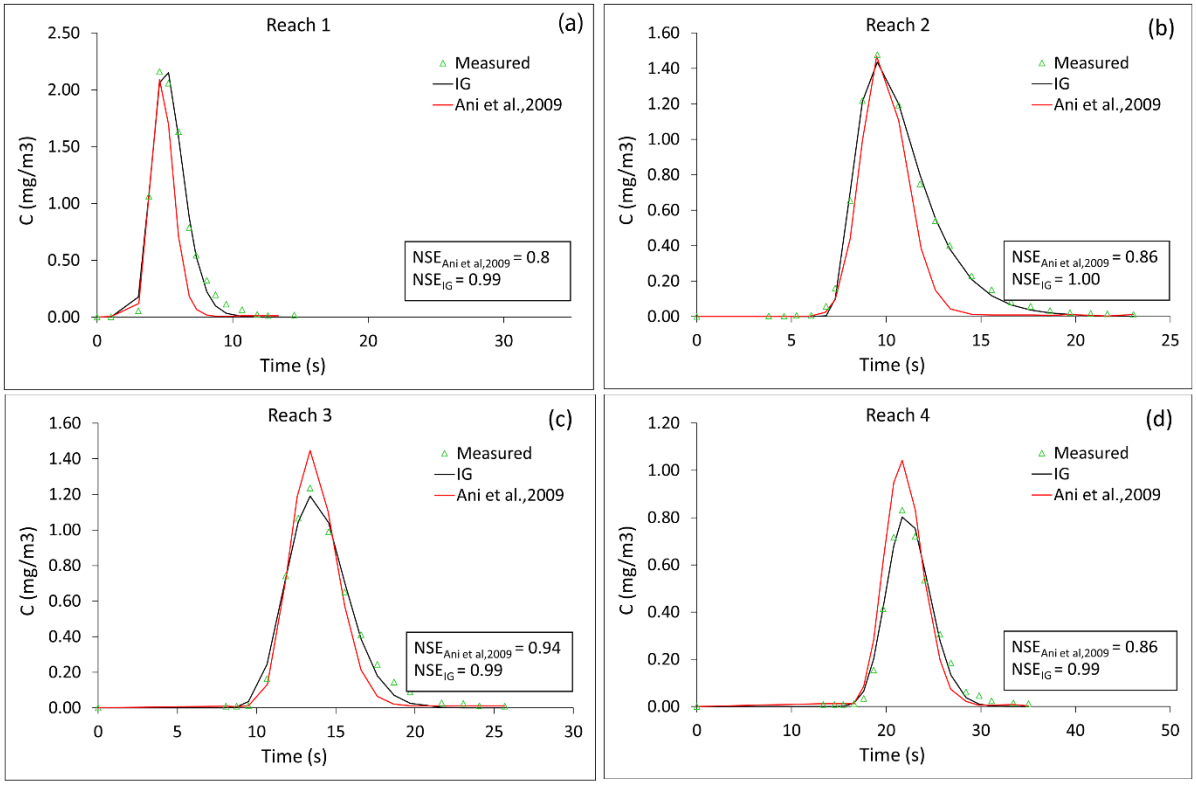

Figure 5.3.3.Comparison of fitting BTCs using IG and method recommended by Ani et al. (2009) *using BTC measurements by* Ani et al. (2009)

5.4. Discussion

5.4.1. Arrival times and changes of Ks

This study involved multiple tracer tests on 9 specimens utilizing NaCl as the tracing element to generate BTCs for each experiment. A flat BTC indicates a longer peak arrival time, signifying slower transport of the tracer solution within the specimen and suggesting a lower Ks. Conversely, a sharper peak indicates a quicker arrival time and higher Ks.

Analysis of the Ks-time graph (Figure 5.3.1) reveals a declining trend in Ks for specimens L1 and L2. However, observation of the corresponding BTCs (Figures 5.3.2 and 5.3.3) shows that peak arrival times at certain hydraulic heads do not necessarily exhibit delays. For example, in specimen L1, the Ks values for experiments 1 (L1-963) and 2 (L1-1163-D1) are 2.38 and 2.30 cm/min, respectively, yet the peak arrival time of experiment 2 is

shorter than that of experiment 1. Similar discrepancies are observed in experiments 8 and 10, and in specimen L2 for specific hydraulic heads (e.g., experiments 2 and 15).

In short-term experiments, two phases of relatively constant Ks and a phase of rapid Ks change can be discerned according to Figure 5.3.1. For instance, in specimen C7, during normalized time intervals 0 to 0.4 and 0.7 to 1.0, Ks remains nearly constant at around 6.6 cm/min and 12 cm/min, respectively. Correspondingly, in Figure 5.3.10, these periods align with experiments 1 to 4 (C7-697, 805, 911, and 1018) where peak arrival times range from 130 to 60 seconds, and experiments 8 to 10 (C7-1527, 1624, and 1758) where peak arrival times range from 30 to 20 seconds. This inconsistency between Ks and peak arrival times suggests that the validity of Ks as a reflective parameter of fluid movement in a porous medium may not always hold true.

Ks values are typically utilized as inputs in surface and subsurface hydraulic models, and are estimated through field tests like slug or pumping tests, or laboratory tests like constant and falling head tests. However, the study suggests that the dynamic nature of fluid movement in saturated porous media challenges the notion of a single Ks value accurately representing this behaviour over time. Therefore, the conventional application of Ks as a parameter for fluid movement in porous media may require re-evaluation in modelling scenarios to better account for temporal changes in fluid movement durations.

5.4.2. Inverse Gaussian distribution and the potential of tracer tests as indicator of fluid transport in porous medium

The IG distribution has been used for simulating particle movement with Brownian motion, notably in scenarios such as the movement of colloidal suspensions under an electric field (Johnson et al., 1994). However, the application of the IG distribution for interpreting BTCs in soil has been limited. Traditionally, BTCs in tracer tests in rivers and aquifers have been analysed using Fickian equations, which assume a dominant diffusion mechanism for particle movement. Estimating coefficients of particle movement based on diffusion mechanisms is often challenging and may lead to inaccuracies in results.

In this study, the utilization of the IG distribution has demonstrated that the simulation of solute transport in porous media can be achieved with greater accuracy compared to diffusion models. The NSEs derived from the fitted BTCs support the effectiveness of the IG distribution for interpreting tracer data. Furthermore, a comparison of NSE values

between an ADE model and the IG distribution indicates the superior predictive capability of the IG model for tracer data analysis.

In the majority of tracer tests conducted, the NSE values exceeded 0.9, demonstrating the high level of accuracy in data interpretation. However, challenges arose in cases where tracer tests lacked a single peak due to very low Ks, specifically observed in experiments with low hydraulic heads in specimen L1. The IG distribution yielded less satisfactory results in these scenarios, leading to delayed travel times in the tracer tests. As depicted in Figure 5.3.11, the plots o, p, r, ar, and as corresponding to experiments L1-1365R-D3, L1-1365R-D5, L1-963R-D7, L2-963R-D5, and C1-591, along with their BTCs in the appendix, all exhibit lower Ks values compared to other experiments, resulting in delayed travel times.

While the method employed in this research may lack accuracy in measuring BTCs with low Ks, this does not undermine the potential of the IG distribution for simulating measured BTCs. Analysis of the tracer data highlights that proper capture of BTCs in tracer experiments allows for the effective use of the IG distribution to fit the data with a high degree of accuracy.

While some may argue that the accuracy of ADE models is sufficient for evaluating solute transport parameters, it is important to note that the evaluation of ADE parameters requires substantial resources in terms of time and computational demand to achieve a satisfactory fit between measured and modelled BTCs. In contrast, the IG distribution can be implemented on BTCs using a simple spreadsheet tool like Excel, with minimal parameters for evaluation.

An inherent reason for the limited widespread application of the IG distribution in tracer tests could stem from the fact that the advection-dispersion equation, a foundation of many models, is rooted in physical mechanisms within the porous medium. In contrast, the IG distribution is purely statistical and lacks explicit physical transport mechanisms. Despite this, studies like Leiva et al. (2008) demonstrate the utility of the IG distribution in interpreting particle movement under Brownian motion, showcasing how statistical methods can aid in establishing physical relationships.

In the context of the IG distribution, Johnson et al. (1994) mentions a correlation between particle diffusion and velocity through IG distribution parameters for Brownian motion. However, further investigation is required to establish a direct link between these IG parameters and hydraulic properties of porous medium, such as hydraulic conductivity.

This exploration could potentially bridge the statistical nature of the IG distribution with the physical properties relevant to porous media transport, enhancing its applicability and understanding in tracer tests.

5.5. Conclusions

The use of IG distribution for interpretation of tracer tests in soil can be a quick, cost effective, and accurate method for fitting the breakthrough curves. The examination of the Ks-time graph revealed a declining trend in Ks for specimens L1 and L2. However, the study also observed discrepancies between Ks values and peak arrival times, highlighting inconsistencies that challenge the conventional application of Ks as a representative parameter for fluid movement within porous media.

The utilization of the IG distribution in simulating solute transport in porous media demonstrated greater accuracy compared to traditional diffusion models. The study indicated that the IG distribution offers superior predictive capabilities for analysing tracer data, as evidenced by higher NSE values and enhanced data interpretation accuracy.

Although the IG distribution showed high accuracy in most tracer tests, challenges arose in cases with very low Ks, leading to delays in travel times. While the IG distribution may lack accuracy in measuring BTCs with low Ks, it remains a valuable tool for simulating measured BTCs with a high degree of accuracy.

In conclusion, the study suggests the need for a re-evaluation of the conventional application of parameters like Ks in modelling scenarios, emphasizing the potential of statistical methods like the IG distribution in enhancing the understanding and interpretation of tracer test data in porous media.

The IG distribution has the potential to be used as initial estimates of solute transport parameters, as inputs in the models. Because the process of calibration of dispersivity and pore velocity is a process of trial and error, therefore finding the mentioned parameters through fitting the BTCs by IG distribution can give the curve fitting parameters, that can be used as inputs in the model, to make the best estimate for the initial run of the models.

Further research exploring the correlation between IG distribution parameters and hydraulic properties could improve the applicability and understanding of statistical methods in tracer tests.

5.6. Acknowledgement

This research was supported by the University of Waikato Doctoral Scholarship.

5.7. Data Availability Statement

All raw tracer data used in this study can be accessed in ZENODO repository (Nikghalb Ashouri, 2024).

5.8. Appendix 1- BTCs of all experiments and IG fitting on the BTCs

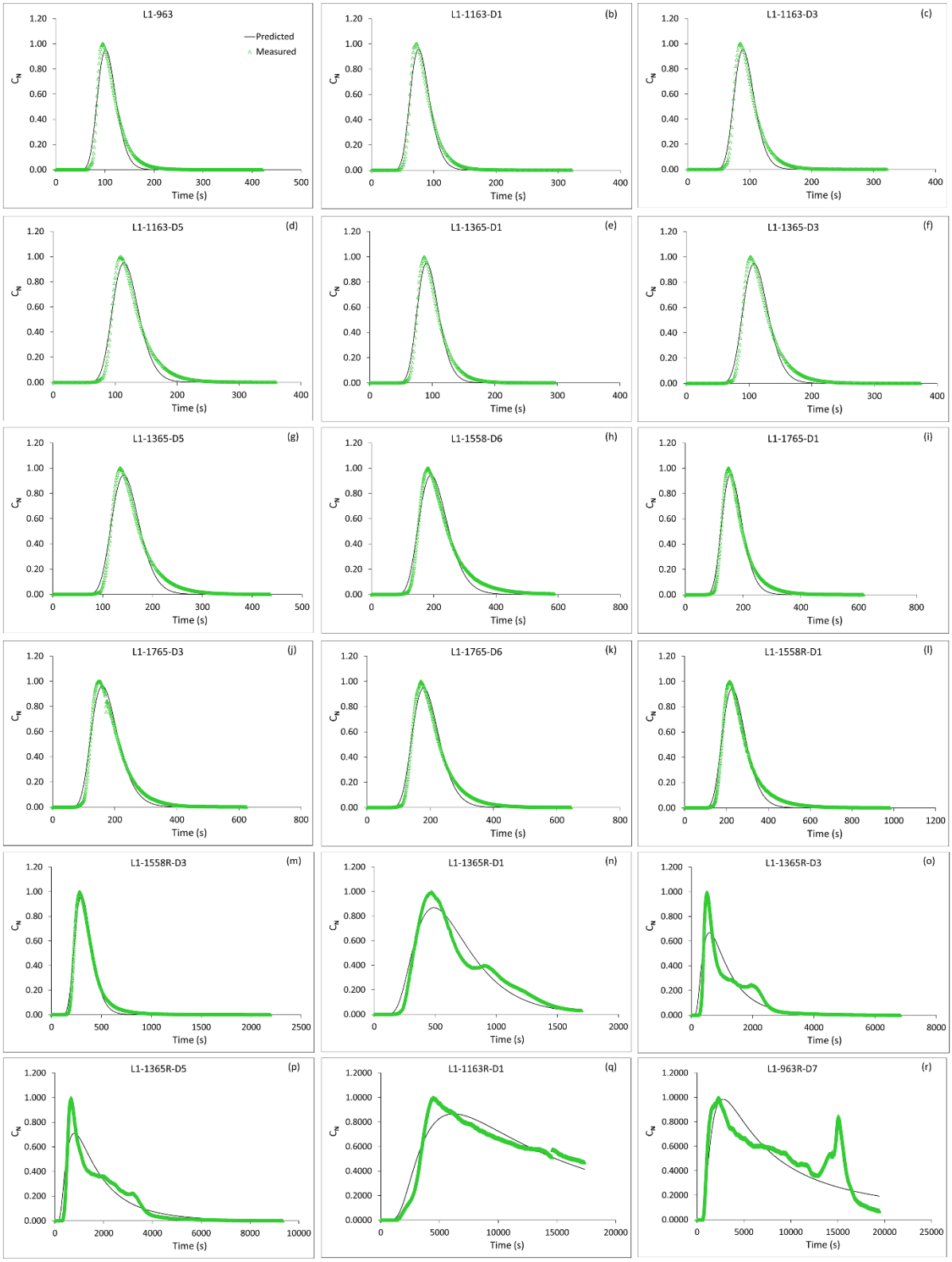

Figure 5.8.1. Breakthrough curves and fitted curves using IG

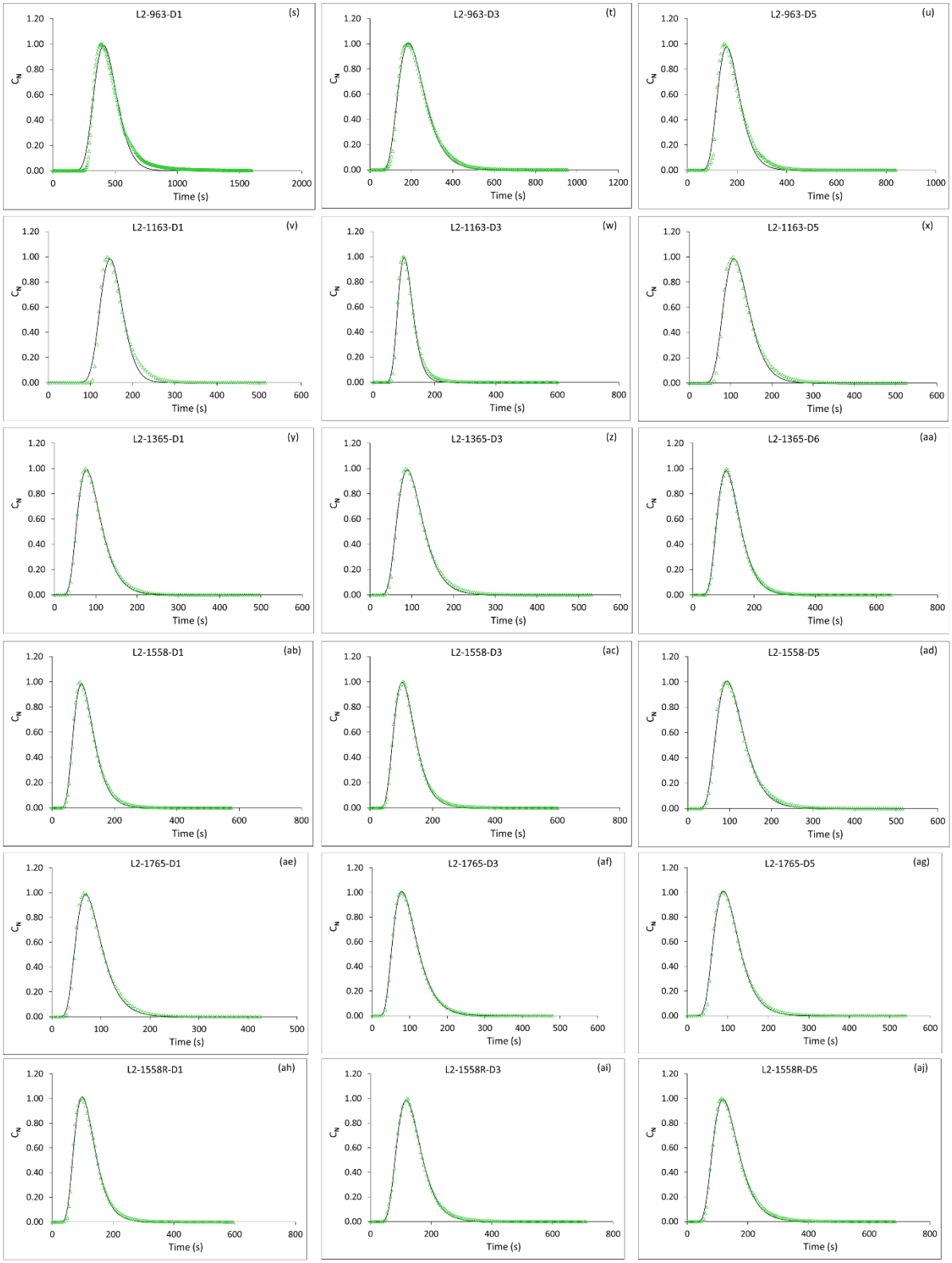

Figure 5.8.2. Breakthrough curves and fitted curves using IG (Continued)

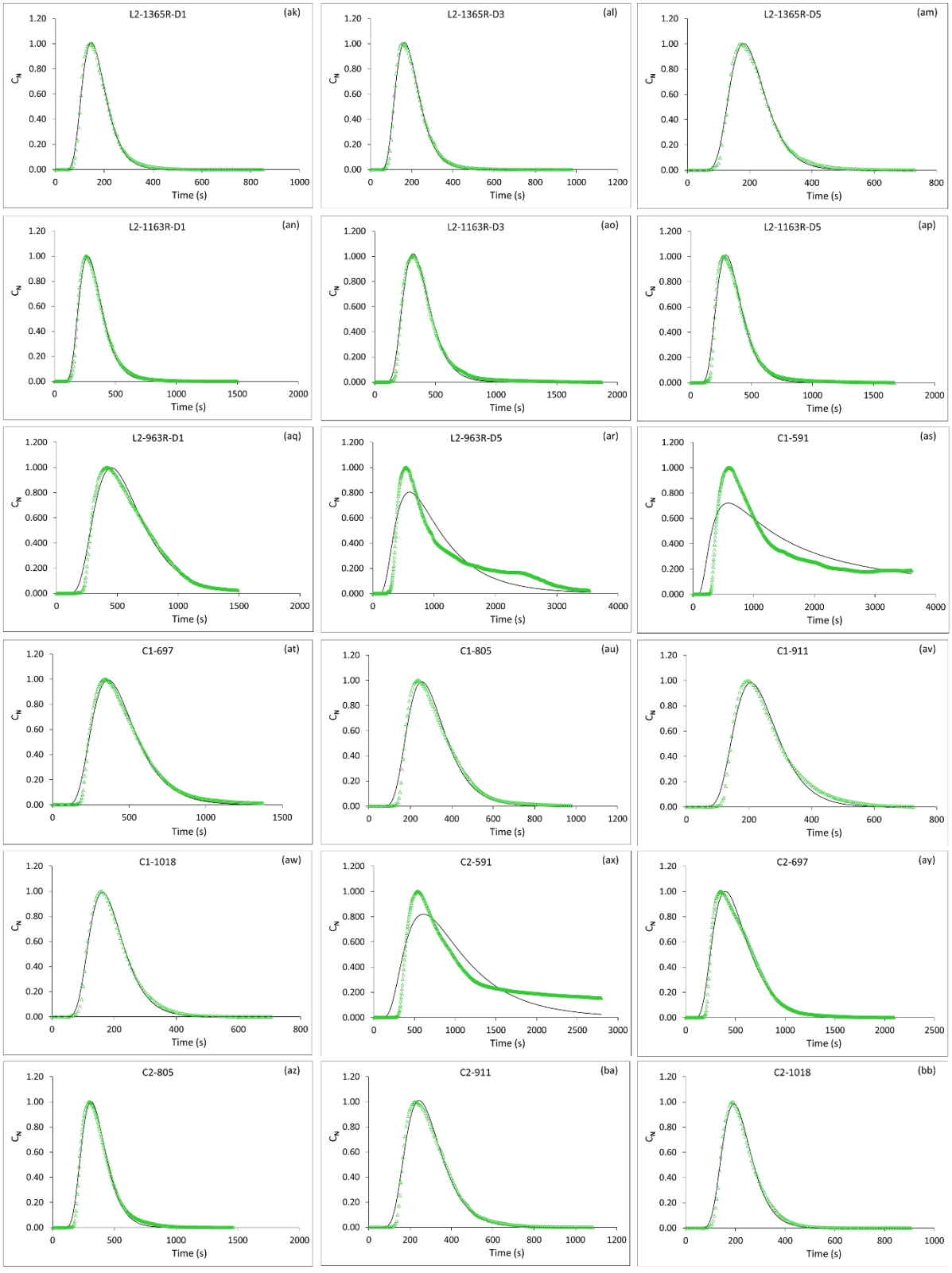

Figure 5.8.3. Breakthrough curves and fitted curves using IG (Continued)

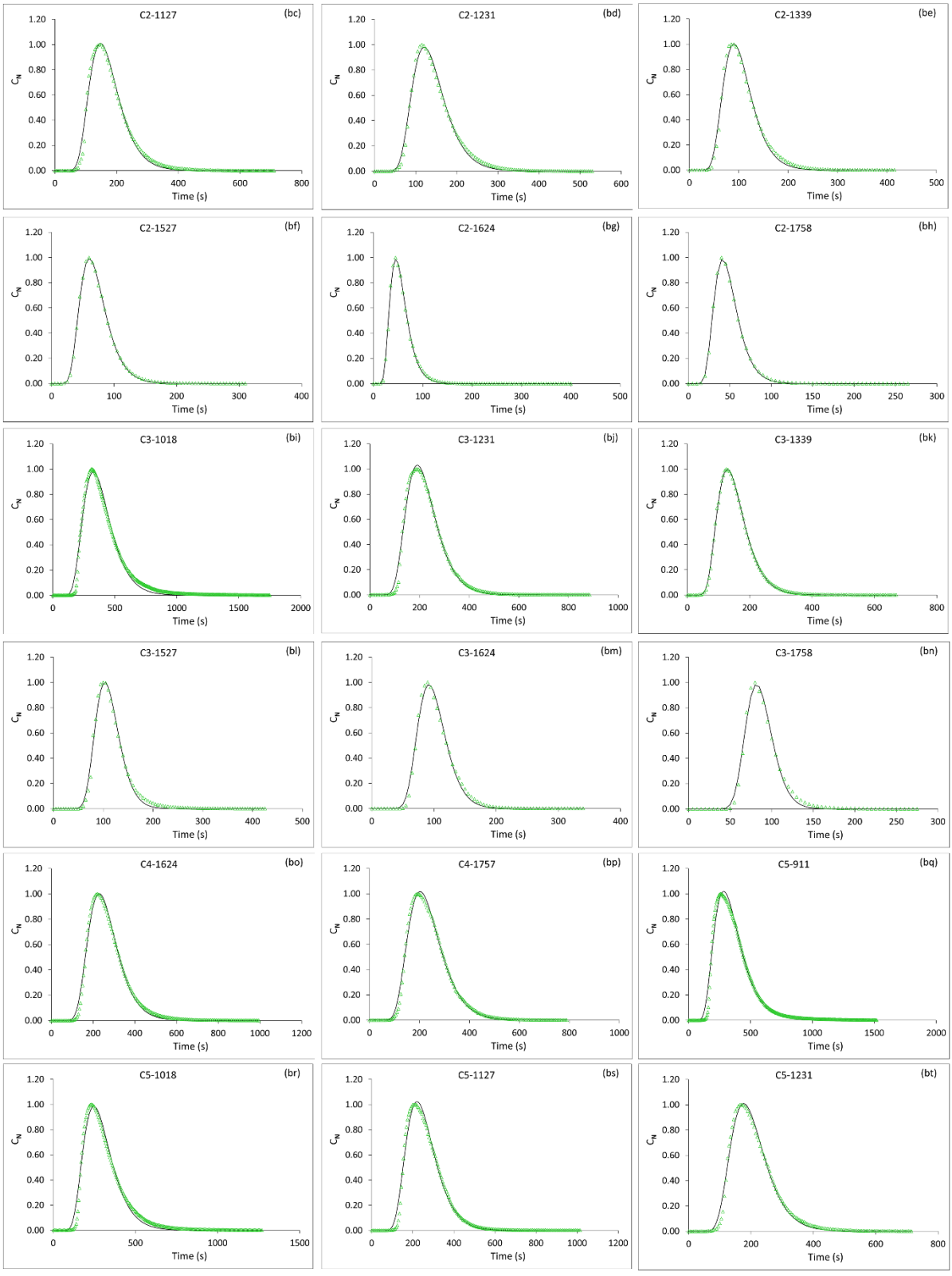

Figure 5.8.4. Breakthrough curves and fitted curves using IG (Continued)

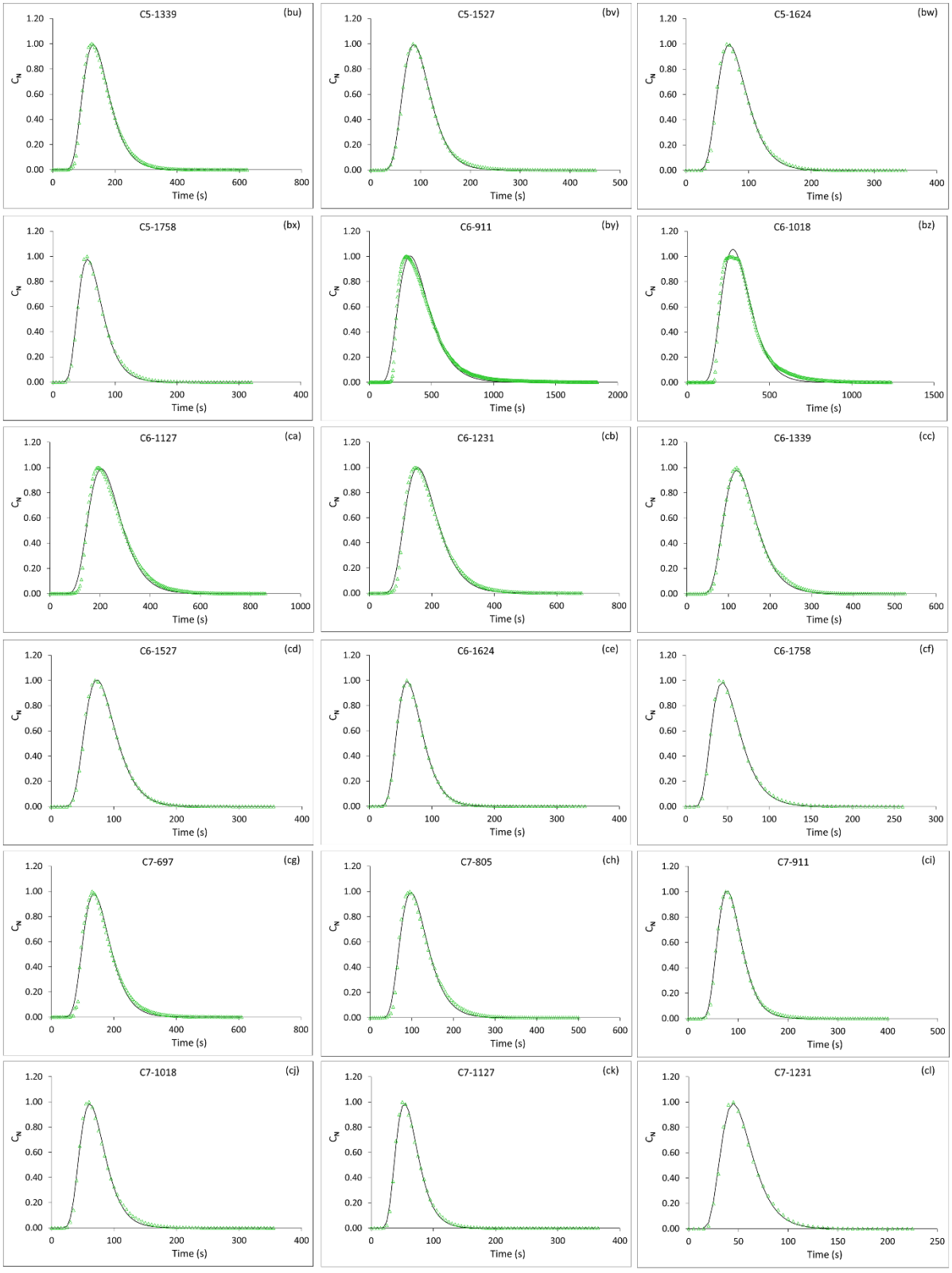

Figure 5.8.5. Breakthrough curves and fitted curves using IG (Continued)

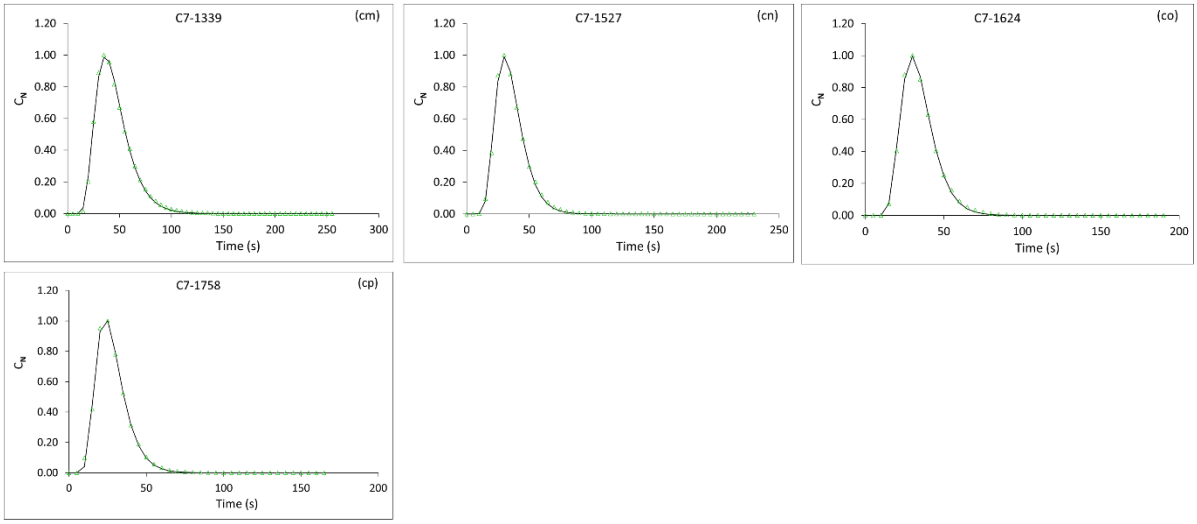

Figure 5.8.6. Breakthrough curves and fitted curves using IG (Continued)

5.9. Appendix 2- Inverse Gaussian Parameters for Each Experiment

Table 5.9.1. IG parameters and the Ks of specimen L1 in different hydraulic heads

Experiment name	c	μ	λ	RMSE	NSE	Measured K (cm/min)
L1-963	45	107	3172	0.042	0.970	2.54
L1-1163-D1	37	80	1971	0.037	0.979	3.43
L1-1163-D3	39	94	2889	0.040	0.976	3.48
L1-1163-D5	50	120	3641	0.044	0.974	3.46
L1-1365-D1	41	96	2794	0.038	0.980	3.46
L1-1365-D3	48	113	3387	0.041	0.976	4.26
L1-1365-D5	65	150	4121	0.044	0.975	4.14
L1-1558-D6	109	208	3746	0.047	0.975	4.45
L1-1765-D1	84	169	3491	0.039	0.979	5.33
L1-1765-D3	104	177	2586	0.041	0.980	5.24
L1-1765-D6	101	194	3620	0.039	0.981	5.2
L1-1558R-D1	131	248	4347	0.040	0.977	4.36
L1-1558R-D3	207	337	4433	0.027	0.986	4.34
L1-1365R-D1	535	673	3110	0.075	0.937	3.46
L1-1365R-D3	796	1154	2374	0.077	0.854	3.36
L1-1365R-D5	1379	1911	2898	0.069	0.900	2.44
L1-1163R-D1	17028	21445	20328	0.078	0.918	4.71
L1-963R-D7	17768	100571192	8348	0.151	0.634	3.65

Table 5.9.2. IG parameters and the Ks of specimen L2 in different hydraulic heads

Experiment name	c	μ	λ	RMSE	NSE	Measured K (cm/min)
L2-963-D1	230	439	8806	0.039	0.980	2.7
L2-963-D3	165	221	1955	0.024	0.994	0.89
L2-963-D5	110	178	2326	0.036	0.982	1.23
L2-1163-D1	65	154	4816	0.038	0.980	2.53
L2-1163-D3	61	110	1969	0.023	0.991	2.86
L2-1163-D5	78	122	1515	0.027	0.991	2.67
L2-1365-D1	73	94	723	0.012	0.998	3.18
L2-1365-D3	77	105	930	0.016	0.997	3.09
L2-1365-D6	93	128	1152	0.009	0.999	2.94
L2-1558-D1	82	111	970	0.016	0.997	4.26
L2-1558-D3	87	121	1141	0.012	0.998	3.29
L2-1558-D5	84	111	959	0.019	0.996	3.7
L2-1765-D1	67	84	608	0.022	0.994	4.49
L2-1765-D3	83	100	643	0.009	0.992	4.19
L2-1765-D5	81	106	913	0.019	0.996	4.2
L2-1558R-D1	89	117	1017	0.018	0.996	3.93
L2-1558R-D3	101	139	1258	0.011	0.999	3.69
L2-1558R-D5	107	141	1159	0.015	0.997	4.02
L2-1365R-D1	127	172	1611	0.018	0.996	3.26
L2-1365R-D3	148	196	1698	0.019	0.996	3.27
L2-1365R-D5	146	209	2165	0.021	0.995	3.19
L2-1163R-D1	241	323	2819	0.022	0.994	2.57
L2-1163R-D3	291	378	3176	0.022	0.994	2.54
L2-1163R-D5	268	348	2863	0.031	0.989	2.22
L2-963R-D1	516	592	3221	0.044	0.984	1.54
L2-963R-D5	868	1055	2653	0.093	0.873	2.2

Table 5.9.3. IG parameters and the Ks of specimen C1 in different hydraulic heads

Experiment name	c	μ	λ	RMSE	NSE	Measured K (cm/min)
C1-591	2624	53551	1740	0.122	0.783	0.95
C1-697	366	451	3057	0.034	0.989	1.43
C1-805	232	307	2493	0.042	0.983	1.42
C1-911	175	243	2221	0.039	0.985	2.06
C1-1018	140	192	1736	0.022	0.995	2.05

Table 5.9.4. IG parameters and the Ks of specimen C2 in different hydraulic heads

Experiment name	c	μ	λ	RMSE	NSE	Measured K (cm/min)
C2-591	840	1014	2862	0.108	0.838	0.92
C2-697	463	526	2807	0.042	0.983	1.56
C2-805	254	361	3665	0.030	0.990	1.95
C2-911	226	293	2379	0.035	0.988	2.12
C2-1018	147	221	2485	0.024	0.993	2.2
C2-1127	124	172	1684	0.029	0.991	2.25
C2-1231	98	141	1396	0.023	0.994	2.16
C2-1339	74	104	1062	0.026	0.993	2.23
C2-1527	52	71	638	0.008	0.999	2.95
C2-1624	43	55	431	0.010	0.998	3.77
C2-1758	35	49	451	0.008	0.999	4.46

Table 5.9.5. IG parameters and the Ks of specimen C3 in different hydraulic heads

Experiment name	c	μ	λ	RMSE	NSE	Measured K (cm/min)
C3-1018	278	386	3484	0.030	0.989	2.79
C3-1231	159	220	2284	0.025	0.994	2.5
C3-1339	112	152	1361	0.008	0.999	2.35
C3-1527	60	112	2161	0.025	0.992	2.68
C3-1624	55	100	1752	0.025	0.993	3.2
C3-1758	39	87	2337	0.025	0.992	4.14

Table 5.9.6. IG parameters and the Ks of specimen C4 in different hydraulic heads

Experiment name	c	μ	λ	RMSE	NSE	Measured K (cm/min)
C4-1624	177	262	2961	0.023	0.994	1.95
C4-1757	169	235	2355	0.023	0.995	2.28

Table 5.9.7. IG parameters and the Ks of specimen C5 in different hydraulic heads

Experiment name	c	μ	λ	RMSE	NSE	Measured K (cm/min)
C5-911	286	350	2494	0.034	0.988	2.86
C5-1018	217	294	2539	0.036	0.985	3.25
C5-1127	185	256	2587	0.032	0.990	3.39
C5-1231	142	203	2158	0.029	0.992	3.43
C5-1339	108	152	1470	0.021	0.995	3.33
C5-1527	71	100	1002	0.011	0.999	3.15
C5-1624	60	82	721	0.018	0.996	3.15
C5-1758	49	67	555	0.016	0.997	3.68

Table 5.9.8. IG parameters and the Ks of specimen C6 in different hydraulic heads

Experiment name	c	μ	λ	RMSE	NSE	Measured K (cm/min)
C6-911	320	401	2932	0.040	0.982	2.85
C6-1018	238	321	3277	0.042	0.983	3.13
C6-1127	164	237	2444	0.033	0.988	3.18
C6-1231	133	182	1673	0.028	0.992	3.11
C6-1339	97	139	1390	0.015	0.998	2.85
C6-1527	63	86	795	0.012	0.998	3.08
C6-1624	51	71	656	0.006	0.999	3.55
C6-1758	44	55	371	0.014	0.998	4.31

Table 5.9.9. IG parameters and the Ks of specimen C7 in different hydraulic heads

Experiment name	c	μ	λ	RMSE	NSE	Measured K (cm/min)
C7-697	109	157	1596	0.030	0.990	1.32
C7-805	84	115	1048	0.026	0.992	1.79
C7-911	62	90	972	0.014	0.998	2.19
C7-1018	52	72	660	0.019	0.995	2.44
C7-1127	46	63	575	0.015	0.997	2.55
C7-1231	40	54	447	0.016	0.997	2.56
C7-1339	35	45	324	0.010	0.999	2.63
C7-1527	26	35	331	0.011	0.998	2.95
C7-1624	24	34	352	0.009	0.999	3.15
C7-1758	22	28	223	0.013	0.998	3.53

Chapter 6. Conclusions, Limitations, and Recommendations for Future Work

This research explores several critical topics related to water movement within porous media. The primary aim was to assess the reliability of laboratory tests in determining saturated hydraulic conductivity (Ks). In this study, for the first time the long-term changes of Ks in a sandy soil in the laboratory were investigated and the results showed a significant reduction in the long-term Ks of the samples. Further, an evaluation was conducted on the reliability of various predictive equations for Ks. A novel method for interpreting tracer test data in porous media was also proposed.

In Chapters 3 and 4, numerous constant head tests were performed and assessed using sand specimen columns. Findings revealed that the duration of laboratory Ks tests significantly impacts results. Long-term tests showcased steady variations in Ks, primarily reductions, whereas short-term tests with varying hydraulic heads resulted in increased Ks, and suggesting a three-phase process.

The research also scrutinized the effectiveness of seven pedotransfer functions (PTFs) for estimating Ks in Chapter 4, followed by adjusting one method's parameters to enhance the accuracy of Ks estimates.

Finally, an innovative approach was introduced for fitting breakthrough curves (BTCs) in tracer tests in Chapter 5, and this was compared with conventional methods. The Inverse Gaussian distribution was employed to fit BTCs from tracer tests executed on soil columns.

6.1. Conclusions

6.1.1. Variations of Ks during long-term constant head tests

Ks is a crucial parameter in all applications that involve the movement of water through porous media. Its significance extends to the calculations related to the stability of slopes, the investigation of seepage in soil layers, the safety assessment of geotechnical structures, hydraulic and hydrological modelling of floodplains, and the design of drainage systems, where it affects the spacing of subsurface drains due to its relationship with the rate of flow in soil.

However, determining Ks in the laboratory presents numerous challenges, as the results can be influenced by inherent flaws in the testing procedures. This research addressed these challenges by conducting several constant head tests on non-cohesive sand samples with less than 10% fine particles and diverse particle size mixtures.

A critical and often overlooked factor in laboratory determination of Ks is the duration of the constant head tests. It is essential for the standards to account for this duration. This research found that during long-term tests exceeding 50 days, the Ks of the samples continuously changed. While changes in Ks were not noticeable over periods of a few hours within these long-term tests, after 50 days, the final Ks for the samples was more than 90% lower than the maximum values recorded during the tests.

Current standards for testing Ks (ASTM D2434-19, 2019; ASTM D5856-15, 2015) do not address the consideration of long-term changes in Ks during the tests. Although variations of Ks noticed over shorter periods were within acceptable ranges for terminating the tests and reporting Ks, the long-term variations observed were significantly larger. Given Ks's critical role in water movement within soil, acknowledging these variations and reductions is important for all applications related to the movement of water in saturated porous media. There is substantial research on the sensitivity of hydrological, hydraulic, and groundwater models to Ks (de Rooij, 2012; Đukić & Radić, 2016; Glose et al., 2019; M. Foster & M. Maxwell, 2019; Mustafa & Darwish, 2022; Reinecke et al., 2019; L. Wu et al., 1996), thus results from these model will be affected by variations in Ks.

Furthermore, the non-linear behaviour of the samples during the tests indicated that the assumption of Darcy's law, even at low hydraulic heads, is not universally valid. While a linear relationship between flow rate and hydraulic gradient could be established in some instances, the majority of cases exhibited a non-linear relationship.

The potential for internal mobility, displacement, and clogging of fine particles during Ks tests must also be considered, as they impact on the changes of Ks. These factors should be mentioned when reporting Ks to ensure that modellers or designers account for possible reductions in Ks, depending on their specific applications. Additionally, the incorporation of time-based Ks variations into surface water or groundwater models should be considered. It is recommended for the conditions where the soil goes under slow saturation, similar to the condition that happens in the aquifer, considering time-based variations for the Ks, or applying a reasonable reduction factor to be conservative.

6.1.2. Ks variations under short-term constant head tests

Typically, laboratory tests for determining Ks using constant head tests are completed within a few hours. The findings from this study demonstrated that Ks exhibits a three-phase behaviour in short-term tests conducted under a wide range of hydraulic heads. Therefore, the variation during short-term tests must also be accounted for when reporting Ks.

Within the short-term tests, different mixtures with varying proportion of coarse or fine particles did not significantly affect the behaviour of Ks in the samples tested in this research. The Ks results from short-term tests underscores the importance of reporting Ks as a range, especially for conditions where the hydraulic head changes rapidly. During rapid changes in the hydraulic head, such as the movement of flood water across/through soil, it is recommended to consider a range of values from low to high for Ks.

6.1.3. Pedotransfer functions for estimation of Ks: useful or not?

Pedotransfer functions (PTFs) hold significant promise for estimating Ks. However, to ensure reliable results, they should be used in conjunction with laboratory or field tests.

This study demonstrated that incorporating the coefficient of uniformity and void ratio into the calculation of the coefficients in Mbonimpa's equation significantly enhances the performance of the PTF for the tested samples. This modified formula offers a more accurate method for estimating the Ks of non-cohesive sandy samples. The results showed that modifications on constant key parameters of Mbonimpa's equation resulted in more accurate predictions of Ks compared with the original equation for the short-term Ks tests.

6.1.4. The use of Inverse Gaussian distribution for interpretation of breakthrough curves

Estimating Ks using tracer models based on advection-dispersion equations is complex and time-intensive. Tracer tests are typically conducted at large scales in the field, involving observations from multiple wells to derive aquifer hydraulic parameters. The calibration of these hydraulic parameters, which includes adjusting the dispersivity coefficient, pore velocity, and Ks, requires iterative trial-and-error procedures. Each trial involves running a groundwater model for the entire study area, checking if the predicted and observed breakthrough curves (BTCs) align, adjusting the hydraulic parameters, and

rerunning the model. Depending on the study area's size, each model run may take from hours to days. Therefore, a method for directly predicting hydraulic parameters from BTCs would significantly reduce the time required by groundwater modellers.

This research demonstrated that the Inverse Gaussian (IG) distribution predicts BTCs with high accuracy. Setting up the statistical distribution can be done using a simple spreadsheet, and the process of determining IG distribution parameters is considerably simpler than running an advection-dispersion equation (ADE) model. The model efficiency (based on the Nash-Sutcliffe model efficiency coefficient) in most cases was found to be close to 1, indicating high accuracy of predicted results compared with the lab measured breakthrough curves.

6.2. Limitations of the study and recommendations for future work

6.2.1. Varying Particle Size Distribution

The fluctuations observed in Ks highlight that the hydraulic conductivity is not a constant, where that approach may lead to inaccuracies in calculations related to water movement in soil. Long-term and short-term experiments were carried out on several sand dominated samples, which is a limitation of this study.There is not enough evidence to suggest whether the observed variations in Ks occur in other soil mixtures. Further experimentation on samples with varying PSDs will provide additional guidance on the anticipated response of Ks over time. Additionally, Ks tests on undisturbed samples will clarify whether undisturbed samples show the same variations in Ks or not.

6.2.2. Non-Linearity of Water Movement

Darcy's law is not sufficient in all situations to explain water movement in porous media, and assuming a constant value for Ks in saturated porous media is unreliable based on the testing completed.

This study did not cover the physical mechanisms behind the recorded changes of the Ks. It is recommended to investigate the physical mechanisms behind the non-linearity in movement of water in porous media. Specifically, understanding the physical process behind the different behaviours of Ks under gradual changes of hydraulic head during long-term tests and rapid changes of hydraulic head during short-term tests, will result in a better understanding of the movement of water in a porous medium.

One of the main factors affecting the variation of Ks is the change in the connectivity of the drainable pores in the samples. In this research the change in connections of the drainable pores was not recorded as this requires special instruments. Visualization of the changes in the drainable pores can be investigated by scanning the samples. X-ray computed tomography (CT) is recommended to observe the dynamic changes of drainable pores. However, using X-ray CT instruments during long-term Ks experiments can be complex and expensive.

6.2.3. Calibrate Regional PTFs

Pedotransfer functions (PTFs) are valuable tools for estimating Ks in data-scarce scenarios. Findings of this research are not sufficient for modification of existing Ks PTFs in New Zealand as developing PTFs will require extensive sampling of different types of soils and carrying out long-term Ks tests. However, it is recommended to calibrate PTFs for various regions in New Zealand and develop an extensive database of Ks values for native soils. Further studies on Ks for different soil types around New Zealand are essential to ensure the accuracy of the adopted PTFs. Caution is advised when using Ks data from other studies or projects to develop PTFs, as laboratory test procedures for determining Ks may lack quality control measures. For instance, full saturation of specimens is often not verified due to the absence of standardized procedures.

6.2.4. Link Inverse Gaussian Distribution to Hydraulic Parameters

The use of the Inverse Gaussian distribution can facilitate the iteration procedure for estimation of solute transport parameters. This distribution is suitable for positively skewed data, making it a favourable choice for the distribution of breakthrough curves (BTCs). However, when BTCs exhibit multiple peaks, the IG distribution may not predict the data accurately, making it less suitable in such cases. The accuracy of EC probes in this study was not enough to smoothly capture the changes of EC versus time during the tests where the Ks was very low. Additionally, this study did not investigate a relation between IG distribution parameters and soil hydraulic properties. The physical link between IG distribution parameters and aquifer hydraulic parameters could be a topic for further investigation.

References

Abdelbaki, A. M. (2016). Using automatic calibration method for optimizing the performance of Pedotransfer functions of saturated hydraulic conductivity. *Ain Shams Engineering Journal*, *7*(2), 653–662. https://doi.org/10.1016/j.asej.2015.05.012

Abdelbaki, A. M. (2021). Selecting the most suitable pedotransfer functions for estimating saturated hydraulic conductivity according to the available soil inputs. *Ain Shams Engineering Journal*, *12*(3), 2603–2615. https://doi.org/10.1016/j.asej.2021.01.030

Adjuik, T. A., Nokes, S. E., Montross, M., Sama, M. P., & Wendroth, O. (2023). Predictor Selection and Machine Learning Regression Methods to Predict Saturated Hydraulic Conductivity From a Large Public Soil Database. *Journal of the ASABE*, *66*(2), 285–296. https://doi.org/10.13031/ja.15068

Águila, J. F., McDonnell, M. C., Flynn, R., Butler, A. P., Hamill, G. A., Etsias, G., Benner, E. M., & Donohue, S. (2023). Comparison of saturated hydraulic conductivity estimated by empirical, hydraulic and numerical modeling methods at different scales in a coastal sand aquifer in Northern Ireland. *Environmental Earth Sciences*, *82*(13), 327. https://doi.org/10.1007/s12665-023-11019-6

Amoozegar, A. (2020). Examination of models for determining saturated hydraulic conductivity by the constant head well permeameter method. *Soil and Tillage Research*, *200*, 104572. https://doi.org/10.1016/j.still.2020.104572

Ani, E.-C., Wallis, S., Kraslawski, A., & Agachi, P. S. (2009). Development, calibration and evaluation of two mathematical models for pollutant transport in a small river. *Environmental Modelling & Software*, *24*(10), 1139–1152. https://doi.org/10.1016/j.envsoft.2009.03.008

Araya, S. N., & Ghezzehei, T. A. (2019). Using Machine Learning for Prediction of Saturated Hydraulic Conductivity and Its Sensitivity to Soil Structural Perturbations. *Water Resources Research*, *55*(7), 5715–5737. https://doi.org/10.1029/2018WR024357

Ashouri, S. N. (2024). *Supplementary Data for Manuscript "Examining the mid to long-term variability in saturated hydraulic conductivity of sandy soils and its influencing factors under constant head test in the laboratory."* https://doi.org/https://zenodo.org/doi/10.5281/zenodo.10538456

ASTM. (2019). Standard Test Method for Permeability of Granular Soils (Constant Head) (D2434-19). *ASTM International, West Conshohocken, PA*. https://doi.org/10.1520/D2434-19

ASTM 6034-96. (2010). Standard Test Method (Analytical Procedure) for Determining the Efficiency of a Production Well in a Confined Aquifer from a Constant Rate Pumping Test. *ASTM International*. https://doi.org/10.1520/D6034-96R10E01

ASTM D2434-19. (2019). Standard Test Method for Permeability of Granular Soils (Constant Head). *ASTM International, West Conshohocken, PA*. https://doi.org/10.1520/D2434-19

ASTM D2487. (2020). Standard Practice for Classification of Soils for Engineering Purposes (Unified Soil Classification System). *ASTM*.

ASTM D4044M. (2015). Standard Test Method for (Field Procedure) for Instantaneous Change in Head (Slug) Tests for Determining Hydraulic Properties of Aquifers. *ASTM International*. https://doi.org/10.1520/D4044_D4044M-15

ASTM D5856-15. (2015). Standard Test Method for Measurement of Hydraulic Conductivity of Porous Material Using a Rigid-Wall, Compaction-Mold Permeameter. *ASTM International, West Conshohocken, PA*.

ASTM, W. C. P. (2012). Standard Test Methods for Laboratory Compaction Characteristics of Soil Using Standard Effort. *ASTM International*. https://doi.org/https://doi.org/10.1520/D0698-12E01

Aubertin, M., Chapuis, R. P., & Mbonimpa, M. (2005). Discussion of "Goodbye, Hazen; Hello, Kozeny-Carman," by W. David Carrier III. *Journal of Geotechnical and Geoenvironmental Engineering*, *131*(8), 1056–1057. https://doi.org/10.1061/(ASCE)1090-0241(2005)131:8(1056)

Batlle-Aguilar, J., Cook, P. G., & Harrington, G. A. (2016). Comparison of hydraulic and chemical methods for determining hydraulic conductivity and leakage rates in argillaceous aquitards. *Journal of Hydrology*, *532*, 102–121. https://doi.org/10.1016/j.jhydrol.2015.11.035

Beach, D. N. H., McCray, J. E., Lowe, K. S., & Siegrist, R. L. (2005). Temporal changes in hydraulic conductivity of sand porous media biofilters during wastewater infiltration due to biomat formation. *Journal of Hydrology*, *311*(1–4), 230–243. https://doi.org/10.1016/j.jhydrol.2005.01.024

Ben-Hur, M., Yolcu, G., Uysal, H., Lado, M., & Paz, A. (2009). Soil structure changes: Aggregate size and soil texture effects on hydraulic conductivity under different saline and sodic conditions. *Australian Journal of Soil Research*. https://doi.org/10.1071/SR09009

Bloem, E., de Gee, M., & de Rooij, G. H. (2012). Parameterizing the Leaching Surface by Combining Curve-Fitting for Solute Breakthrough and for Spatial Solute Distribution. *Transport in Porous Media*, *92*(3), 667–685. https://doi.org/10.1007/s11242-011-9927-2

Boadu, F. K. (2000a). Hydraulic Conductivity of Soils from Grain-Size Distribution: New Models. *Journal of Geotechnical and Geoenvironmental Engineering*, *126*(8), 739–746. https://doi.org/10.1061/(ASCE)1090-0241(2000)126:8(739)

Boadu, F. K. (2000b). Hydraulic Conductivity of Soils from Grain-Size Distribution: New Models. *Journal of Geotechnical and Geoenvironmental Engineering*, *126*(8), 739–746. https://doi.org/10.1061/(ASCE)1090-0241(2000)126:8(739)

Breyer, W. (1964). Zur Bestimmung der Wasserdurchlässigkeit von Kiesen und Sanden aus der Kornverteilung. *Wasserwirtschaft- Wassertechnik 14*, 165–169.

Butler, J. J. (2005). *Hydrogeological Methods for Estimation of Spatial Variations in Hydraulic Conductivity* (pp. 23–58). https://doi.org/10.1007/1-4020-3102-5_2

Cabalar, A. F., & Akbulut, N. (2016). Evaluation of actual and estimated hydraulic conductivity of sands with different gradation and shape. *SpringerPlus*, *5*(1), 820. https://doi.org/10.1186/s40064-016-2472-2

Carman, P. C. (1939). Permeability of saturated sands, soils and clays. *The Journal of Agricultural Science*, *29*(2), 262–273. https://doi.org/10.1017/S0021859600051789

Carrier, W. D. (2003). Goodbye, Hazen; Hello, Kozeny-Carman. *Journal of Geotechnical and Geoenvironmental Engineering*, *129*(11), 1054–1056. https://doi.org/10.1061/(ASCE)1090-0241(2003)129:11(1054)

Chabokpour, J. (2020). Study of pollution transport through the rivers using aggregated dead zone and hybrid cells in series models. *International Journal of Environmental Science and Technology*, *17*(10), 4313–4330. https://doi.org/10.1007/s13762-020-02741-w

Chapuis, R. (2004). Permeability Tests in Rigid-Wall Permeameters: Determining the Degree of Saturation, its Evolution, and its Influence of Test Results. *Geotechnical Testing Journal*, *27*(3), 304–313. https://doi.org/10.1520/GTJ10905

Chapuis, R. P. (2004). Predicting the saturated hydraulic conductivity of sand and gravel using effective diameter and void ratio. *Canadian Geotechnical Journal*, *41*(5), 787–795. http://ezproxy.waikato.ac.nz/login?url=https://www.proquest.com/scholarly-journals/predicting-saturated-hydraulic-conductivity-sand/docview/213421795/se-2?accountid=17287

Chapuis, R. P. (2012a). Predicting the saturated hydraulic conductivity of soils: a review. *Bulletin of Engineering Geology and the Environment*, *71*(3), 401–434. https://doi.org/10.1007/s10064-012-0418-7

Chapuis, R. P. (2012b). Predicting the saturated hydraulic conductivity of soils: a review. *Bulletin of Engineering Geology and the Environment*, *71*(3), 401–434. https://doi.org/10.1007/s10064-012-0418-7

Chapuis, R. P., & Aubertin, M. (2010). Discussion of "Influence of relative compaction on the hydraulic conductivity of completely decomposed granite in Hong Kong"Appears in Canadian Geotechnical Journal, **46** (10): 1229–1235. *Canadian Geotechnical Journal*, *47*(6), 704–707. https://doi.org/10.1139/T10-035

Chapuis, R. P., Gill, D. E., & Baass, K. (1989). Laboratory permeability tests on sand: influence of the compaction method on anisotropy. *Canadian Geotechnical Journal*, *26*(4), 614–622. https://doi.org/10.1139/t89-074

Chen, J., Qian, H., Yang, M., Qin, J., & Qu, W. (2021a). Effects of bacterial activity on the saturated hydraulic conductivity of remolded loess. *Engineering Geology*, *287*, 106101. https://doi.org/10.1016/j.enggeo.2021.106101

Chen, J., Qian, H., Yang, M., Qin, J., & Qu, W. (2021b). Effects of bacterial activity on the saturated hydraulic conductivity of remolded loess. *Engineering Geology*, *287*, 106101. https://doi.org/10.1016/j.enggeo.2021.106101

Cheng, C., & Chen, X. (2007). Evaluation of methods for determination of hydraulic properties in an aquifer–aquitard system hydrologically connected to a river. *Hydrogeology Journal*, *15*(4), 669–678. https://doi.org/10.1007/s10040-006-0135-z

Cheong, J.-Y., Hamm, S.-Y., Kim, H.-S., Ko, E.-J., Yang, K., & Lee, J.-H. (2008). Estimating hydraulic conductivity using grain-size analyses, aquifer tests, and numerical modeling in a riverside alluvial system in South Korea. *Hydrogeology Journal*, *16*(6), 1129. https://doi.org/10.1007/s10040-008-0303-4

Cherif Taiba, A., Mahmoudi, Y., Hazout, L., Belkhatir, M., & Baille, W. (2019). Evaluation of hydraulic conductivity through particle shape and packing density characteristics of sand–silt mixtures. *Marine Georesources & Geotechnology*, *37*(10), 1175–1187. https://doi.org/10.1080/1064119X.2018.1539891

Chhikara, R. (1988). *The Inverse Gaussian Distribution: Theory: Methodology, and Applications*. Taylor & Francis. https://books.google.co.nz/books?id=bGyHxrEALI0C

Cichota, R., Vogeler, I., Snow, V. O., & Webb, T. H. (2013). Ensemble pedotransfer functions to derive hydraulic properties for New Zealand soils. *Soil Research*, *51*(2), 94. https://doi.org/10.1071/SR12338

Cihan, A., Petrusak, R., Bhuvankar, P., Alumbaugh, D., Trautz, R., & Birkholzer, J. T. (2022a). Permeability Decline by Clay Fines Migration around a Low-Salinity Fluid Injection Well. *Groundwater*, *60*(1), 87–98. https://doi.org/10.1111/gwat.13127

Cihan, A., Petrusak, R., Bhuvankar, P., Alumbaugh, D., Trautz, R., & Birkholzer, J. T. (2022b). Permeability Decline by Clay Fines Migration around a Low-Salinity Fluid Injection Well. *Groundwater*, *60*(1), 87–98. https://doi.org/10.1111/gwat.13127

Daneshian, B., Habibagahi, G., & Nikooee, E. (2021). Determination of unsaturated hydraulic conductivity of sandy soils: a new pore network approach. *Acta Geotechnica*, *16*(2), 449–466. https://doi.org/10.1007/s11440-020-01088-3

de Rooij, G. H. (2012). Transient flow between aquifers and surface water: analytically derived field-scale hydraulic heads and fluxes. *Hydrology and Earth System Sciences*, *16*(3), 649–669. https://doi.org/10.5194/hess-16-649-2012

Deb. (2012). VARIABILITY OF HYDRAULIC CONDUCTIVITY DUE TO MULTIPLE FACTORS. *American Journal of Environmental Sciences*, *8*(5), 489–502. https://doi.org/10.3844/ajessp.2012.489.502

Devi, A., Chandel, A., & Shankar, V. (2025). Modelling hydraulic conductivity of porous media using machine learning techniques. *Journal of Hydroinformatics*, *27*(3), 381–405. https://doi.org/10.2166/hydro.2025.161

Dikinya, O., Hinz, C., & Aylmore, G. (2006). Dispersion and re-deposition of fine particles and their effects on saturated hydraulic conductivity. *Soil Research*, *44*(1), 47. https://doi.org/10.1071/SR05067

Du, X., Wang, Z., & Ye, X. (2013). Potential Clogging and Dissolution Effects During Artificial Recharge of Groundwater Using Potable Water. *Water Resources Management*, *27*(10), 3573–3583. https://doi.org/10.1007/S11269-013-0365-5/FIGURES/13

Du, X., Zhang, H., Ye, X., & Lu, Y. (2018). Flow Velocity Effects on Fe(III) Clogging during Managed Aquifer Recharge Using Urban Storm Water. *Water 2018, Vol. 10, Page 358*, *10*(4), 358. https://doi.org/10.3390/W10040358

Duan, R., Fedler, C. B., & Borrelli, J. (2012). Comparison of Methods to Estimate Saturated Hydraulic Conductivity in Texas Soils with Grass. *Journal of Irrigation and Drainage Engineering*, *138*(4), 322–327. https://doi.org/10.1061/(ASCE)IR.1943-4774.0000407

Đukić, V., & Radić, Z. (2016). Sensitivity Analysis of a Physically Based Distributed Model. *Water Resources Management*, *30*(5), 1669–1684. https://doi.org/10.1007/s11269-016-1243-8

Elhakim, A. F. (2016). Estimation of soil permeability. *Alexandria Engineering Journal*, *55*(3), 2631–2638. https://doi.org/10.1016/j.aej.2016.07.034

Fang, Y., Kong, L., Zhang, P., Zhang, L., Zhao, H., Xiang, X., Cheng, S., Zhang, H., Ju, F., & Li, L. (2022). Fifteen-year analysis of constructed wetland clogging: A critical review. *Journal of Cleaner Production*, *365*, 132755. https://doi.org/https://doi.org/10.1016/j.jclepro.2022.132755

Feng, S., & Vardanega, P. J. (2019). A database of saturated hydraulic conductivity of fine-grained soils: probability density functions. *Georisk: Assessment and Management of Risk for Engineered Systems and Geohazards*, *13*(4), 255–261. https://doi.org/10.1080/17499518.2019.1652919

Ferrer Julià, M., Estrela Monreal, T., Sánchez del Corral Jiménez, A., & García Meléndez, E. (2004). Constructing a saturated hydraulic conductivity map of Spain using pedotransfer functions and spatial prediction. *Geoderma*, *123*(3–4), 257–277. https://doi.org/10.1016/j.geoderma.2004.02.011

Ferris, J. G. (1952). *Cyclic fluctuations of water level as a basis for determining aquifer transmissibility*. https://doi.org/10.3133/70133368

Field, M. S. (2003). A review of some tracer-test design equations for tracer-mass estimation and sample-collection frequency. *Environmental Geology*, *43*(8), 867–881. https://doi.org/10.1007/s00254-002-0708-7

Fienen, M. N., Luo, J., & Kitanidis, P. K. (2006). A Bayesian geostatistical transfer function approach to tracer test analysis. *Water Resources Research*, *42*(7). https://doi.org/10.1029/2005WR004576

Francisca, F. M., & Glatstein, D. A. (2010). Long term hydraulic conductivity of compacted soils permeated with landfill leachate. *Applied Clay Science*. https://doi.org/10.1016/j.clay.2010.05.003

Ghanbarian, B., Taslimitehrani, V., & Pachepsky, Y. A. (2017). Accuracy of sample dimension-dependent pedotransfer functions in estimation of soil saturated hydraulic conductivity. *CATENA*, *149*, 374–380. https://doi.org/10.1016/j.catena.2016.10.015

Ghibus, T., Gaitanaru, D., & Gogu, C. R. (2023). *Evaluation of In-Situ Test Methods for the Assessment of Saturated Hydraulic Conductivity of Unsaturated Urban Soils*. https://doi.org/10.2139/ssrn.4594435

Glose, T. J., Lowry, C. S., & Hausner, M. B. (2019). Vertically Integrated Hydraulic Conductivity: A New Parameter for Groundwater-Surface Water Analysis. *Groundwater*, *57*(5), 727–736. https://doi.org/10.1111/gwat.12864

Goldenberg, L. C., Magaritz, M., & Mandel, S. (1983). Experimental investigation on irreversible changes of hydraulic conductivity on the seawater-freshwater interface in coastal aquifers. *Water Resources Research*, *19*(1), 77–85. https://doi.org/10.1029/WR019i001p00077

Hangen, E., & Vieten, F. (2018). A Comparison of Five Different Techniques to Determine Hydraulic Conductivity of a Riparian Soil in North Bavaria, Germany. *Pedosphere*, *28*(3), 443–450. https://doi.org/10.1016/S1002-0160(17)60385-0

Hazen, A. (1892). Some Physical Properties of Sands and Gravels, with Special Reference to Their Use in Filtration. *24th Annual Report, Massachusetts State Board of Health*, 539–556.

He, H., Zou, W., Jones, S. B., Robinson, D. A., Horton, R., Dyck, M., Filipović, V., Noborio, K., Bristow, K., Gong, Y., Sheng, W., Wu, Q., Feng, H., & Liu, Y. (2023). *Critical review of the models used to determine soil water content using TDR-measured apparent permittivity* (pp. 169–219). https://doi.org/10.1016/bs.agron.2023.06.004

Hess, K. M., Wolf, S. H., & Celia, M. A. (1992). Large-scale natural gradient tracer test in sand and gravel, Cape Cod, Massachusetts: 3. Hydraulic conductivity variability and calculated macrodispersivities. *Water Resources Research*, *28*(8), 2011–2027. https://doi.org/10.1029/92WR00668

Hördt, A., Blaschek, R., Kemna, A., & Zisser, N. (2007). Hydraulic conductivity estimation from induced polarisation data at the field scale — the Krauthausen case history. *Journal of Applied Geophysics*, *62*(1), 33–46. https://doi.org/10.1016/j.jappgeo.2006.08.001

Hoseini, Y. (2023). Optimization of saturated hydraulic conductivity estimation using kriging in drainage networks. *Applied Water Science*, *13*(4), 94. https://doi.org/10.1007/s13201-023-01897-3

Huang, M., Lee Barbour, S., Elshorbagy, A., Zettl, J. D., & Cheng Si, B. (2011). Infiltration and drainage processes in multi-layered coarse soils. *Canadian Journal of Soil Science*, *91*(2), 169–183. https://doi.org/10.4141/cjss09118

Hwang, H., Jeen, S., Suleiman, A., & Lee, K. (2017). Comparison of Saturated Hydraulic Conductivity Estimated by Three Different Methods. *Water*, *9*(12), 942. https://doi.org/10.3390/w9120942

Hwang, H. T., Jeen, S. W., Suleiman, A. A., & Lee, K. K. (2017). Comparison of saturated hydraulic conductivity estimated by three different methods. *Water (Switzerland)*. https://doi.org/10.3390/w9120942

Ibrahim, M., & Aliyu, J. (2016). Comparison of Methods for Saturated Hydraulic Conductivity Determination: Field, Laboratory and Empirical Measurements (A Pre-view). *British Journal of Applied Science & Technology*, *15*(3), 1–8. https://doi.org/10.9734/BJAST/2016/24413

Islam, A., Mailapalli, D. R., & Behera, A. (2019). Comparison of Saturated Hydraulic Conductivity Methods for Sandy Loam Soil with Different Land Uses. In *Water Resources and Environmental Engineering I* (pp. 99–117). Springer Singapore. https://doi.org/10.1007/978-981-13-2044-6_10

Jabro, J. D. (1992). Estimation of Saturated Hydraulic Conductivity of Soils From Particle Size Distribution and Bulk Density Data. *Transactions of the ASAE*, *35*(2), 557–560. https://doi.org/10.13031/2013.28633

Jardani, A., Revil, A., & Dupont, J. P. (2013). Stochastic joint inversion of hydrogeophysical data for salt tracer test monitoring and hydraulic conductivity imaging. *Advances in Water Resources*, *52*, 62–77. https://doi.org/10.1016/j.advwatres.2012.08.005

Jeong, H. Y., Jun, S.-C., Cheon, J.-Y., & Park, M. (2018a). A review on clogging mechanisms and managements in aquifer storage and recovery (ASR) applications. *Geosciences Journal*, *22*(4), 667–679. https://doi.org/10.1007/s12303-017-0073-x

Jeong, H. Y., Jun, S.-C., Cheon, J.-Y., & Park, M. (2018b). A review on clogging mechanisms and managements in aquifer storage and recovery (ASR) applications. *Geosciences Journal*, *22*(4), 667–679. https://doi.org/10.1007/s12303-017-0073-x

Jo, H. Y., Benson, C. H., Shackelford, C. D., Lee, J.-M., & Edil, T. B. (2005). Long-Term Hydraulic Conductivity of a Geosynthetic Clay Liner Permeated with Inorganic Salt Solutions. *Journal of Geotechnical and Geoenvironmental Engineering*. https://doi.org/10.1061/(asce)1090-0241(2005)131:4(405)

Johnson, N. Lloyd., Kotz, Samuel., & Balakrishnan, N. (1994). *Continuous univariate distributions*. Wiley.

Kabala, Z. J. (1993). The dipole flow test: A new single-borehole test for aquifer characterization. *Water Resources Research*, *29*(1), 99–107. https://doi.org/10.1029/92WR01820

Keïta, A., Zorom, M., Faye, M. D., Damba, D. D., Konaté, Y., Hayde, L. G., & Lidon, B. (2023). Achieving Real-World Saturated Hydraulic Conductivity: Practical and Theoretical Findings from Using an Exponential One-Phase Decay Model. *Hydrology*, *10*(12), 235. https://doi.org/10.3390/hydrology10120235

Kenney, T. C., Lau, D., & Ofoegbu, G. I. (1984). Permeability of compacted granular materials. *Canadian Geotechnical Journal*, *21*(4), 726–729. https://doi.org/10.1139/t84-080

Khaja, M. A., Shah, S. R., & Jha, R. (2022). Evaluation of empirical models for estimating hydraulic conductivity using gradation characteristics of unconsolidated fluvial sediments. *Arabian Journal of Geosciences*, *15*(8), 720. https://doi.org/10.1007/s12517-022-10002-y

Knöll, P., & Scheytt, T. (2018). A tracer test to determine a hydraulic connection between the Lauchert and Danube karst catchments (Swabian Alb, Germany). *Hydrogeology Journal*, *26*(2), 429–437. https://doi.org/10.1007/s10040-017-1678-x

Konikow, L. F., August, L. L., & Voss, C. I. (2001a). Effects of Clay Dispersion on Aquifer Storage and Recovery in Coastal Aquifers. *Transport in Porous Media*, *43*(1), 45–64. https://doi.org/10.1023/A:1010613525547

Konikow, L. F., August, L. L., & Voss, C. I. (2001b). Effects of Clay Dispersion on Aquifer Storage and Recovery in Coastal Aquifers. *Transport in Porous Media*, *43*(1), 45–64. https://doi.org/10.1023/A:1010613525547

Kotlar, A. M., Iversen, B. V., & de Jong van Lier, Q. (2019). Evaluation of Parametric and Nonparametric Machine-Learning Techniques for Prediction of Saturated and Near-Saturated Hydraulic Conductivity. *Vadose Zone Journal*, *18*(1), 1–13. https://doi.org/10.2136/vzj2018.07.0141

Kozeny, J. (1927a). Ueber kapillare Leitung des Wassers im Boden. *Sitzungsber Akad*, 271–306.

Kozeny, J. (1927b). Ueber kapillare Leitung des Wassers im Boden. Sitzungsber Akad. *Sitzungsber Akad. Wiss., Wien, 136(2a)*, 271–306.

Kretzschmar, R., Borkovec, M., Grolimund, D., & Elimelech, M. (1999). *Mobile Subsurface Colloids and Their Role in Contaminant Transport* (pp. 121–193). https://doi.org/10.1016/S0065-2113(08)60427-7

Krumbein, W. C., & Monk, G. D. (1942). *Permeability as a Function of the Size Parameters of Unconsolidated Sand*. American Institute of Mining and Metallurgical Engineers. https://books.google.co.nz/books?id=Ru-3XwAACAAJ

Ladd, R. (1978). Preparing Test Specimens Using Undercompaction. *Geotechnical Testing Journal*, *1*(1), 16. https://doi.org/10.1520/GTJ10364J

Landcare Research. (2023). *SMAP (Digital Soil Map of New Zealand)*. Landcare Research (Manaaki Whenua).

Lebron, I., Schaap, M. G., & Suarez, D. L. (1999). Saturated hydraulic conductivity prediction from microscopic pore geometry measurements and neural network analysis. *Water Resources Research*, *35*(10), 3149–3158. https://doi.org/10.1029/1999WR900195

Lee, J., & Lee, K. (1999). Analysis of the Quality of Parameter Estimates from Repeated Pumping and Slug Tests in a Fractured Porous Aquifer System in Wonju, Korea. *Groundwater*, *37*(5), 692–700. https://doi.org/10.1111/j.1745-6584.1999.tb01161.x

Lei, D., Sun, H., Zhang, Y., Blaszczyk, T., & Yu, Z. (2023). Upscaling solute transport in rough single-fractured media with matrix diffusion using a time fractional advection-dispersion equation. *Journal of Hydrology*, *627*, 130280. https://doi.org/10.1016/j.jhydrol.2023.130280

Leibundgut, C., Speidel, U., & Weisner, H. (1993). TRANSPORT PROCESSES IN RIVERS INVESTIGATED BY TRACER EXPERIMENTS. *Tracers in Hydrology (Proceedings of the Yokohama Symposium)*.

Leiva, V., Hernández, H., & Sanhueza, A. (2008). An R Package for a General Class of Inverse Gaussian Distributions. *Journal of Statistical Software*, *26*(4). https://doi.org/10.18637/jss.v026.i04

Li, K., Chen, Y., Ye, W., & Wang, Q. (2023). Modelling the evolution of dual-pore structure for compacted clays along hydro-mechanical paths. *Computers and Geotechnics*, *157*, 105308. https://doi.org/https://doi.org/10.1016/j.compgeo.2023.105308

Libohova, Z., Schoeneberger, P., Bowling, L. C., Owens, P. R., Wysocki, D., Wills, S., Williams, C. O., & Seybold, C. (2018). Soil Systems for Upscaling Saturated Hydraulic Conductivity for Hydrological Modeling in the Critical Zone. *Vadose Zone Journal*, *17*(1), 1–20. https://doi.org/10.2136/vzj2017.03.0051

Liu, G., Butler, J. J., Reboulet, E., & Knobbe, S. (2012). Hydraulic conductivity profiling with direct push methods. *Grundwasser*, *17*(1), 19–29. https://doi.org/10.1007/s00767-011-0182-9

Liu, Y., & Liu, J. (2020). The BioChemical Clogging of Landfill Leachate Collection System: Based on Laboratory Studies. *International Journal of Environmental Research and Public Health*, *17*(7), 2299. https://doi.org/10.3390/ijerph17072299

Loudon, A. G. (1952). The Computation of Permeability from Simple Soil Tests. *Géotechnique*, *3*(4), 165–183. https://doi.org/10.1680/geot.1952.3.4.165

Lu, H., Wang, C., Li, D., Li, J., & Wan, Y. (2020). Permeability, Pore, and Structural Parameters of Undisturbed Silty Clay Presented in Landfill Leachate. *Water, Air, & Soil Pollution*, *231*(5), 190. https://doi.org/10.1007/s11270-020-04568-0

M. Foster, L., & M. Maxwell, R. (2019). Sensitivity analysis of hydraulic conductivity and Manning's *n* parameters lead to new method to scale effective hydraulic conductivity across model resolutions. *Hydrological Processes*, *33*(3), 332–349. https://doi.org/10.1002/hyp.13327

Mallants, D. (2014). Field-scale solute transport parameters derived from tracer tests in large undisturbed soil columns. *Soil Research*, *52*(1), 13. https://doi.org/10.1071/SR13143

Masipan, T., Chotpantarat, S., & Boonkaewwan, S. (2016). Experimental and modelling investigations of tracer transport in variably saturated agricultural soil of Thailand: Column study. *Sustainable Environment Research*, *26*(2), 97–101. https://doi.org/10.1016/j.serj.2016.04.005

Mavis, F. T., & Wilsey, E. F. (1936). *A study of the permeability of sand*. State University of Iowa. https://doi.org/10.17077/006163

Mays, D. C., & Hunt, J. R. (2005). Hydrodynamic Aspects of Particle Clogging in Porous Media. *Environmental Science & Technology*, *39*(2), 577–584. https://doi.org/10.1021/es049367k

Mbonimpa, M., Aubertin, M., Chapuis, R. P., & Bussière, B. (2002). Practical pedotransfer functions for estimating the saturated hydraulic conductivity. *Geotechnical and Geological Engineering*, *20*(3), 235–259. https://doi.org/10.1023/A:1016046214724

McCuen, R. H., Knight, Z., & Cutter, A. G. (2006). Evaluation of the Nash–Sutcliffe Efficiency Index. *Journal of Hydrologic Engineering*, *11*(6), 597–602. https://doi.org/10.1061/(ASCE)1084-0699(2006)11:6(597)

McDonald, M. G., & Harbaugh, A. W. (1988). *A modular three-dimensional finite-difference ground-water flow model*. https://doi.org/10.3133/twri06A1

McNeill, S. J., Lilburne, L. R., Carrick, S., Webb, T. H., & Cuthill, T. (2018). Pedotransfer functions for the soil water characteristics of New Zealand soils using S-map information. *Geoderma*, *326*, 96–110. https://doi.org/10.1016/j.geoderma.2018.04.011

Melville, J. G., Molz, F. J., Güven, O., & Widdowson, M. A. (1991). Multilevel Slug Tests with Comparisons to Tracer Data. *Groundwater*, *29*(6), 897–907. https://doi.org/10.1111/j.1745-6584.1991.tb00577.x

Millham, N. P., & Howes, B. L. (1995). A Comparison of Methods to Determine K in a Shallow Coastal Aquifer. *Groundwater*, *33*(1), 49–57. https://doi.org/10.1111/j.1745-6584.1995.tb00262.x

Minasny, B., McBratney, A. B., & Bristow, K. L. (1999). Comparison of different approaches to the development of pedotransfer functions for water-retention curves. *Geoderma*, *93*(3–4), 225–253. https://doi.org/10.1016/S0016-7061(99)00061-0

Minutti, C., Illman, W. A., & Gomez, S. (2020). A New Inverse Modeling Approach for Hydraulic Conductivity Estimation Based on Gaussian Mixtures. *Water Resources Research*, *56*(9). https://doi.org/10.1029/2019WR026531

Mitrinović, D., Kovačević, S., Vojt, P., Pušić, M., & Dimkić, M. (2019). Tracer test analysis using flow and transport simulation code and new analytical transport model 27 April 2019. *Water Environment Research*, *91*(9), 940–953. https://doi.org/10.1002/wer.1135

Mohan, K. K., Vaidya, R. N., Reed, M. G., & Fogler, H. S. (1993). Water sensitivity of sandstones containing swelling and non-swelling clays. *Colloids and Surfaces A: Physicochemical and Engineering Aspects*, *73*, 237–254. https://doi.org/10.1016/0927-7757(93)80019-B

Mojid, M. A. (2024). Performance of Six Methods in Determining Solute-Transport Parameters from Breakthrough Curves. *Communications in Soil Science and Plant Analysis*, 1–20. https://doi.org/10.1080/00103624.2024.2319801

Monego, M., Cassiani, G., Deiana, R., Putti, M., Passadore, G., & Altissimo, L. (2010). A tracer test in a shallow heterogeneous aquifer monitored via time-lapse surface electrical resistivity tomography. *GEOPHYSICS*, *75*(4), WA61–WA73. https://doi.org/10.1190/1.3474601

Montoro, M. A., & Francisca, F. M. (2010). Soil Permeability Controlled by Particle-Fluid Interaction. *Geotechnical and Geological Engineering*. https://doi.org/10.1007/s10706-010-9348-y

Moosavi, A. A., Nematollahi, M. A., & Omidifard, M. (2024). Comparing machine learning approaches for estimating soil saturated hydraulic conductivity. *PLOS ONE*, *19*(11), e0310622. https://doi.org/10.1371/journal.pone.0310622

Mustafa, S., & Darwish, M. (2022). Effect of Hydraulic Conductivity on Three Dimensional Contaminant Transport in Riverbank Filtration System. *Asian Journal of Water, Environment and Pollution*, *19*(6), 1–9. https://doi.org/10.3233/AJW220082

Nagatsuka, H., & Balakrishnan, N. (2013). A consistent method of estimation for the parameters of the three-parameter inverse Gaussian distribution. *Journal of Statistical Computation and Simulation*, *83*(10), 1915–1931. https://doi.org/10.1080/00949655.2012.674130

Naik, A. P., Norbu, T., & Pekkat, S. (2024). Comparison of flux-based and head-based methods for determination of near-surface saturated hydraulic conductivity. *Hydrological Sciences Journal*, *69*(3), 275–293. https://doi.org/10.1080/02626667.2024.2305745

Nash, J. E., & Sutcliffe, J. V. (1970). River flow forecasting through conceptual models part I — A discussion of principles. *Journal of Hydrology*, *10*(3), 282–290. https://doi.org/10.1016/0022-1694(70)90255-6

Nikghalb Ashouri, S. (2024). EC-t dataset for: Using Inverse Gaussian Distribution for Analysis of Breakthrough Curves in Tracer Tests for Sandy Samples in Rigid Wall Cell. *Zenodo Respository*.

Nikghalb Ashouri, S., Pittari, A., Moon, V., & Shokri, A. (2023). Examining long-term variability in saturated hydraulic conductivity of sandy soils and its influencing factors. *ESS OPEN ARCHIVE (Pre-Print)*. https://essopenarchive.org/users/664099/articles/665992-examining-long-term-variability-in-saturated-hydraulic-conductivity-of-sandy-soils-and-its-influencing-factors

Niu, C., Guo, X., Xu, W., & Zhu, L. (2014). Testing equality of shape parameters in several inverse Gaussian populations. *Metrika*, *77*(6), 795–809. https://doi.org/10.1007/s00184-013-0465-5

Novák, V., & Hlaváčiková, H. (2019). *Soil-Water Movement in Water-Saturated Capillary Porous Media* (pp. 97–117). https://doi.org/10.1007/978-3-030-01806-1_8

Nowak, W., & Cirpka, O. A. (2006). Geostatistical inference of hydraulic conductivity and dispersivities from hydraulic heads and tracer data. *Water Resources Research*, *42*(8). https://doi.org/10.1029/2005WR004832

Oliveira, M. A., Vaz, A. S. L., Siqueira, F. D., Yang, Y., You, Z., & Bedrikovetsky, P. (2014). Slow migration of mobilised fines during flow in reservoir rocks: Laboratory study. *Journal of Petroleum Science and Engineering*, *122*, 534–541. https://doi.org/10.1016/j.petrol.2014.08.019

Olson, N. C., Gulliver, J. S., Nieber, J. L., & Kayhanian, M. (2013). Remediation to improve infiltration into compact soils. *Journal of Environmental Management*, *117*, 85–95. https://doi.org/10.1016/j.jenvman.2012.10.057

Passos, R. G., Dias, D. F. C., Matos, M. P., & von Sperling, M. (2018). Sodium chloride as a tracer for hydrodynamic characterization of a shallow maturation pond. *Water Practice and Technology*, *13*(1), 30–38. https://doi.org/10.2166/wpt.2018.009

Pásztor, L., Szabó, B., Makó, A., Kocsis, M., Mészáros, J., Laborczi, A., Takács, K., & Szatmári, G. (2025). *Elaboration of 3D Soil Hydraulic Databases in Hungary*. https://doi.org/10.5194/egusphere-egu24-11606

Pedescoll, A., Samsó, R., Romero, E., Puigagut, J., & García, J. (2011). Reliability, repeatability and accuracy of the falling head method for hydraulic conductivity measurements under laboratory conditions. *Ecological Engineering*, *37*(5), 754–757. https://doi.org/10.1016/j.ecoleng.2010.06.032

Picciafuoco, T., Morbidelli, R., Flammini, A., Saltalippi, C., Corradini, C., Strauss, P., & Blöschl, G. (2019). A Pedotransfer Function for Field-Scale Saturated Hydraulic Conductivity of a Small Watershed. *Vadose Zone Journal*, *18*(1), 1–15. https://doi.org/10.2136/vzj2019.02.0018

Piccinini, L., Fabbri, P., & Pola, M. (2016). Point dilution tests to calculate groundwater velocity: an example in a porous aquifer in northeast Italy. *Hydrological Sciences Journal*, *61*(8), 1512–1523. https://doi.org/10.1080/02626667.2015.1036756

Pillsbury, A. F., & Appleman, D. (1945). Factors in permeability changes of soils and inert granular material. *Soil Science*, *59*(2), 115–123. https://doi.org/10.1097/00010694-194502000-00002

Pollock, D., & Cirpka, O. A. (2010). Fully coupled hydrogeophysical inversion of synthetic salt tracer experiments. *Water Resources Research*, *46*(7). https://doi.org/10.1029/2009WR008575

Prych, E. A. (1999). A tracer test to estimate hydraulic conductivities and dispersivities of sediments in the shallow aquifer at the East Gate Disposal Yard, Fort Lewis, Washington. In *Water-Resources Investigations Report*. https://doi.org/10.3133/wri994244

Ptak, T., Piepenbrink, M., & Martac, E. (2004). Tracer tests for the investigation of heterogeneous porous media and stochastic modelling of flow and transport—a review of some recent developments. *Journal of Hydrology*, *294*(1–3), 122–163. https://doi.org/10.1016/j.jhydrol.2004.01.020

Pucko, T., & Verbovšek, T. (2015). Comparison of hydraulic conductivities by grain-size analysis,pumping, and slug tests in Quaternary gravels, NE Slovenia. *Open Geosciences*, *7*(1). https://doi.org/10.1515/geo-2015-0032

Punzo, A. (2019). A new look at the inverse Gaussian distribution with applications to insurance and economic data. *Journal of Applied Statistics*, *46*(7), 1260–1287. https://doi.org/10.1080/02664763.2018.1542668

Qiu, H., Hu, R., Luo, N., Illman, W. A., & Hou, X. (2023). Comparison of travel-time and geostatistical inversion approaches for hydraulic tomography: Synthetic modeling study on data density and well configuration issues. *Journal of Hydrology*, *618*, 129247. https://doi.org/10.1016/j.jhydrol.2023.129247

Quinton, W. L., Hayashi, M., & Carey, S. K. (2008). Peat hydraulic conductivity in cold regions and its relation to pore size and geometry. *Hydrological Processes*, *22*(15), 2829–2837. https://doi.org/10.1002/hyp.7027

Radcliffe, D. E., & Simunek, J. (2018). *Soil Physics with HYDRUS*. CRC Press. https://doi.org/10.1201/9781315275666

Rajabi, M. M., Hajizadeh Javaran, M. R., Bah, A., Frey, G., Le Ber, F., Lehmann, F., & Fahs, M. (2022). Analyzing the efficiency and robustness of deep convolutional neural networks for modeling natural convection in heterogeneous porous media. *International Journal of Heat and Mass Transfer*, *183*, 122131. https://doi.org/10.1016/j.ijheatmasstransfer.2021.122131

Ranieri, E., Gorgoglione, A., & Solimeno, A. (2013). A comparison between model and experimental hydraulic performances in a pilot-scale horizontal subsurface flow constructed wetland. *Ecological Engineering*, *60*, 45–49. https://doi.org/10.1016/j.ecoleng.2013.07.037

Rehman, Z. ur, Khalid, U., Ijaz, N., Mujtaba, H., Haider, A., Farooq, K., & Ijaz, Z. (2022). Machine learning-based intelligent modeling of hydraulic conductivity of sandy soils considering a wide range of grain sizes. *Engineering Geology*, *311*, 106899. https://doi.org/10.1016/j.enggeo.2022.106899

Reinecke, R., Foglia, L., Mehl, S., Herman, J. D., Wachholz, A., Trautmann, T., & Döll, P. (2019). Spatially distributed sensitivity of simulated global groundwater heads and flows to hydraulic conductivity, groundwater recharge, and surface water body parameterization. *Hydrology and Earth System Sciences*, *23*(11), 4561–4582. https://doi.org/10.5194/hess-23-4561-2019

Ren, X., Zhao, Y., Deng, Q., Kang, J., Li, D., & Wang, D. (2016). A relation of hydraulic conductivity — void ratio for soils based on Kozeny-Carman equation. *Engineering Geology*, *213*, 89–97. https://doi.org/10.1016/j.enggeo.2016.08.017

Rinck-Pfeiffer, S. (2000). Interrelationships between biological, chemical, and physical processes as an analog to clogging in aquifer storage and recovery (ASR) wells. *Water Research*, *34*(7), 2110–2118. https://doi.org/10.1016/S0043-1354(99)00356-5

Rodgers, M., & Mulqueen, J. (2004). Field-saturated hydraulic conductivity of soils from laboratory constant-head well tests. *Irrigation and Drainage Systems*, *18*(4), 315–327. https://doi.org/10.1007/s10795-004-3265-2

ROWIŃSKI, P. M., GUYMER, I., & KWIATKOWSKI, K. (2008). Response to the slug injection of a tracer—a large-scale experiment in a natural river / Réponse à l'injection impulsionnelle d'un traceur—expérience à grande échelle en rivière naturelle. *Hydrological Sciences Journal*, *53*(6), 1300–1309. https://doi.org/10.1623/hysj.53.6.1300

Sadeghi, H., & AliPanahi, P. (2020). Saturated hydraulic conductivity of problematic soils measured by a newly developed low-compliance triaxial permeameter. *Engineering Geology*, *278*, 105827. https://doi.org/10.1016/j.enggeo.2020.105827

Sanzeni, A., Colleselli, F., & Grazioli, D. (2013). Specific Surface and Hydraulic Conductivity of Fine-Grained Soils. *Journal of Geotechnical and Geoenvironmental Engineering*, *139*(10), 1828–1832. https://doi.org/10.1061/(ASCE)GT.1943-5606.0000892

Sarki, A., Mirjat, M. S., Mahessar, A. A., Kori, S. M., & Qureshi, A. L. (2014). Determination of Saturated Hydraulic Conductivity of Different Soil Texture Materials. *IOSR Journal of Agriculture and Veterinary Science (IOSR-JAVS)*, *7*(12), 56–62.

Sarris, T. S., Close, M., & Abraham, P. (2018). Using solute and heat tracers for aquifer characterization in a strongly heterogeneous alluvial aquifer. *Journal of Hydrology*, *558*, 55–71. https://doi.org/10.1016/j.jhydrol.2018.01.032

Schaap, M. G., Leij, F. J., & van Genuchten, M. Th. (2001). rosetta : a computer program for estimating soil hydraulic parameters with hierarchical pedotransfer functions. *Journal of Hydrology*, *251*(3–4), 163–176. https://doi.org/10.1016/S0022-1694(01)00466-8

Segismundo, E. Q., Koo, B.-H., Kim, L.-H., & Lee, B.-S. (2016). Effects of Media Breakage on Infiltration Characteristics in Stormwater Management System. *Journal of the Korean Geotechnical Society*, *32*(2), 31–41. https://doi.org/10.7843/kgs.2016.32.2.31

Seifert, D., & Engesgaard, P. (2007a). Use of tracer tests to investigate changes in flow and transport properties due to bioclogging of porous media. *Journal of Contaminant Hydrology*, *93*(1–4), 58–71. https://doi.org/10.1016/j.jconhyd.2007.01.014

Seifert, D., & Engesgaard, P. (2007b). Use of tracer tests to investigate changes in flow and transport properties due to bioclogging of porous media. *Journal of Contaminant Hydrology*, *93*(1–4), 58–71. https://doi.org/10.1016/j.jconhyd.2007.01.014

Shaver, E. (2020). *Waikato stormwater management guideline*.

Simunek, J., van Genuchten, M. Th., Sejna, M., Torride, N., & Leiji, F. J. (1999). The STANMOD Computer Software for Evaluating Solute Transport in Porous Media Using Analytical Solutions of Convection-Dispersion Equation. *U. S. SALINITY LABORATORY AGRICULTURAL RESEARCH SERVICE U. S. DEPARTMENT OF AGRICULTURE RIVERSIDE, CALIFORNIA*.

Singha, K., & Gorelick, S. M. (2005). Saline tracer visualized with three-dimensional electrical resistivity tomography: Field-scale spatial moment analysis. *Water Resources Research*, *41*(5). https://doi.org/10.1029/2004WR003460

Siriwardene, N., Deletic, A., & Fletcher, T. (2007). Clogging of stormwater gravel infiltration systems and filters: Insights from a laboratory study. *Water Research*, *41*(7), 1433–1440. https://doi.org/10.1016/j.watres.2006.12.040

Slichter, C. (1898). *Theoretical investigation of the motion of ground waters*. U.S. Geological Survey, 19th Annual Report.

Snehota, M., Jelinkova, V., Sobotkova, M., Sacha, J., Vontobel, P., & Hovind, J. (2015). Water and entrapped air redistribution in heterogeneous sand sample: Quantitative neutron imaging of the process. *Water Resources Research*, *51*(2), 1359–1371. https://doi.org/10.1002/2014WR015432

Song, W., Liu, X., Zheng, T., & Yang, J. (2020). A review of recharge and clogging in sandstone aquifer. *Geothermics*, *87*, 101857. https://doi.org/10.1016/j.geothermics.2020.101857

Strom, E. W. (1998). *Hydrogeology and simulation of groundwater flow in the Cretaceous-Paleozoic aquifer system northern Mississippi*. https://pubs.usgs.gov/wri/1998/4171/report.pdf

Su, W., Cui, Y.-J., Qin, P.-J., Zhang, F., Ye, W.-M., & Conil, N. (2018). Application of instantaneous profile method to determine the hydraulic conductivity of unsaturated natural stiff clay. *Engineering Geology*, *243*, 111–117. https://doi.org/10.1016/j.enggeo.2018.06.012

Su, W., Cui, Y.-J., Zhang, F., & Ye, W. (2020). Revisiting the methods of determining hydraulic conductivity of saturated expansive clays in low-compressibility zone. *Journal of Rock Mechanics and Geotechnical Engineering*, *12*(5), 1131–1136. https://doi.org/10.1016/j.jrmge.2020.01.004

Suleiman, A. A., & Ritchie, J. T. (2001). Estimating saturated hydraulic conductivity from soil porosity. *Transactions of the American Society of Agricultural Engineers*. https://doi.org/10.13031/2013.4683

Tan, Y., Zhang, P., Chen, J., Shamet, R., Hyun Nam, B., & Pu, H. (2023). Predicting the hydraulic conductivity of compacted soil barriers in landfills using machine learning techniques. *Waste Management*, *157*, 357–366. https://doi.org/10.1016/j.wasman.2023.01.003

Tanaka, H., Shiwakoti, D. R., Omukai, N., Rito, F., Locat, J., & Tanaka, M. (2003). Pore Size Distribution of Clayey Soils Measured by Mercury Intrusion Porosimetry and its Relation to Hydraulic Conductivity. *Soils and Foundations*, *43*(6), 63–73. https://doi.org/10.3208/sandf.43.6_63

Tangparitkul, S., Saul, A., Leelasukseree, C., Yusuf, M., & Kalantariasl, A. (2020). Fines migration and permeability decline during reservoir depletion coupled with clay swelling due to low-salinity water injection: An analytical study. *Journal of Petroleum Science and Engineering*, *194*, 107448. https://doi.org/10.1016/j.petrol.2020.107448

Tatone, B., Donnelly, C. R., Protulipac, D., & Clarke, C. (2009). EVALUATION OF THE HYDRAULIC EFFICIENCY OF A NEWLY CONSTRUCTED PLASTIC CONCRETE CUT-OFF WALL. *Proceedings of the 2009 Canadian Dam Association Conference*. https://doi.org/10.13140/2.1.3540.1284

Taylor, D. (1948). *Fundamentals of soil mechanics*. John Wiley & Sons.

Terzaghi, C. (1925). Principles of soil mechanics. *Engineering News Record*, 95–832.

Terzaghi, K. (1922). *Erdbaumechanik auf Bodenphysicalisher Grundlagen*. Franz Deuticke.

Tian, L. (2006). Testing equality of inverse Gaussian means under heterogeneity, based on generalized test variable. *Computational Statistics & Data Analysis*, *51*(2), 1156–1162. https://doi.org/10.1016/j.csda.2005.11.012

Tian, L., Hu, L., Wang, D., & Cao, X. (2024). Site-scale groundwater pollution risk assessment using surrogate models and statistical analysis. *Journal of Contaminant Hydrology*, *261*, 104288. https://doi.org/10.1016/j.jconhyd.2023.104288

Torkzaban, S., Bradford, S. A., Vanderzalm, J. L., Patterson, B. M., Harris, B., & Prommer, H. (2015a). Colloid release and clogging in porous media: Effects of solution ionic strength and flow velocity. *Journal of Contaminant Hydrology*, *181*, 161–171. https://doi.org/10.1016/j.jconhyd.2015.06.005

Torkzaban, S., Bradford, S. A., Vanderzalm, J. L., Patterson, B. M., Harris, B., & Prommer, H. (2015b). Colloid release and clogging in porous media: Effects of solution ionic strength and flow velocity. *Journal of Contaminant Hydrology*, *181*, 161–171. https://doi.org/10.1016/j.jconhyd.2015.06.005

Torride, N., Leij, F. J., & van Genuchten, M. Th. (1999). The CXTFIT Code for Estimating Transport Parameters from Laboratory or Field Tracer Experiments. *U.S. SALINITY LABORATORY AGRICULTURAL RESEARCH SERVICE U.S. DEPARTMENT OF AGRICULTURE RIVERSIDE, CALIFORNIA*.

Touze-Foltz, N., Duquennoi, C., & Gaget, E. (2006). Hydraulic and mechanical behavior of GCLs in contact with leachate as part of a composite liner. *Geotextiles and Geomembranes*, *24*(3), 188–197. https://doi.org/https://doi.org/10.1016/j.geotexmem.2006.01.004

Valencia-González, Y., Quintero-Ramírez, A., & Lara-Valencia, L. A. (2022). A laboratory methodology for predicting variations in the geotechnical parameters of soil exposed to solid waste leachates in the field. *Results in Engineering*, *14*, 100398. https://doi.org/https://doi.org/10.1016/j.rineng.2022.100398

van Genuchten, M. Th., Simunek, J., Leij, F. J., Toride, N., & Sejna, M. (2012). STANMOD: Model Use, Calibration, and Validation. *Transactions of the ASABE*, *55*(4), 1355–1368. https://doi.org/10.13031/2013.42247

van Genuchten, M. Th., Simunek, J., Leij, F., & Sejna, M. (2012). STANMOD: Model Use, Calibration, and Validation. *Transactions of the ASABE*, *55*(4), 1355–1368. https://doi.org/10.13031/2013.42247

Vanderzalm, J. L., Page, D. W., Barry, K. E., & Gonzalez, D. (2020). Evaluating Treatment Requirements for Recycled Water to Manage Well Clogging during Aquifer Storage and Recovery: A Case Study in the Werribee Formation, Australia. *Water 2020, Vol. 12, Page 2575*, *12*(9), 2575. https://doi.org/10.3390/W12092575

Vandevivere, P., & Baveye, P. (1992). Effect of bacterial extracellular polymers on the saturated hydraulic conductivity of sand columns. *Applied and Environmental Microbiology*, *58*(5), 1690–1698. https://doi.org/10.1128/aem.58.5.1690-1698.1992

VanGulck, J. F., & Rowe, R. K. (2004). Evolution of clog formation with time in columns permeated with synthetic landfill leachate. *Journal of Contaminant Hydrology*. https://doi.org/10.1016/j.jconhyd.2004.06.001

Vienken, T., & Dietrich, P. (2011). Field evaluation of methods for determining hydraulic conductivity from grain size data. *Journal of Hydrology*, *400*(1–2), 58–71. https://doi.org/10.1016/j.jhydrol.2011.01.022

Vienken, T., Huber, E., Kreck, M., Huggenberger, P., & Dietrich, P. (2017). How to chase a tracer – combining conventional salt tracer testing and direct push electrical conductivity profiling for enhanced aquifer characterization. *Advances in Water Resources*, *99*, 60–66. https://doi.org/10.1016/j.advwatres.2016.11.010

Villaseñor, J. A., González-Estrada, E., & Ochoa, A. (2019). On Testing the Inverse Gaussian Distribution Hypothesis. *Sankhya B*, *81*(1), 60–74. https://doi.org/10.1007/s13571-017-0148-8

Vuković, M., & Soro, A. (1992). *Determination of hydraulic conductivity of porous media from grain-size composition*.

Wang, B., Chen, L., & Niu, Z. (2022a). Critical hydraulic gradient and fine particle migration of sand under upward seepage flow. *Scientific Reports*, *12*(1), 14440. https://doi.org/10.1038/s41598-022-18720-9

Wang, B., Chen, L., & Niu, Z. (2022b). Critical hydraulic gradient and fine particle migration of sand under upward seepage flow. *Scientific Reports*, *12*(1), 14440. https://doi.org/10.1038/s41598-022-18720-9

Wang, C., Dou, Z., Zhu, Y., Zhuang, C., Yang, Z., & Zou, Z. (2025). Enhancing hydraulic conductivity field characterization through integration of hydraulic head and tracer data using multi-

modal neural network models. *Journal of Hydrology*, *647*, 132295. https://doi.org/10.1016/j.jhydrol.2024.132295

Wang, H., Qian, H., & Gao, Y. (2020). Non-darcian flow in loess at low hydraulic gradient. *Engineering Geology*. https://doi.org/10.1016/j.enggeo.2020.105483

Wang, J., François, B., & Lambert, P. (2017). Equations for hydraulic conductivity estimation from particle size distribution: A dimensional analysis. *Water Resources Research*, *53*(9), 8127–8134. https://doi.org/10.1002/2017WR020888

Wang, J., Wu, Y., Zhang, X., Li, Z., & Chen, L. (2023). Analytical Delay Modeling for a Sub-Threshold Cell Circuit with the Inverse Gaussian Distribution Function. *Electronics*, *12*(6), 1387. https://doi.org/10.3390/electronics12061387

Wang, W., Dong, L., Zhai, T., Wang, W., Wu, H., Kong, F., Cui, Y., & Wang, S. (2023). Bio-clogging mitigation in constructed wetland using microbial fuel cells with novel hybrid air-photocathode. *Science of The Total Environment*, *881*, 163423. https://doi.org/https://doi.org/10.1016/j.scitotenv.2023.163423

Wang, Y., Wei, Y., Du, Y., Li, Z., & Wang, T. (2024). Causality analysis and prediction of soil saturated hydraulic conductivity by combining empirical modeling and machine learning techniques. *Journal of Hydrology*, *644*, 132104. https://doi.org/10.1016/j.jhydrol.2024.132104

Wang, Y., Yu, M., Bo, Z., Bedrikovetsky, P., & Le-Hussain, F. (2021). Effect of temperature on mineral reactions and fines migration during low-salinity water injection into Berea sandstone. *Journal of Petroleum Science and Engineering*, *202*, 108482. https://doi.org/10.1016/j.petrol.2021.108482

Wang, Z., Du, X., Yang, Y., & Ye, X. (2012). Surface clogging process modeling of suspended solids during urban stormwater aquifer recharge. *Journal of Environmental Sciences*, *24*(8), 1418–1424. https://doi.org/10.1016/S1001-0742(11)60961-3

Watson, K. K. (1966). An instantaneous profile method for determining the hydraulic conductivity of unsaturated porous materials. *Water Resources Research*, *2*(4), 709–715. https://doi.org/10.1029/WR002i004p00709

Weihermüller, L., Lehmann, P., Herbst, M., Rahmati, M., Verhoef, A., Or, D., Jacques, D., & Vereecken, H. (2021). Choice of Pedotransfer Functions Matters when Simulating Soil

Water Balance Fluxes. *Journal of Advances in Modeling Earth Systems*, *13*(3). https://doi.org/10.1029/2020MS002404

Weir, G. (2018). Deriving permeability distributions from fractal Gaussian tracer returns. *ANZIAM Journal*, *59*, 205. https://doi.org/10.21914/anziamj.v59i0.12611

Wietsma, T. W., Oostrom, M., Covert, M. A., Queen, T. E., & Fayer, M. J. (2009). An Automated Tool for Three Types of Saturated Hydraulic Conductivity Laboratory Measurements. *Soil Science Society of America Journal*, *73*(2), 466–470. https://doi.org/10.2136/sssaj2008.0154

Wu, J.-C., An, M., & Ma, W.-G. (2019). Spontaneous rectification and absolute negative mobility of inertial Brownian particles induced by Gaussian potentials in steady laminar flows. *Soft Matter*, *15*(36), 7187–7194. https://doi.org/10.1039/C9SM00853E

Wu, L., Allmaras, R. R., Lamb, J. B., & Johnsen, K. E. (1996). Model Sensitivity to Measured and Estimated Hydraulic Properties of a Zimmerman Fine Sand. *Soil Science Society of America Journal*, *60*(5), 1283–1290. https://doi.org/10.2136/sssaj1996.03615995006000050001x

Yang, S., Sheng, Z., Liu, W., Song, Z., Wu, M., & Zhang, J. (2008). Evaluation and prevention of formation damage in offshore sandstone reservoirs in China. *Petroleum Science*, *5*(4), 340–347. https://doi.org/10.1007/s12182-008-0057-6

Ye, X., Cui, R., Du, X., Ma, S., Zhao, J., Lu, Y., & Wan, Y. (2019). Mechanism of Suspended Kaolinite Particle Clogging in Porous Media During Managed Aquifer Recharge. *Groundwater*, *57*(5), 764–771. https://doi.org/10.1111/gwat.12872

Yeh, Y. J., Lee, C. H., & Chen, S. T. (2000). A tracer method to determine hydraulic conductivity and effective porosity of saturated clays under low gradients. *Ground Water*. https://doi.org/10.1111/j.1745-6584.2000.tb00244.x

Yin, J.-H. (2009). Influence of relative compaction on the hydraulic conductivity of completely decomposed granite in Hong Kong. *Canadian Geotechnical Journal*, *46*(10), 1229–1235. https://doi.org/10.1139/T09-053

Zebarth, B. J., De Jong, E., & Henry, J. L. (1989). Water flow in a hummocky landscape in central Saskatchewan, Canada, II. Saturated flow and groundwater recharge. *Journal of Hydrology*, *110*(1–2), 181–198. https://doi.org/10.1016/0022-1694(89)90243-6

Zeitfogel, H., Feigl, M., & Schulz, K. (2023). Soil information on a regional scale: Two machine learning based approaches for predicting saturated hydraulic conductivity. *Geoderma*, *433*, 116418. https://doi.org/10.1016/j.geoderma.2023.116418

Zhang, Y., & Schaap, M. G. (2019). Estimation of saturated hydraulic conductivity with pedotransfer functions: A review. *Journal of Hydrology*, *575*, 1011–1030. https://doi.org/10.1016/j.jhydrol.2019.05.058

Zhao, Z., Berg, S. J., Illman, W. A., & Qi, Y. (2022). Improving predictions of solute transport in a laboratory sandbox aquifer through high-resolution characterization with hydraulic tomography. *Journal of Hydrology*, *615*, 128673. https://doi.org/10.1016/j.jhydrol.2022.128673